AD-A083 764 GEORGIA INST OF TECH ATLANTA SCHOOL OF AEROSPACE ENG--ETC F/G 21/8.2
ROCKET RESEARCH AT GEORGIA TECH.(U)
NOV 79 E W PRICE, W C STRAHLE, B T ZINN F49620-78-C-0003
UNCLASSIFIED AFOSR-TR-80-0305 NL

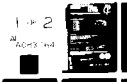

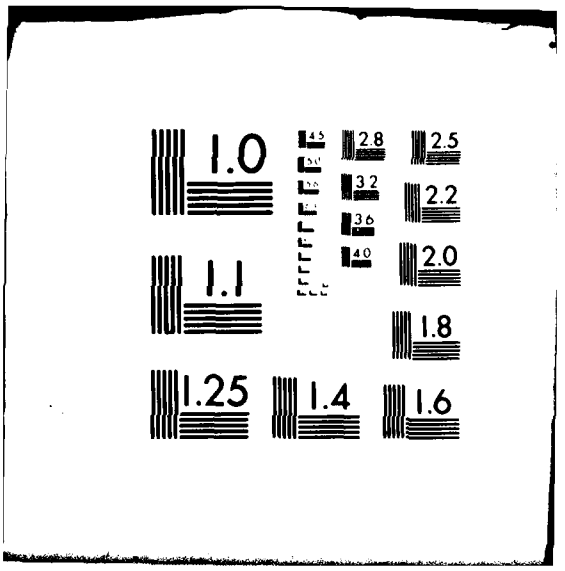
1.0
1.1
1.25
1.4
1.6
1.8
2.0
2.2
2.5
2.8
3.2
3.6
4.0

DISCLAIMER NOTICE

THIS DOCUMENT IS BEST QUALITY PRACTICABLE. THE COPY FURNISHED TO DTIC CONTAINED A SIGNIFICANT NUMBER OF PAGES WHICH DO NOT REPRODUCE LEGIBLY.

UNCLASSIFIED
SECURITY CLASSIFICATION OF THIS PAGE (When Data Entered)

REPORT DOCUMENTATION PAGE	READ INSTRUCTIONS BEFORE COMPLETING FORM
(19) AFOSR-TR-80-0855 2. GOVT ACCESSION NO. AD-A083 764	3. RECIPIENT'S CATALOG NUMBER
4. TITLE (and Subtitle) ROCKET RESEARCH AT GEORGIA TECH.	5. TYPE OF REPORT & PERIOD COVERED (9) INTERIM Rept. 1 OCT 78-30 SEP 79,
7. AUTHOR(s) (5070) E. W. Price, W. C. Strahle, B. T. Zinn, J. E. Hubbartt, D. H. Neale [redacted]	8. CONTRACT OR GRANT NUMBER(s) (15) F49620-78-C-0034
9. PERFORMING ORGANIZATION NAME AND ADDRESS GEORGIA INSTITUTE OF TECHNOLOGY SCHOOL OF AEROSPACE ENGINEERING ATLANTA, GA 30332 403914	10. PROGRAM ELEMENT, PROJECT, TASK AREA & WORK UNIT NUMBERS (16) 23[redacted] 61102F (17) A1
11. CONTROLLING OFFICE NAME AND ADDRESS AIR FORCE OFFICE OF SCIENTIFIC RESEARCH/NA BLDG 410 BOLLING AIR FORCE BASE, D.C. 20332	12. REPORT DATE (11) NOV 79 13. NUMBER OF PAGES [redacted]
14. MONITORING AGENCY NAME & ADDRESS(if different from Controlling Office) (12) 132	15. SECURITY CLASS. (of this report) UNCLASSIFIED
	15a. DECLASSIFICATION/DOWNGRADING SCHEDULE

16. DISTRIBUTION STATEMENT (of this Report)

Approved for public release; distribution unlimited

17. DISTRIBUTION STATEMENT (of the abstract entered in Block 20, if different from Report)

18. SUPPLEMENTARY NOTES

19. KEY WORDS (Continue on reverse side if necessary and identify by block number)

SOLID PROPELLANT COMBUSTION; UNSTEADY COMBUSTION; ALUMINUM; NOISE; TURBULENCE NOISE; VIBRATION; EXTERNAL BURNING PROPULSION; BASE FLOW; SUPERSONIC FLOW

20. ABSTRACT (Continue on reverse side if necessary and identify by block number)

Progress is reported on four distinct projects which are administered as a group. The individual projects are identified as tasks and reported on separately. A summary for each task follows.

TASK I. Work concerned improvement and application of the impedance tube method for measurement of the pressure-coupled combustion response of solid propellants and measurement of the bulk damping in the product flow. Improvements included 403914 increased sites and amplitude range of pressure measurements; increased

of the data acquisition system; and a modified, more rapid data reduction program. Admittances and bulk loss coefficients of nonaluminized and aluminized propellants were measured over a range of frequencies.

TASK II. Studies were continued on external burning using an axisymmetric model at Mach 3. Early work using contoured test section walls and cold gas base region injection is reviewed to demonstrate wake detail and length scale changes under the influence of simulated external/base burning. Tests with actual combustion of radially and axially injected hydrogen are then reported. Outstanding performance values with significant base drag reduction is shown for injection and burning directly in the near-wake (base burning). Current attemp ts at radial injection and burning in the free stream (external burning) have not yet succeeded. These tests, however, have defined an envelope within which external burning, if feasible, will presently be achieved.

TASK III. Investigations continued of the accumulation processes of aluminum on the propellant burning surface that lead to formation of agglomerate droplets, the size of which dominates aluminum combustion. Using dry-pressed mixtures of ammonium perchlorate, aluminum and carnauba wax powders, the effects of particle sizes, mixture ratios and pressure were studied by high speed photography. Results were correlated with a scenario describing the effects of propellant microstructure, retention processes for aluminum on the burning surface, response of aluminum powders to heating, and inflamation process for sintered aluminum.

Quench tests at atmospheric pressure on the combustion plume above the burning surface showed that the agglomerates in these tests burned much as aluminum droplets in earlier single particle-controlled atmosphere tests. An exception resulted in tests with large (95 μm) aluminum particles which did not ignite completely. An apparatus for tests at elevated pressure was designed and partially fabricated.

TASK IV. Experimental and analytical studies were continued on the subject of turbulence-induced pressure fluctuations in a rocket-like cavity. To overcome prior deficiencies in theory, a new theory was constructed for the generation of pressure disturbances by the turbulence. Undeniable separation has been achieved between propagational and local pressure fluctuations, and the agreement between theory and experiment are adequate. Measurements include microphone and hot film anemometry, and time series analysis is applied to the results.

Unclassified

AFOSR INTERIM SCIENTIFIC REPORT

AFOSR-TR-79-

ROCKET RESEARCH AT GEORGIA TECH

Prepared for

Air Force Office of Scientific Research
Aerospace Sciences Directorate
Bolling Air Force Base, D.C.

Co-Principal Investigators

E. W. Price
W. C. Strahle
B. T. Zinn
J. E. Hubbartt
D. H. Neale
R. K. Sigman
B. R. Daniel

School of Aerospace Engineering
Georgia Institute of Technology
Atlanta, GA 30332

Approved for public release; distribution unlimited
Contract No. F49620-78-C-0003 November 1979

TABLE OF CONTENTS

General Introduction

Progress is reported for the second year effort of four distinct projects under contract AFOSR F49620-78-C-0003. The individual projects are identified as distinct tasks, this distinction being preserved because it reflects also distinct test facilities and personnel assignments. Each task report contains its own abstract, introduction, and progress report.

Task I is concerned with combustion stability, with particular reference to measurement of the response of solid propellant combustion to oscillatory flow environments. Primary effort is on development of the impedance tube method for measuring response functions. This includes improving its accuracy, economy of operation, and versatility of application. Exploration of other methods of measuring response functions is also conducted.

Task II is concerned with combined external and base burning as a means of developing sustained thrust for missiles with minimum weight and volume demands on the propulsion system. A facility was developed previously for injection and combustion of hydrogen in and around the near-wake shear flow of an axisymmetric body. Initial studies were made of the flow field using nonreactive gases, and the present report covers recent studies with hydrogen injection and burning.

Task III is concerned with the role of the aluminum powder ingredient in propellant combustion and 2-phase product flow. The steps in the metal "metabolism" are traced through the phase of accumulation on the burning surface, the melting and coalescing of particles into relatively large droplets, the ignition

and combustion of the droplets, effect of combustor gas flow on these steps, and their response to gas oscillations. The present report summarizes combustion photographs, tests of burning surface behavior of model propellants (dry-pressed powders) involving various combinations of aluminum, ammonium perchlorate and hydrocarbon wax powder. Also reported are results of quench tests, including quench-collection of condensed material in the combustion phase.

Task IV is concerned wtih the source of pressure fluctuations in rocket motors. It is believed that a significant contribution is made by the interaction of turbulence of the flow with the nozzle. A facility was constructed previously to measure this effect, and modifications are continuing. Recent testing is reported here, and a new theory is presented.

TASK I

SOLID PROPELLANT RESPONSE FACTOR MEASUREMENTS

BEN T. ZINN

BRADY R. DANIEL

YOSSI D. BAUM

Abstract

Results obtained under an AFOSR sponsored research program that is concerned with the development of experimental techniques for the determination of the admittances of burning solid propellants under conditions simulating those observed in unstable rocket motors and the determination of the admittances of various solid propellant are described. As part of this program, much effort has gone into improving the accuracy of the impedance tube technique that was developed earlier under this program. These improvements included increasing the number of transducers utilized to measure the standing wave structure to fifteen, increasing the dynamic measurement range to cover 110-165 db, increasing the sampling rate of the mini computer based data acquisition system, and reducing the number of numerical iterations required for determining the propellant admittance from the measured acoustic pressure data. The improved impedance tube set-up was then used to determine the frequency dependence of the admittances and bulk loss coefficients of aluminized and non-aluminized propellants and some of these results are presented in this report. Finally, efforts dealing with the development of a direct admittance measurement technique are described.

I. Introduction

This report summarizes progress made under Task I of AFOSR Contract No. F49620-78-C-0003 during the period October 1, 1978 to September 30, 1979. This research was concerned with the development of the experimental techniques for the determination of the admittances of burning solid propellants under a variety of conditions simulating those observed in unstable solid rockets and the measurement of the admittances of various aluminized and non-aluminized composite solid propellants. The ability to predict and measure the burning rate characteristics of solid propellants under a variety of unsteady rocket motor operating conditions is of great scientific and practical importance. Such data is needed for the apriori prediction of the combustion stability characteristics of proposed solid propellant rocket motor designs as well as the determination of the relative driving capabilities of various solid propellant formulations. Also, there is a need to correlate the predictions of theoretical solid propellant combustion models and relevant experimental data. Establishing the validity of theoretical combustion models would demonstrate a level of technology which would greatly reduce future development testing requirements. The progress made in reaching the goals of this program are briefly outlined in the remainder of this report.

As the objectives and background for this research program have been discussed in much detail in Ref. 1 only a brief review of this material will be provided herein. The propellant in unstable solid rockets is exposed to regions of primarily pressure oscillations, regions of primarily velocity oscillations and regions that contain both pressure and velocity oscillations. To predict solid rocket motor stability, data describing the propellants burning rate at each of these regions, at different frequencies, different oscillation amplitudes and different engine operating conditions are needed. Most of the research efforts in this area to date have concentrated on the pressure coupled response that describes the propellant burning rate response when exposed to small-amplitude pressure

oscillations only. Most of the experimental efforts in this area to date depend upon the utilization of the T-burner[2] which provided much useful data in spite of some obvious shortcomings[1]. Careful considerations of what has been done in this area to date clearly indicate the need for the development of alternate experimental approaches that are hopefully devoid of some of the difficulties that affect T-burners. Results provided by these new measurement techniques could also be used to check the accuracy of the T-burner data.

The work conducted under this program can be generally divided into two parts; namely, (1) the development of experimental techniques for the measurement of the admittances of solid propellants under different conditions simulating those observed in unstable rockets and (2) the acquisition of solid propellant admittance data.

The efforts concerned with the development of new experimental techniques included the improvement of the impedance tube technique developed earlier under this program and the investigation of the so-called "direct" burn rate measurement techniques. In this case the term "direct" implies experimental techniques that are capable of directly measuring the mass loss of the propellant sample or its surface regression. These efforts are still in progress and their state of development is described in the following section of this report.

The efforts to acquire solid propellant admittance data concentrated on the determination of the admittances of two non-aluminized and two aluminized propellants at 300 psig over the frequency range from 300 to 1000 Hz. Of special significance are the investigations of the admittances of aluminized propellants where the utilization of the impedance tube allowed the simultaneous determination of the gas phase losses caused by the aluminum oxide particles in the impedance tube and the admittance at the propellant surface. The capability to perform these two measurements simultaneously offers the

possibility for the determination of the manner in which the addition of aluminum or metal particles affects combustion instabilities; that is, whether the addition of aluminum particles attenuate or amplify combustion instabilities by providing gas phase damping or amplification and/or modifying the combustion response of the solid propellants. The resolution of this problem will require the utilization of the developed impedance tube technique in a series of tests in which the same propellants will be tested with and without metal additives and the results will be compared. Some of the propellant admittance data measured in the course of this investigation will be presented in the following section.

The ability to utilize the impedance tube technique in the measurement of the admittances of aluminized propellants is of special significance as other experimental techniques, such as the pulse and variable area T-burners, have experienced considerable difficulties in the determination of the admittances of aluminum solid propellants.

Results obtained under this program were presented during the reporting period at the 17th Aerospace Sciences Meeting in New Orleans, La. and the 16th JANNAF Combustion Meeting at Naval Post Graduate School in Monterey, Calif. These works also appeared as the following publications:

1. M. Salikuddin and B. T. Zinn,"Adaptation of the Impedance Tube Technique for the Measuement of Combustion Process Admittances," AIAA Paper No. 79-0167, January 1978.
2. " Experimental Determination of Solid Propellant Admittances by the Impedance Tube Method", to appear in the Proceedings of the 16th JANNAF Combustion Conference, Sept. 10-14, 1979.

Paper No. 1 above has also been accepted for publication in the December issue of the Journal of Sound and Vibrations.

In addition, the paper

3. Baum, J. D., Daniel, B. R. and Zinn, B. T., "Determination of Solid Propellant Admittances of Impedance Tube Method," has been accepted for presentation at the18th AIAA Aerospace Sciences Meeting that will be held in Pasadena, California.

All of the above papers are included in Appendix I-A of this report.

Finally, the Ph.D. thesis of Dr. M. Salikuddin that was supported under this program was published and approved by the Georgia Tech faculty in April 1978. This thesis is entitled:

"Application of the Impedance Tube Technique in the Measurement of Burning Solid Propellant Admittances"

In the following section a brief summary of the progress made during the reporting period is provided. More detailed descriptions of these efforts can be found in the papers included in Appendix I-A.

II. Program Progress

(A) Improvements in the Impedance Tube Technique

The principles of the operation of the impedance tube technique are provided in Paper No. 1 in App. I-A. As with any newly developed experimental technique, much effort was expended during the reporting period on the improvement of the operation and accuracy of the impedance tube technique. These efforts can be divided into three parts; namely, (a) improvement of the experimental procedure; (b) improvement of the data acquistion procedure; and (c) improvement of the data reduction procedure. Item (a) involved the use of additional transducers (up to 15) in the acoustic pressure measurements and the development of a new calibration procedure that increased the previously available dynamic measurement range to cover the range of 110-165 db. Item (b) involved the inclusion of a "direct memory access" into the mini computer based data acquisition system which greatly increased the data sampling rate. This change resulted in considerable improvement in the quality of the measured acoustic data. Finally, Item (c) involved the mathematical reformulation of the data reduction procedure in order to eliminate the majority of the previously used numerical iterations. This improvement considerably reduces the amount of computer time required to obtain the desired admittances from the measured acoustic pressure data.

Since the efforts covered under items (a), (b) and (c) above are described in detail in Papers 2 and 3 of App. I-A of this write up, further discussion of these efforts will not be repeated herein. In addition, these references contain data illustrating the repeatability and consistency of the data measured by the impedance tube technique.

(B) Measured Solid Propellant Admittance Data

During the report period, the impedance tube technique was utilized to measure the admittances of two non-aluminized composite propellants (i.e., A-13 and A-14) provided to this group by NWC, China Lake, Calif. and two aluminized propellants. The latter

consisted of a UTP-3001 propellant that is a Titan III C Booster Propellant provided by Prof. E. W. Price at Georgia Tech who uses it in his research program, and a UTP-19360 propellant provided by Dr. L. Strand from the JPL Laboratories in Pasadena, California.

Typical results obtained with the UTP- 3001 aluminized propellant are presented in Figs. 1 through 4 of this report. In this case, Figs. 1 and 2 present a comparison between the instantaneous pressure amplitude and phase profiles predicted utilizing the determined propellant admittances and the measued experimental data. Excellent agreement between the two sets of data is demonstrated. Furthermore, attention should be given to the increase in the magnitude of the second amplitude minima, as compared to the first amplitude minima. This change was caused by the gas phase attenuation provided by the presence of aluminum oxide particles in the flow. The large gas phase damping is also supported by the change in the positive slope of the phase space curve near the respective minimum points. The frequency dependence of the UTP-3001 propellant driving characteristics, as described by the real part of the admittance Y_R, and the gas phase damping, as described by the gas phase damping coefficient G, are plotted in Figs. 3 and 4, respectively. Similar data for the UTP-19360 propellant has also been obtained during the research period covered by this report.

(C) Evaluation of the Feasibility of the "Direct" Impedance Measurement Techniques.

As stated earlier, the "direct" measurement techniques involve the direct measurement of the propellant mass loss and/or the regression of its surface, when exposed to an oscillatory flow field. The difficulty in performing these measurements is that they require the measurement of extremely small mass or distance changes over extremely short time periods. In contrast to the "direct" measurements, most of the currently used techniques for admittance measurement (e.g., the T-burner and the impedance tube) utilize measured acoustic pressure data to determine the propellant admittance. In these cases the accuracy of the determined admittances depends, among other things, upon the accuracy of the theoretical model used to describe the system

acoustics.

Some of the research efforts conducted under this program were concerned with the investigation of the feasibility of the some potentially promising direct measurement techniques. In the first part of this program the feasibility of utilizing the Optron, an optical target follower, to follow the regression of a burning solid propellant surface was considered. The characteristics of the Optron System were discussed in last year's proposal[3] and they will not be repeated herein.

Part of the efforts conducted under this part of the program involved the borrowing of an Optron system that was available at AFRPL. Upon receipt of this system much effort went into its checkout and, unfortunately, this system did not perform adequately. Simultaneously with the Optron's checkout, the ability of the Optron system to accurately measure the small changes in propellant surface regression in response to an oscillatory flow field were considered. This analysis indicated that the distance changes that one would need to measure in order to determine the propellant admittance are of the same order of magnitude as the surface irregularities caused by the presence of ammonium pechlorate in the binder. Consequently, the ability of the Optron to distinguish the "oscillatory" changes in the propellant regression caused by the propellant response to an oscillatory environment from "random" regression rate fluctuations is uncertain. To answer this question, a newer and more accurate Optron system will have to be utilized. Considering the uncertainty of the results of such an effort and the high cost of a new Optron system, a decision has been made to terminate these efforts for the time being and, instead, focus our efforts on the possibility of directly measuring propellants mass losses.

The other portion of this study was concerned with the development of an accurate experimental technique for direct mass loss measurement. Efforts conducted in this area in the Soviet Union[4,5] concentrated on the development of a system whose mass change could be related to a frequency change that can be measured with much accuracy. A

schematic of one of these setups where the change in the natural frequency of an equivalent mass-spring-dashpot system is measured as shown in Fig. 5. In this experiment, a change in the mass of the burning propellant is reflected by a proportional change in the natural frequency of the system. The major shortcoming of this effort is the low natural frequency of the developed mechanical system. Therefore, the relatively small change in the natural frequency due to the propellant mass flux precludes the high degree of resolution required for meaningful propellant admittance measurements.

The most promising technique for direct mass loss measurement is a modification of the mass-spring-dashpot system which uses the high natural frequency characteristics of piezoelectric crystals. A schematic of the setup currently being investigated under this program is also shown in Fig. 5 . In initial investigations with this setup, quartz crystals were used as the basic oscillatory system. Unfortunately, the oscillatory characteristics of the quartz crystals is such that the crystals will not oscillate with the relatively high propellant mass loadings that are necessary for mass flux measurements.

More recent work in this area has been directed toward using a ceramic crystal as the oscillating system. Progress in this area to-date includes the selection and purchase of several configurations of piezo-ceramic crystals with unloaded natural frequencies of the order of 9 Mega Hertz. It is anticipated that at this relatively high frequency the change in the natural frequency of the system due to propellant mass loading will be of an order which will make measurement of the mass flux of a burning solid propellant possible. However, the feasibility of the application of the ceramic crystals for direct mass measurement will depend on the static loading tests which will be conducted as soon as the crystal elements are delivered from the manufacturer. This work is currently in progress.

III. Future Research

This program is still committed to the objective of improving current experimental capabilities for measuring the admittances of various solid propellants under a variety of conditions simulating these observed in unstable rocket motors and the acquisition of propellant response factor data for a variety of aluminized and non-aluminized propellants over frequency ranges that are of interest to the propulsion community. Specifically, the following studies will continue under this program: (a) the investigation of the feasibility of utilizing a piezo-ceramic crystal for the direct measurement of the propellant mass loss; (b) the determination of the admittances of various aluminized and non-aluminized propellants with special emphasis given to the determination of the effect of metal addition upon the propellant admittance; and (c) an effort will be undertaken to determine whether the impedance tube technique can be used to determine the velocity-coupled response of solid propellants.

References

1. "Rocket Research", a proposal submitted by the School of Aerospace Engineering to AFOSR on May 6, 1977.

2. T-Burner Manual, CPIA Publication No. 191, Nov. 1969.

3. B. T. Zinn, "Rocket Research at Georgia Tech", Task I, Research Proposal submitted by the School of Aerospace Engineering at Georgia Tech to AFOSR on June 22, 1978.

4. Mikheev, V. F., Zarko, V. E., Borin, S. M., Kutsenogii, K. P. and Simonenko, V. N., "Measurement of Burning Rates in Transient Combustion Processes Under the Influence of External Radiation," published in Experimental Diagnostics in Combustion Solids (Boggs and Zinn editors), AIAA Progress in Astronautics and Aeronautics, Volume 63, pp. 173-187.

5. Romanov, O. Ya., Tarkhov, V. S., and Shelukhin, G. G., "Measurement of Mass Rate of Nonstationary Combustion of a Condensed Substance by A Frequency Method," published in Combustion, Explosion, and Shock Waves, Volume 13, No. 6, Nov.-Dec. 1977.

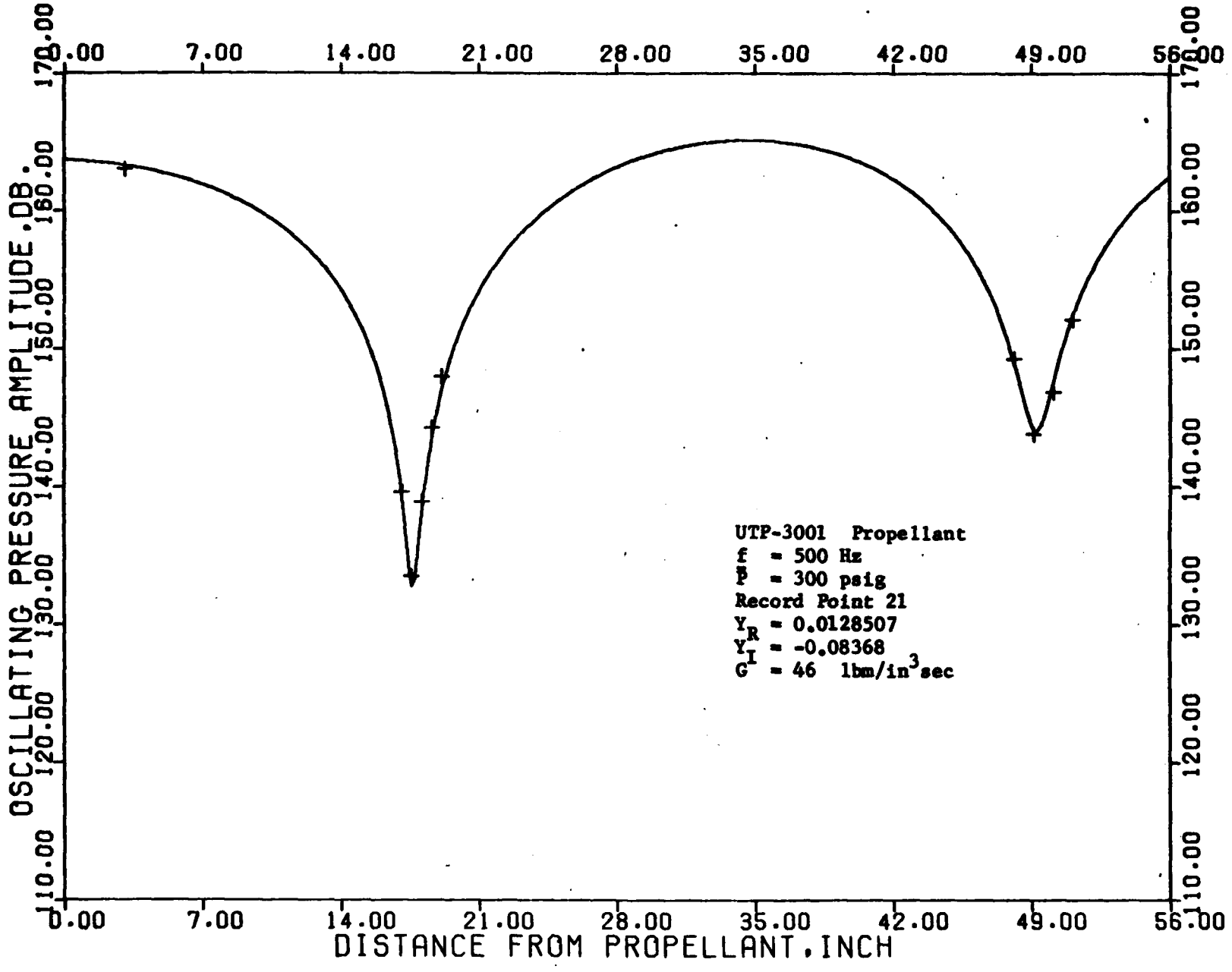

Figure 1. Predicted (——) and Measured (+) Axial Variations of the Instantaneous Pressure Amplitude.

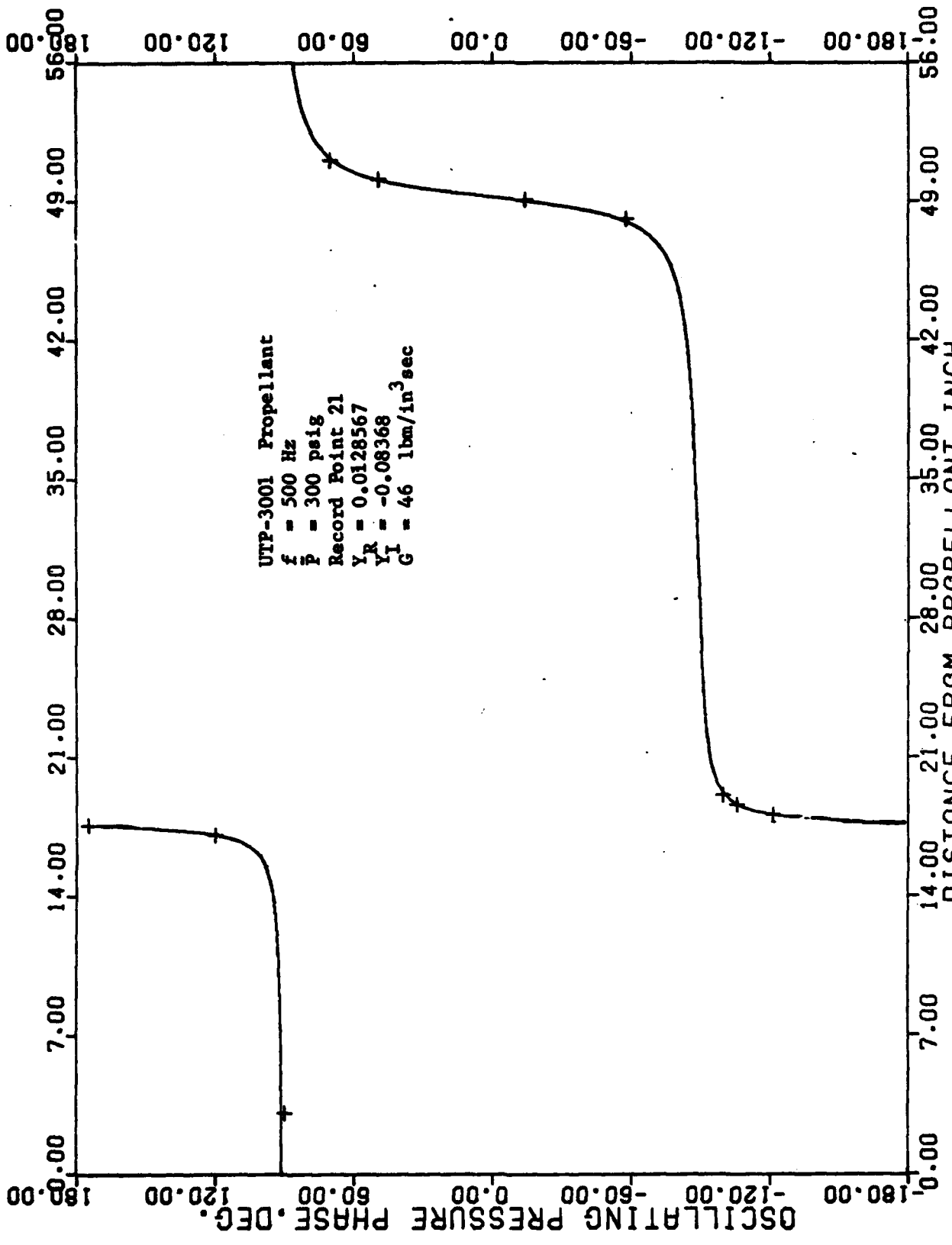

Figure 2. Predicted (——) and Measured (+) Axial Variation of the Instantaneous Pressure Phase.

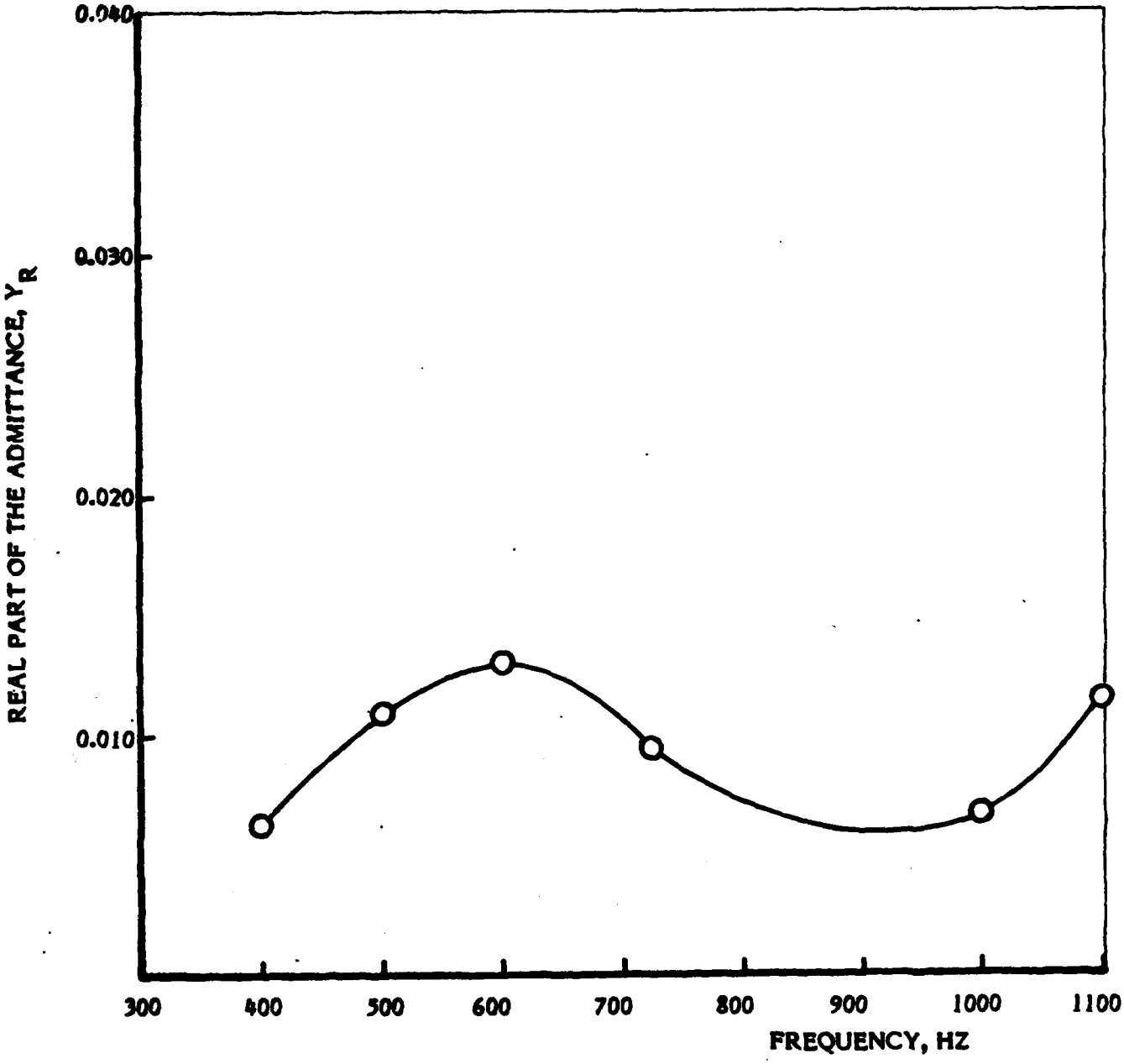

Figure 3. The Frequency Dependence of Real Part of the Admittance of a UTP-3001 Aluminized Propellant.

/w

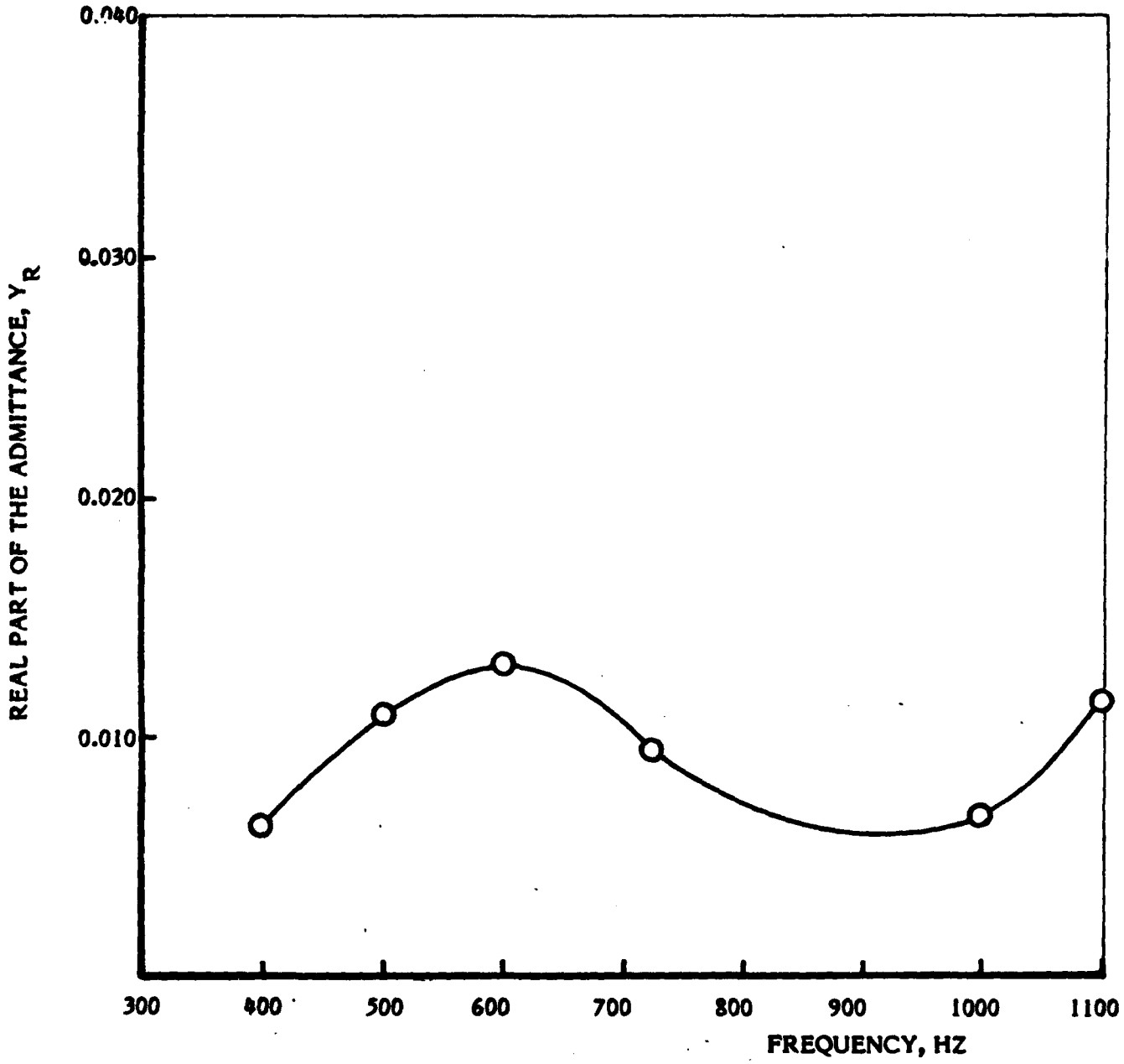

Figure 4. The Frequency Dependence of the Bulk Loss Coefficient G for a UTP-3001 Aluminized Propellant Tested at 300 psig.

SCHEMATICS FOR DIRECT MASS LOSS MEASUREMENTS

(A) ROMANOV ET AL SETUP IS EQUIVALENT TO THE FOLLOWING

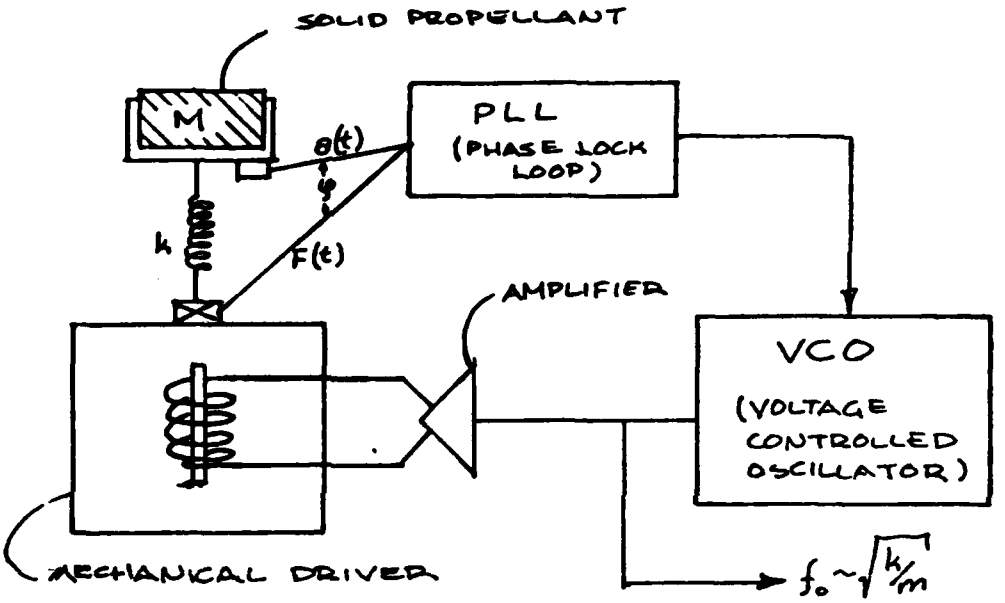

(B) SETUP UNDER CONSIDERATION AT GEORGIA TECH

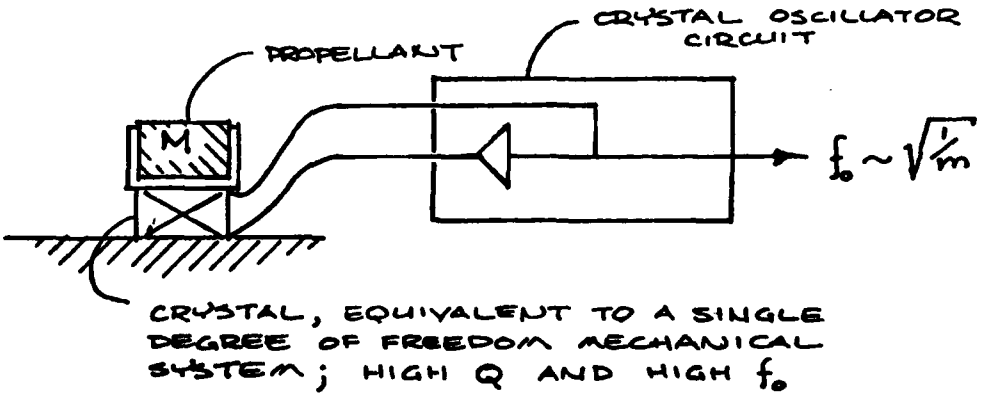

Figure 5. Schematics for Direct Mass Loss Measurements.

TASK II

EXTERNAL BURNING FOR PROPULSION

DOUGLAS H. NEALE

JAMES E. HUBBARTT

WARREN C. STRAHLE

Abstract

Experimental studies of base pressure manipulation for an axisymmetric model at Mach 3 with simulated and actual external base burning are described. Early work using contoured test section walls and cold gas base region injection is reviewed to demonstrate wake detail and length scale changes under the influence of simulated external/base burning. Tests with actual combustion of radially and axially injected hydrogen are then reported. Outstanding performance values with significant base drag reduction is shown for injection and burning directly in the near-wake (base burning). Current attempts at radial injection and burning in the free stream (external burning) have not yet succeeded. These tests, however, have defined an envelope within which external burning, if feasible, will presently be achieved.

I. Introduction

The application of burning, either in the near wake (base) or in the free stream adjacent to the near wake (external), can provide significant base drag reduction for projectiles operating at airbreathing altitudes. The coupling of attractive performance values with hardware simplicity makes this a particularly interesting propulsion concept.

The feasibility of external/base burning for propulsion in which the subsonic near-wake transmits elevated downstream pressures to the projectile base has been established. At present, however, no analytical model exists which adequately treats the complex base flows that result from combustion in and near the wake. A major contribution in understanding these flows, establishing and optimizing performance criteria and providing direction for theory can be supplied experimentally through detailed pressure and temperature measurements in the wake region for various modes of external/base combustion. Current studies in the School of Aerospace Engineering at Georgia Tech seek to provide this information.

A versatile experimental facility has been established for both simulation and actual combustion testing of axisymmetric external/base burning configurations at Mach 3 with a 5.72 cm dia. model in a 15.2 cm dia. test section (Reynolds number based on model diameter = 3.0×10^6). The blow-down facility is shown in Figures 1 and 2 in Appendix II-A. The hollow cylindrical model is mounted in the subsonic flow, passes through the nozzle throat and terminates in the plexiglass test section. Gases for base region injection are brought in through four of the eight support strut access ports. The remaining four ports are used to bring model surface static pressure tubes to the external data acquisition system. Detailed pressure and temperature wake measurements are made with computer controlled traverses of probes introduced through the constant-area diffuser downstream of the test

section. Run times range from 4-7 minutes depending on the stagnation pressure selected. Tunnel flow is not heated and stagnation temperatures drift downward from ambient to approximately -20^{o}C during typical tests.

II. Program Progress

Investigations of external/base burning with hydrogen have continued this year in the Georgia Tech Mach 3 Test Facility. The experiments were designed to meet the following goals:

1. Measurement of over-all performance and wake detail with pure base burning
2. Determination of pure external burning feasibility with subsequent performance and flow detail measurements
3. Investigation of base burning in combination with external burning to define optimum performance.

Progress in fulfilling these goals is summarized briefly in the following paragraphs and is documented in detail in Appendix II-A (text to be presented at the AIAA 18th Aerospace Sciences Meeting, January 1980).

Tests with pure base burning have thoroughly documented the encouraging base pressure rise and associated performance values for this apparatus. A reliable firing procedure featuring consumable igniters was developed and repeatable measurements were obtained. Wake surveys to measure pressure and temperature detail were completed for a range of hydrogen injection rates. Severe deflection of the pitot-static and thermocouple probes during these tests resulted in binding and slippage in the vertical portion of the traverse program. The measurements, therefore, are questionable for determining precise spatial pressure or temperature distributions. The temperature measurements, however, are valuable for demonstration of the lean-burning nature of the wake. Temperatures were highest within two model diameters of the base and decreased continuously with distance from the base. In all cases, wake temperatures remained significantly below the flame temperature for stoichiometric burning of hydrogen. Further measurements

with the present probe design were not continued so that "pure" external burning tests could be pursued. If judged valuable, wake detail measurements may be resumed in the coming year using re-designed probes.

Attempts to achieve pure external burning have not yet suceeded. The original radial injection configuration using six orifices recessed in an annular channel and operating subsonically ($M < 0.1$) yielded base pressure rises and performance values similar to the base injection tests. Burning was obtained in the annular channel as well as in the wake; however, no combustion in the free stream was evident. Orifice sizes were reduced and supersonic injection was attempted to increase jet penetration. Ignition with jet Mach numbers greater than about 2.1 was not obtained either in the channel or in the wake. With injection at $1.5 < M < 2.1$, ignition was sustained in the channel but not in the wake and base pressures were not significantly elevated. Further tests with this configuration are currently in progress to explore the range of subsonic and supersonic injection conditions between the extremes defined by the original tests.

Investigation of combined external/base burning was effected by superimposing simulated axisymmetric and asymmetric external burning on actual base burning. These tests revealed that, for the three simulated burning fields applied, the resulting base pressure is very nearly the simple sum of the individual base and external contributions when acting alone. These results confirm earlier tests in this program with simulated external and base burning showing that base pressures can be elevated substantially above free stream (i.e., base thrust) and are consistent with those recently presented by Schadow and Chieze.[1] Tests exploring actual combined external/base burning are being conducted concurrently with those attempting to achieve "pure" external burning. Radial injection at decreasing Mach numbers is combined with base injection through sintered plugs of varying porosity

to maintain an approximately equal split. The success of these, of course, will closely parallel the success of tests with attempted pure external burning.

Preparation for the coming year's proposed base burning tests of diluted hydrogen was begun in the current year. Design calculations were completed for purchase of flow meters to obtain the desired molecular weight ranges with the specified diluent gases. Two rotameters each with two alternate floats have been purchased and delivered. Gas regulators and pressure gages have been purchased and received. All other plumbing hardware will be bought at the time of assembly. Model adjustmenets for these tests are minor. All designs are complete and fabrication is now in progress.

References

1. Schadow, K. C. and D. J. Chieze, "Experimental Study on Base Drag Reduction with Combined Lateral and Axial Injection," AIAA Journal, Vol. 16, No. 10, October, 1978, pp. 1084-1089.

TASK III

BEHAVIOR OF ALUMINUM IN SOLID PROPELLANT COMBUSTION

E. W. PRICE

R. K. SIGMAN

J. K. SAMBAMURTHI

T. S. SHESHADRI

C. J. PARK

Abstract

Investigations continued of the accumulation processes of aluminum on the propellant burning surface that lead to formation of agglomerate droplets, the size of which dominates aluminum combustion. Using dry-pressed mixtures of ammonium perchlorate, aluminum and carnauba wax powders, the effects of particle sizes, mixture ratios and pressure were studied by high speed photography. Results were correlated with a scenario describing the effects of propellant microstructure, retention processes for aluminum on the burning surface, response of aluminum powders to heating, and inflamation process for sintered aluminum.

Quench tests at atmospheric pressure on the combustion plume above the burning surface showed that the agglomerates in these tests burned much as aluminum droplets in earlier single particle-controlled atmosphere tests. An exception resulted in tests with large (95 μm) aluminum particles which did not ignite completely. An apparatus for tests at elevated pressure was designed and partially fabricated.

I. Introduction

It was noted in earlier progress reports[1-4] that the primary unknowns in combustion behavior of aluminum in solid rockets arise from the complicated behavior of the aluminum on the propellant burning surface. While the combustion occurs primarily after the aluminum leaves the burning surface, the nature of the burning droplets is determined by surface processes involving accumulation and agglomeration of original ingredient particles. The present studies have been aimed at determining the nature of these processes, the nature of the burning droplets, and the effect on combustion behavior.

Initial work on this program concentrated on the behavior of the propellant ingredients during heating, including formation of binder melts and interaction of particles (particularly aluminum). These studies established the conditions necessary for concentration, adhesion and sintering of particles on the propellant surface. Studies were then made of the evidence of these processes in propellant-like systems chosen to control such critical conditions as the presence of binder melts, proximity of aluminum particles in the matrix of the solid, and oxidizing character of the surroundings of the aluminum particles. These studies (on samples made from AP/Al mixtures) suggested that molten binder was not essential to retention and accumulation of aluminum on the burning surface (although it was conducive to accumulation under some conditions). The results showed that the aluminum was resistant to ignition in the AP flame, but that accumulating particles would sinter together. This latter process was favored by particle size combinations that provided proximity of aluminum particles to each other.

Introduction of a hydrocarbon fuel in graduated amounts showed that ignition events occurred in the accumulating aluminum, with surface-wise spreading of

inflamation sweeping up adjoining aluminum accumulations to give burning agglomerates. These results, and tests on samples with thin fuel laminations show that diffusion flamelets associated with the H.C. fuel vapors act to pilot the aluminum ignition. Tests along these lines have been continued and are described below.

At the beginning of this report period, preliminary tests had been made to further evaluate the aluminum behavior after leaving the burning surface. Experiments provided samples of agglomerates quenched at various distances from the burning surface. The limited results available suggested transformation of accumulates to liquid aluminum droplets near the surface, followed by combustion to burnout without any singular events.

While the previously reported work did not pretend to determine details of aluminum behavior at the molecular or submicron level, it established a basis for recognition of the dominant processes governing aluminum behavior; and hence provided some rational basis for modification of behavior. More recent work has sought to consolidate the basis of understanding by extending previous test series and by development of a mechanistic model embodying the understanding to date. In addition, observations of behavior of droplets after detachment from the burning surface have been continued.

II. Program Progress

A. Burning Surface Behavior: AP/Al Systems

Various studies have been reported on combustion of solid samples made by dry-pressing mixtures of AP and Al powders .[5-7] There is a tendency for such works to be provincial in nature, exploring a limited range of experimental variables and making a broad interpretation based on the rather limited range of observational data (e.g., argument about aluminum behavior based on determinations of sample burning rate). In the present studies, more direct observation of the samples was made using high speed cinemicrophotography. Test variables were chosen to reflect rocket motor-like conditions (within the limits of the window-bomb type of experiment). Observations were also made of samples quenched by various methods. State and behavior of the aluminum itself was addressed in these observations. Work during this reporting period on the AP/Al system included extension of the previous test series and more thorough examination of results. Table III-1 summarizes the complete series and test conditions. In many cases the tests are duplicates, run to obtain more decisive information or better motion pictures.

The most productive tests were the motion pictures. These were viewed independently by several observers, who evaluated the behavior relative to the different aspects of behavior listed in Table III-2. After recording these evaluations, the observers compared results and agreed on the following observations.

1. Aluminum accumulates, concentrates and sinters on the burning surface before detaching.

2. Samples containing AP and Al of comparable particle size showed only

Table III-1

Summary of Tests on Dry-Pressed AP / Al Mixtures*

Sample / Pressure		85% 10 μmAP 15% 5 μmAl (H-5)	85% 60 μmAP 15% 30 μmAl (H-30)	85% 100 μmAP 15% 30 μmAl (H-30)			85% 100 μmAP 15% 95 μmAl (H-95)		
					Movie			Movie	
MPa	PSI	Movie	Movie	dp/dt Quench	Hi Mag	Lo Mag	dp/dt Quench	Hi Mag	Lo Mag
4.2	600			✓✓✓✓			✓✓✓✓		
5.5	800			✓	35	38		5,9,13	c
6.9	1000	55	57	✓✓✓	33	4	✓✓✓	1,10,14	

*Check marks denote tests. Numbers identify the pertinent film.

Table III-2
Topics to Evaluate From Movies

1. Degree of surface accumulation (s.a.)

2. Connectedness of s.a.

3. Looseness of attachment of connected s.a. (c.s.a.) (i.e., apparent rigidity vs. freedom of movement while attached)

   crust? filigree?

4. To what extent do aluminum particles or accumulates ignite in the field of view?

5. Is the ignition primarily before, during or after detachment

6. Are most of the particles leaving the surface

   original Al particles

   accumulates of Al particles (typically how many?)

   ignited agglomerates

7. Describe size and size distribution of burning droplets.

8. How vigorous is the Al combustion? "Vigorous" is

   many small bright droplets

   overall plume bright

   smoke density in plume builds up close to surface (don't count recirculating smoke, etc.)

9. Is flux of Al from the burning surface macroscopically continuous; spasmodic (in time or location); periodic; surface propagative (e.g., in accumulate layer)?

limited accumulation and sintering. Coarse AP with fine Al showed massive accumulation and sintering.

3. The environment of the AP flame is not effective in igniting the aluminum in the condition present on the burning surface. In the case of coarse Al particles, most left the surface without igniting (i.e., without visible flame envelopes). The sintered accumulate obtained with fine particles did not ignite readily, and when it did ignite, the conditions suggested that break-up of the accumulate played a causative role (i.e., onset of mobility and detachment seemed to precede ignition).

4. When ignition occurred in the sintered accumulate, it tended to spread through the accumulate. In the process, the accumulate layer coalesced into a number of large burning droplets (referred to here as "agglomerates"), in a progressive process involving also progressive detachment from the surface.

5. Aluminum that experienced detachment without ignition usually did not ignite later. In the case of sintered fine Al, sintered structures broke up some during detachment, and those fragments that were already ignited somewhere in the fragment became fully inflamed.

6. The behavior described above was affected only moderately by pressure over the pressure range tested (4.1 to 6.9 MPa, 600-1000 psi).

7. Fine ingredient particle size (10/5) led to sporadic inflamation and agglomeration at the surface; inflamation and combustion of the Al was then extremely vigorous.

In terms of mechanistic arguments relative to propellant combustion, the observations 1-7 (combined with results reported earlier on behavior of Al particles during heating) imply the following:*

---

* The numbered mechanistic arguments pertain to the correspondingly numbered observations of the preceding list.

1. Whatever the state of the aluminum particles and the AP surface when the AP particles emerge on the burning surface, there is some adhesive process that prevents immediate detachment of the particles. Under suitable conditions (e.g., AP size large compared to Al size), retention is long enough to result in emergence of more Al particles, concentration of particles and sintering. Retention may initially involve the liquid state of the AP surface, and conditions at the surface suggest that sintering is similar to that observed slightly above the aluminum melting point in heating tests on Al powders in oxidizing atmospheres.

2. Formation of aggregates of metal particles depends on both the mechanism and the opportunity. Work to date has focused on mechanisms by which aluminum particles stick to each other (sintering, coalescence), and the necessity and means for adhesion to the burning surface to permit particle concentration (opportunity for particle interaction). However the opportunity is governed also by how long a particle must "wait" on the surface before it is joined by other particles, and by the nature of its environment during the wait. Thus opportunity is dependent on microstructure of the sample, including particularly the grouping of aluminum in pockets and connective arrays between pockets. When the number of oxidizer and aluminum particles are equal, the opportunity for aluminum particle interaction is low, the wait for interaction long, and the retention environment poor, so that sintering is minimal. When the aluminum particle size is small, the particles group into packing voids among AP particles, and may even form connective arrays among the voids. This provides the opportunity for accumulation and sintering of groups of particles and interconnecting bridges between groups, giving the sintered layers observed in tests.

3. Mechanistically, the reluctance of aluminum to ignite in most of these

tests indicates that the oxide coating on the particles is resistive to breakdown in the chemical and thermal environment of the AP flame. This is analogous to results of hot plate experiments where agglomeration of aluminum powders occurred at or near to the aluminum melting point in an Argon atmosphere, but not in an oxygen enriched one. It appears that the oxide "skin" is reinforced before ignition, even in the AP flame, thus delaying ignition. This exceptional behavior of aluminum (and some other metals) is unique among fuels: oxidation temporarily inhibits combustion. In any case, the protective property of the oxide skin in conventional propellants contributes to the opportunity for sintering and agglomeration, by delaying ignition, even in the AP flame.

4. From observations 3 and 4 above, it is concluded that sintered accumulates consist of interconnected oxide shells containing molten aluminum that is exposed when the sintered structure is broken. This can lead to local inflamation of aluminum, with corresponding local temperature rise. Given the relatively low thermal conductivity of a sintered accumulate (compared to aluminum), the local temperature rise is sufficient to melt the surrounding oxide, permitting propagation of the ignition front through the accumulate. The aluminum is drawn by surface tension into one or more burning droplets.

5. The interpretation in 4 is further supported by the observation in 5 that ignition rarely occurs in single or sintered particles if they do not ignite during the mechanical stresses of detachment from the burning surface. However, this support must be tempered by recognition that the tests were made with small samples, that slow reaction probably continues without flame type combustion, and that other investigators have obtained intense combustion using very fine AP and Al particle size.

6. The insensitivity of behavior to pressure may be in part related to the limited pressure range tested (4.1 to 6.9 MPa). Lower pressures were not tested because the samples would not support combustion. This is a significant point because other investigators have gone to much lower pressures, but used very fine AP and Al. Their observations regarding the role of condensed phase reactions in determining burning rate are apparently not relevant to samples made from propellant-size ingredients. Such reactions are involved in sintering and in delay of aluminum ignition, and are not conspicuously pressure-dependent.

7. Behavior with very fine ingredients has been studied by others as well, and collected results suggest that substantial surface reaction of Al particles takes place at the propellant burning surface due to the high specific surface of the reactants. This may involve burning off small areas of the heated AP/Al surface layer rather than outright aluminum accumulation. In that case the arguments for non-accumulation due to Al particle isolation in the microstructure may be irrelevant to the tests with 10/5 mixtures.

B. Burning Surface Behavior in AP/Al Systems With Modified Aluminum

In view of the obvious important role of the oxide skin in controlling the onset of sintering, agglomeration and ignition of aluminum particles, it is reasonable to seek beneficial modification of the oxide. A method explored by Krauetle[9] was to enhance the oxide by further oxidation by holding powders at elevated temperature in oxidizing atmospheres. This method was called "pre-oxidation", and was conducted at temperatures below the aluminum melting point.

A method explored earlier in the present project was called "pre-stretching" the oxide by heating particles through the aluminum melting point. The oxide skin deforms to accomodate the increased volume of the aluminum, probably by both

inelastic stretching and cracking. In the presence of a low concentration of oxygen, the cracked areas will close rapidly by further oxidation. Upon cooling, the particles will shrink, the oxide skin will wrinkle or exhibit depressions, but the oxide surface area will remain sufficient to enclose the aluminum when the particle melts in the combustion zone. This argument was developed from growing understanding of preignition behavior of aluminum powder, and was evaluated earlier in the project using the hot stage microscope to produce and test the pre-stretched oxide particles. In those tests the tendency of aluminum powders to sinter and agglomerate when heated was sharply reduced by pre-stretching the oxide.

In the present report period, aluminum with pre-stretched oxide was produced in greater quantity by heating the powder in an open quartz tube to 700°C, using a tube furnace flushed with a nitrogen flow (with some entrained air). Evaluation was then made by preparation and combustion of dry-pressed samples of 85%, 100 μm AP and 15% Alcoa 123 Al. Similar tests were also run on samples with untreated Alcoa 123 Al, and samples with pre-oxidized Alcoa 123Al (provided by Karl Kraeutle of Naval Weapons Center). Tests were run at 6.9 MPa (1000 psi), and observations were made by combustion photography (Table III-3).

Tests on the samples with untreated aluminum were similar to earlier ones (Table III-1) with 100 μm AP and H-30 aluminum, exhibiting massive accumulation and sintering of aluminum on the burning surface, with ignition occurring only during break-up of detaching accumulate layers. Very large agglomerates formed. Results with the pre-oxidized and with the pre-stretched aluminum were alike. Only small accumulates were evident, with more or less continual detachment of fragments. Aluminum ignition was only occasional. This result supports the

Table III-3

Evaluation of Aluminum Pretreatment Table Identifies Combustion Photography Tests. All samples from dry-pressed mixtures of 85% 100 μm AP and 15% Alcoa 123 aluminum tested at 6.9 MPa.

Type of Aluminum Treatment	None	Pre-oxidized	Pre-stretched
Film #	63 64, 70	66, 69, 72	65, 67 71
Test Outcome	Fair Quality (smoke)	Fair Quality (smoke)	Fair Quality (smoke)

mechanistic argument that led to "pre-stretching" experiments, and suggests a means of controlling accumulate size, using a modification of aluminum powder that is economically viable in production, possibly by simply changing process control variables in the original powder manufacture.

C. Burning Surface Behavior: AP/Al/Wax Systems

In view of the reluctance of aluminum to ignite in the AP flame, it was concluded that the diffusion flamelets from the oxidizer-binder vapors played a role in aluminum ignition in propellant flames (a postulate advanced earlier in connection with tests on "sandwiches" with aluminized binders[9] and other tests with aluminized AP.[3] It has often been suggested that aluminum ignition would not be effectively accomplished unless the hydrocarbon fuel-AP (HC-AP) mixture

ratio was suitable for an equilibrium combustion temperature above the melting point of aluminum oxide, thereby assuring breakdown of all protective oxide. However, our observations of the local, propagative nature of the ignition of accumulate layers suggest that satisfactory ignition would occur if a reasonable distribution of local HC-AP diffusion flames occurred, even though that might correspond to a relatively small mass fraction of HC fuel.

Since the accumulation process (and hence agglomerate size) tends to be limited by local ignition events, it seems important to understand what local diffusion flamelet situations are sufficient for ignition. This was explored by adding a hydrocarbon (carnauba) wax to the AP/Al mixture for dry-pressed samples. Combustion photography tests were run that were similar to those for AP/Al samples. The complete series of tests is identified in Table III-4, and the test results were reviewed in the same manner as the AP/Al tests. Observations were as follows:

1. Addition of 2% HC wax reduced surface accumulation to a mininum, giving a steady flow of mostly nonburning Al from the surface.

2. 4% wax resulted in increased surface accumulation of Al (much less than for 0% wax, comparable to propellants), with sporadic detachment and considerable inflamation.

3. 8% wax resulted in formation of burning agglomerates on the surface, which immediately detached and burned vigorously in the outward flow.

4. In all cases, increased pressure led to smaller accumulates and more extensive ignition of aluminum on or near the surface.

Table III - 4

Summary of Tests on Dry-Pressed Ap / Al / Wax Mixtures*

Sample / Pressure		AP / H30 AL / Wax											
		2% Wax 85% AP, 13% Al			4% Wax 85% AP, 11% Al			8% Wax 78.2% AP, 13.8%Al			10% Wax 74% AP, 16% Al		
			Movie			Movie			Movie			Movie	
MPa	PSI	dp/dt Quench	Hi Mag	Lo Mag	dp/dt Quench	Hi Mag	Lo Mag	dp/dt Quench	Hi Mag	Lo Mag	dp/dt Quench	Hi Mag	Lo Mag
4.2	600			20		18	24		19		25		
5.5	800			21		6	A		7		B		
6.9	1000			22		8 11 15 2	23		12 16 17 3			34	

D. Theory of Accumulation-Agglomeration

The processes involved in the behavior of aluminum on the burning surface are clearly rather intricate, and may never be well described by a quantitative theory. However it is important to develop an approximate theory, in order to pursue intelligent design of experiments and to fully exploit results of past experiments in both future experiments and practical applications. Certain steps in the aluminum behavior have been defined in order to assure that relevant processes are considered, and the relation of these steps are identified in Figure III-1 and discussed below. Items 1 and 2 are initial conditions, while the others are processes.

1. First are the many questions about the nature of the individual propellant ingredients, such as the condition of the oxide coating on the aluminum particles.

2. Second is the microstructure of the propellant, which reflects such variables as particle size or specific surface, proximity of Al particles to each other, and nature of the material near the aluminum.

3. Third, as the burning surface approaches one or a group of aluminum particles, the temperature rises until the surrounding binder is softened and gasifying. In effect, the aluminum particle is wetted by melting binder, and scattered particles may be concentrated in the "melt" as binder is removed by vaporization. In a heterogeneous propellant, this behavior is statistically distributed.

4. Aluminum particles must each be reached by the regressing surface between condensed and gas phase. At that point they evidently are retained on the surface, by adhesion to the melt and/or underlying Al particles, leading to continued accumulation. Ignition may be delayed by a continuing fuel-rich environment, and by protectiveness of the oxide on the particles at temperatures

present at the burning surface.

5. Increasing interaction among the adjoining particles leads to sintering by either carbonaceous material or direct particle interaction (oxidation), or both in that order. Temperatures at this point may exceed the aluminum melting point. The microstructure of the propellant (especially spatial distribution of aluminum) plays a key role in determining the opportunity for particles to encounter each other in or on the burning surface, and in determining the extent and nature of sintering. Exposure to an increasingly oxidizing atmosphere can cause sintering without causing ignition.

6. It is helpful to consider the formation of sintered accumulates in two or three ways. In its simplest form, very small numbers of particles may contact each other before detachment from the surface. A more deterministic process is the accumulation, sintering and detachment of all particles in each packing void in the AP array (assemblages of small aluminum particles, created during preparation of the propellant). This description of accumulate size distribution is called the pocket model. A more complete model would have to consider formation of bridges between pocket accumulates, leading to filigrees, flakes or layers. Bridging is related to the nature and aluminum content of the passages between voids in the AP packing array.

7. Agglomeration and ignition are usually closely coupled events, both being governed by breakdown of oxide and exposure of aluminum. To describe the occurrence on a propellant surface, one must first describe the development of accumulates and exposure to diffusion flamelets, and then consider how an ignition site spreads through the accumulate to form one or more agglomerates, and consider what limits the extent of this surface-wise inflamation. In an ordinary propellant, a proper statement of this ignition-inflamation problem would normally

have to be made in statistical terms related to propellant microstructure. To get started, however, one considers the inflamation process through a uniform sintered structure, and then applies the results to a non-uniform one having the characteristics of a propellant surface.

8. The extent of the accumulation-sintering-agglomeration process is dependent always on opportunity, and is statistically variable in more ways than the surface-wise inflamation. Aluminum detaches from the burning surface, at which point the opportunity for further sintering or agglomeration is drastically reduced. Detachment results from the interplay of restraining and removing forces at the surface, which change progressively during accumulation and differ greatly from point to point on the surface, from one propellant to the next, and from one flow environment to the next. Description of these forces has been attempted for only the most simplistic situations (e.g., spheres in an evaporating viscous layer). At present it seems more important to identify the nature of an accumulate, the nature of its attachments to a real propellant surface, the way in which the ignition-agglomeration process changes the interplay of forces, and what conditions precipitate ignition (in most AP-HC binder propellants, detachment is precipitated by ignition, and growth of the agglomerate is terminated by completion of detachment).

A comprehensive theory of accumulation-agglomeration would have to encompass the concepts 1-8. The experimental work has been aimed at identifying the most important steps and clarifying them. Analytical-computational studies of flame spreading from ignition sites have also been made in the present program. These studies were aimed at describing periodic accumulation-ignition-inflamation observed in some AP/Al combustion tests. A second study has examined the void structure resulting from packing particles (i.e., the microstructure of the volume

filled by binder and aluminum in an AP propellant). The goal of this latter study is to determine appropriate statistical variables to characterize the distribution of fine aluminum particles in the propellant microstructure. These two studies are in early phases.

E. Quench Studies of the Combustion Plume

In a rocket motor, the majority of the aluminum in the propellant burns as droplets while moving out with the flow from the propellant surface. Because of the agglomeration process, these droplets are large enough to require appreciable time to burn. In extreme cases, droplets may not be completely burned at the nozzle entrance, in which case loss of efficiency occurs. In all cases, there exists a significant volume containing burning droplets, a volume that also participates in erosive burning processes and in oscillatory combustion-damping phenomena. The effects of this participation have not been addressed for a variety of reasons, the most basic being ignorance of the characteristics of the droplet cloud. This subject was addressed in another project[10] in which some success was achieved in quench-collection of aluminum droplets at various distances from the burning surface (atmospheric pressure).

The scenario for agglomerate combustion has been described before,[10,11] and the object of the tests was to obtain more decisive evidence, and explore the limitations of the scenario. It is widely (but not uniformly) believed that aluminum agglomerates burn like aluminum droplets, with oxidation in a detached flame and on the droplet surface. Products are predominantly Al_2O_3 smoke from the detached flame, with perhaps 20% of the Al_2O_3 forming on the droplet surface and yielding one or more relatively large "residual" oxide droplets after aluminum burnout. In this scenario, a sample quenched from the plume should contain smoke oxide (<2 μm diameter), residual oxide (typically 10-60 μm diameter), and aluminum

particles that are partly burned and have oxide lobes that are the source of "residual" oxide particles upon droplet burnout. The size of the partially burned aluminum droplets depends on the degree of agglomeration on the burning surface (i.e., original agglomerate size) and the distance out to the quench site.

The above scenario for agglomerate combustion is based on contributions from many sources, very few of which were known to be directly applicable to propellant combustion (which is very difficult to observe unambiguously). Outstanding practical questions to be addressed in the present and future work are:

1. Nature of the original agglomerate, and relevance of single particle combustion studies on pure aluminum (this includes the question of how much oxide is already present on the agglomerate by the time it is fully inflamed ("pre-ignition oxide")).

2. Amount of additional oxide accumulation on the agglomerate during burning.

3. Effect of surface oxide on the burning history and burning time.

4. Extent of subdivision of surface oxide, either by ejection during burning or division during droplet burnout.

5. Effect of a convective flow around the burning agglomerate.

6. Responsiveness of droplet burning to oscillatory flow.

7. Dependence of 1-6 on pressure.

8. Dependence of 1-7 on chemistry and temperature of the atmosphere, and radiation field in the rocket motor environment.

In the present studies, the quench-collection procedure in Ref. 10 was used to sample the combustion plume of a variety of model propellant formulations (dry-pressed), and the collected samples were studied to clarify the details of the combustion plume. Tests were run at atmospheric pressure, and construction was

started on a test chamber for testing at elevated pressure. Table III-5 shows a summary of the tests conducted. Variables were:

Aluminum Particle Size

Alcoa 123 ~ 25 μm

H-95 ~ 95 μm

Ammonium Perchlorate Particle Size

Fine ~ 5μm

Coarse ~ 100 μm

% Al

2, 4, 8, 12, 15

AP/Wax ratio (HC fuel content)

88/10, 88/3

Quenching Distance (cm)

5.3, 10.6, 15.9, 31.8

"Q" entries in the table indicate conditions for which quench tests were run, "M" designates motion pictures.

The results of the combustion experiments can be summarized as follows:

1. Quench samples showed the smoke oxide, residual oxide and agglomerates described in the classical scenarios above, in all tests where agglomeration was possible. Coarse aluminum yielded also "large" particles of irregular shape that were judged to be original particles that did not spheroidize but burned slowly to yield substantial surface oxide. In tests showing only these irregular aluminum particles, no other oxide was evident.

2. Agglomerate particles obtained in this experiment appeared black with dull, slightly grainy surfaces. They decreased in size with quenching distance, and

TABLE III - 5
Summary of Atmospheric Pressure Droplet Quench Tests on AP/Al/Wax Samples
Standard conditions: fine AP, fine AL, AP/Al/Wax = 88/10/2
Collection distance = 7.62 cm, p = 1 atm

Table III-5a
Effect of AP Particle Size

	Alcoa 123					75 - 125 μm				
AP \ %Al	2%	4%	8%	12%	15%	2%	4%	8%	12%	15%
Fine				Q M			Q	Q	Q M	Q
Coarse			Q	Q 4D			Q	Q	Q	Q

Table III-5b
Effect of Al Particle Size

Al Size \ %Al	2%	4%	8%	12%	15%	2%	4%	8%	12%	15%
Alcoa 123				Q M				Q	Q 4D	Q
75 - 125 μm		Q	Q	Q M	Q		Q	Q	Q	Q

Table III-5c
Effect of Al Concentration

AP Size	Fine		Coarse	
% Al \ Al Size	Fine Alcoa 123	Coarse 75 - 125 μm	Fine Alcoa 123	Coarse 75 - 125 μm
2				
4		Q		Q
8		Q	Q	Q
12	Q M	Q M	Q 4D W2D	Q
15		Q	Q	Q

Table III-5d
Effect of Quenching Distances

Quenching Distances			3.8	5.1	7.6	15.2
Ap/Wax Ratio	AP Size	Al Size				
88/10	Fine (5 μm)	Fine Alcoa 123			Q	
		Coarse H-95			Q	
	Coarse (100 μm)	Fine Alcoa 123	Q	Q	Q	Q
		Coarse H-95			Q	
88/3	Fine (5 μm)	Fine Alcoa 123				
		Coarse H-95				
	Coarse (100 μm)	Fine Alcoa 123	Q	Q		
		Coarse H-95				

usually develop oxide lobes at increasing quench distance. The agglomerates were spherical except for the lobes and some other anomalies attributed to the quench process and subsequent HCl acid attack. In samples with low aluminum concentration (2 and 4%) agglomerates are very small. In all tests, agglomerates were largely consumed at 7.6 cm. Similar spherical particles occurred in some tests involving coarse aluminum, with similar evolution of form with distance. These "agglomerates" are evidently the classical burning droplets with oxide lobes. Their detailed structure was not determined, but they dissolved in 10% HCl in water leaving the oxide lobes.

3. Residual oxide spheres (translucent, 10-60 μm diameter) were produced only in combustion plumes having the type of spherical particles described in 2 above, presumed to be fully burning droplets. About one in five residual oxide spheres is shiny black in character; these are believed to have inclusions, possibly of aluminum. The oxide spheres did not dissolve in acid. The number and size of the spheres increases with distance from the burning surface, and follows the same trend as "agglomerate" size with increase in % Al in the sample.

4. Oxide smoke was conspicuously present in those tests that had "agglomerate" spheres, was minimal or absent in tests yielding exclusively non-spheroidized aluminum. No attempt was made to study the smoke oxide because it was only partially recovered in the tests, and tended to obscure the rest of the particles. The smoke was mostly removed with the HCl in the washing operation. The presence of smoke exclusively with tests having "agglomerate" spheres is evidence that the non-spherical aluminum particles have burned without detached flame envelope.

5. In general, the observations conform with the results of the high pressure combustion photography tests relative to agglomeration of aluminum on the burning

surface. Coarse aluminum particles leave the burning surface individually, fine particles agglomerate if present in higher concentrations. Fine AP, with fine Al in lower concentrations gives very vigorous Al combustion.

6. Photographic observations revealed no fragmentation events, but technical difficulties have continued to prevent observation of the burnout phase of agglomerates unambiguously.

In general, the quench tests supported the scenario for agglomerate combustion, except in the case of coarse Al particles, which usually did not get hot enough to melt the oxide and give vigorous burning at this pressure.

References

1. Price, E. W. and R. K. Sigman, "Behavior of Aluminum in Solid Propellant Combustion," AFOSR-TR 7750, November, 1976.
2. Price, E. W., R. K. Sigman and J. K. Sambamurthi, "Behavior of Aluminum in Solid Propellant Combustion," AFOSR-TR-78-0468, November, 1977.
3. Price, E. W., R. K. Sigman, J. K. Sambamurthi and T. S. Sheshadri, "Behavior of Aluminum in Solid Propellant Combustion," Task III of AFOSR Interim Scientific Report: Rocket Research at Georgia Tech, November, 1978.
4. Price, E. W. and R. K. Sigman, "Behavior of Aluminum in Solid Propellant Combustion," 14th JANNAF Combustion Meeting, CPIA Publication 292, Vol. I, December, 1977, p. 195.
5. Cohen-Nir, E., "Combustion of Powdered Metals in Contact of Powdered Metals in Contact with a Solid Oxidizer," 13th Symposium (International) on Combustion, The Combustion Institute, Pittsburgh, PA, 1971, pp. 1019-1029.
6. Pai Verneker, V. R., D. Seetharamacharyulu, and R. M. Mallya, "Combustion of Ammonium Perchlorate-Aluminum Mixtures," Journal of Spacecraft and Rockets, Vol. 16, No. 6, November-December 1979, pp. 436-438.
7. Price, E. W., D. W. Rice and J. E. Crump, "Low Frequency Combustion Instability of Solid Rocket Propellants," NOTS TP 3524, July, 1964.
8. Kraeutle, K. J., "The Behavior of Aluminum During Subignition Heating and Its Dependence on Environmental Conditions and Particle Properties," 9th JANNAF Combustion Meeting, CPIA Publication 231, Vol. I, December, 1972, p. 325.
9. Boggs, T. L., D. E. Zurn, W. C. Strahle, J. C. Handley and T. T. Milkie, "Mechanisms of Combustion," Naval Weapons Center TP 5514, July, 1973.

10. Price, E. W., W. L. Meyer, W. C. Strahle, S. S. Samant, E. A. Powell, R. K. Sigman and J. C. Handley, "The Fire Environment of a Solid Rocket Propellant Burning in Air," AFWL-TR-78-34, March 1979.

11. Price, E. W., "Combustion of Aluminum in Solid Propellant Flames," AGARD Conference Proceedings No. 259, Solid Rocket Motor Technology, July, 1979, p. 14-1.

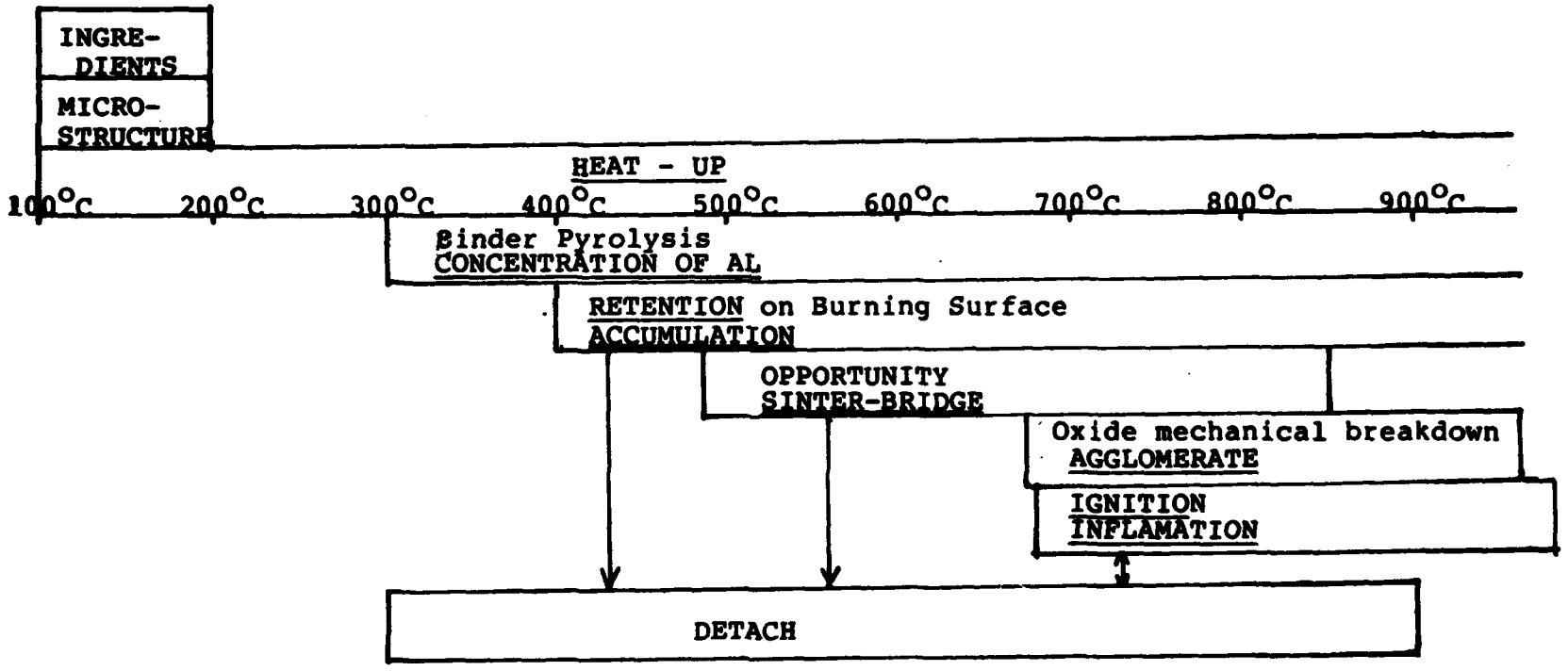

Figure III-1. Progression of aluminum behavior on the propellant surface.

TASK IV

ROCKET MOTOR AEROACOUSTICS

WARREN C. STRAHLE

DOUGLAS H. NEALE

Abstract

Facility modification was completed and extensive testing was performed on an apparatus to investigate turbulence induced pressure fluctuations in a rocket-like cavity. To overcome prior deficiencies in theory, a new theory was constructed for the generation of pressure disturbances by the turbulence. Undeniable separation has been achieved between propagational and local pressure fluctuations, and the agreement between theory and experiment are adequate. Measurements include microphone and hot film anemometry, and time series analysis is applied to the results.

I. Introduction

The background pressure fluctuation level in a rocket motor (liquid or solid) is generally of the order of 1-2%, even under nominally stable operating conditions. These fluctuations are random noise, modified by the chamber acoustics to favor frequencies near acoustic resonant mode frequencies. This background noise level is the source of several real or potential problem areas. It is a) a source of motor vibration, b) a possible disturbance for determining the location of transition from laminar to turbulent flow in the chamber, and c) a possible disturbance to trigger nonlinear instability.

Motor vibration interacts in a detrimental way with guidance accuracy and missile weight. Somewhat recent problems with Poseidon Stage II attest to this fact.[1] More recently, troubles have occurred with the space shuttle solid rocket booster,[2] However, a cause of the motor vibration, internal-pressure fluctuations, has not been investigated, nor is

the background fluctuation level usually measured. The reason for a lack of information is that pressure instrumentation is usually set up with a sufficiently low gain to capture large amplitude instabilities - not noise. The relatively intense acoustic background noise is the source of the disturbances which may be amplified if the motor is unstable. Moreover, it is possible that even if the motor is not unstable in a linear sense it may be driven unstable by the background noise. For these reasons it is desirable to characterize this noise and its cause.

Prior work on this and another contract have pointed to the natural turbulence in the rocket cavity gases as the culprit in generation of unwanted pressure fluctuations. The purpose of this program is to quantify the relation between the turbulence and the generated pressure field.

II. Program Progress

The details of the past year's progress are located in Ref. (3), attached as App. IV-A of this report. The tasks completed during the past year are as follows:

a) Modification of the facility to improve signal to noise ratio and characterization of the signal into propagational sound and local noise

b) Extensive testing using microphone and hot film anemometry measurements. Time series analysis has been applied to the results

c) Generation of a new theory of the aeroacoustics of the device which explains the experimental results.

At the close of the contract year modifications were being made to the apparatus to allow side wall blowing, to simulate combustion gas inflow from the sides.

References

1. Pendelton, L. R., "Sinusoidal Vibration of Poseidon Solid Propellant Motors," Shock and Vibration Bulletin, 3, Naval Research Laboratory, Washington, D.C., 1972.

2. Mathes, H. B., "Assessment of Chamber Pressure Oscillations in the Shuttle SRB," 16th JANNAF Combustion Meeting, Monterey, CA, September, 1979.

3. Strahle, W. C. and Neale, D. H., "Turbulence Generated Pressure Fluctuations in a Rocket-Like Cavity, AIAA Paper No. 80-0208, 1980.

APPENDIX I-A

This appendix contains reproductions of the following papers:

Paper No. 1 "Adaptation of the Impedance Tube Technique for the Measurement of Combustion Process Admittances", M. Salikuddin and B. T. Zinn.

Paper No. 2 "Experimental Determination of Solid Propellant Admittances by the Impedance Tube Method", J. D. Baum, B. R. Daniel and B. T. Zinn.

Paper No. 3 "Determination of Solid Propellant Admittances by the Impedance Tube Method", J. D. Baum, B. R. Daniel and B. T. Zinn.

Journal of Sound and Vibration (1979) 67(4), 000–000

ADAPTATION OF THE IMPEDANCE TUBE TECHNIQUE FOR THE MEASUREMENT OF COMBUSTION PROCESS ADMITTANCES†

M. SALIKUDDIN‡ AND B. T. ZINN

School of Aerospace Engineering, Georgia Institute of Technology, Atlanta, Georgia 30332, U.S.A.

(*Received 23 April 1979, and in revised form 7 August 1979*)

This paper describes the development and application of the impedance tube technique in the measurement of localized combustion process admittances. The latter are needed for combustor stability analyses. The experimental setup consists of a tube with the combustion process to be investigated at one end and an acoustic driver at the other end. The latter is used to excite a standing wave in the tube whose structure depends upon its interaction with the combustion process. The needed combustion process admittance is determined from acoustic pressure measurements taken at several locations along the tube. The paper discusses the theoretical foundation of the experiment and the developed data reduction procedure which accounts for the presence of steady state temperature gradient, mean flow gradient and gas-phase losses in the tube. Results showing the applicability of the developed experimental technique are provided.

1. INTRODUCTION

This paper describes the adaptation of the impedance tube technique in the measurement of the admittances of localized combustion processes. The discussed measurement technique has been developed as part of an AFOSR research grant that was concerned with the measurement of the admittances at the surfaces of burning solid propellant samples. The latter are needed either as inputs in solid rocket stability analyses or as means for evaluating the relative driving capabilities of different solid propellants [1]. While the research described herein is specifically concerned with solid propellant admittances, the developed measurement technique is quite general and it is applicable to other situations involving high temperature admittance measurements. As a matter of fact, the developed measurement technique has recently been used successfully in the measurement of the admittances of gaseous rocket injectors [2]. Other examples of such applications include the determination of the impedances of fibrous materials that are used in exhaust silencers [3, 4].

Because of the complexity of the combustion process, no satisfactory theoretical analysis currently exists for the accurate determination of the admittances of combustion zones and various experimental techniques are being employed to determine the unknown

† Research supported under AFOSR Grant No. 73-2571. AIAA Paper 79-0167, presented at the 17th Aerospace Sciences Meeting, New Orleans, U.S.A., January 1979.

‡ Current address: Lockheed-Georgia Company, Department 72-74, Zone 403, Marietta, Georgia 30063, U.S.A.

0022-460X/79/000000+10$02.00/0

admittances. The development of such an experimental technique that is based upon a modified [illegible] of the impedance tube method [5] is the object of [illegible]

In the classical impedance tube technique the experimental arrangement consists of a tube with an acoustic driver at one end and the sample whose admittance is to be measured at the other end. During an experiment, the driver generates an incident wave of a desired frequency that propagates along the tube until it impinges upon the sample under test. The interaction between the incident wave and the test sample results in a reflected wave with modified amplitude and phase. The reflected wave then combines with the incident wave to form a standing wave pattern in the tube whose structure depends, among other parameters, upon the admittance of the tested sample. The structure of the standing wave is measured by traversing a microphone probe along the tube. The unknown admittance is then computed by using the solution for the standing wave which relates the wave structure to the sample admittance. The classical impedance experiment is restricted to situations involving a constant temperature gas in the tube and no mean flow and this set-up needs to be drastically modified in order to be used in the measurement of the admittances of localized combustion processes which introduces a high temperature steady flow into the impedance tube. In the modified experimental set-up (see Figure 1) which was developed in the course of this investigation, the test sample is replaced by the combustion process under investigation (e.g., the surface of a burning solid-propellant) and a nozzle is provided at the other end for exhausting the combustion products. The acoustic driver, located just upstream of the nozzle, is used to generate an incident wave, P_I of a given frequency f, that propagates along the tube. The interaction of the incident wave with the combustion process results in a reflected wave, P_R, with a modified amplitude and phase. The presence of an axial temperature gradient and an axial mean flow gradient in the tube result in continuous reflection of the incident and reflected waves as they propagate along the tube and the two systems of incident and reflected waves interact to form in the tube a standing wave pattern whose structure depends upon the admittance of the combustion process, the mean flow properties, the frequency and the gas phase losses.

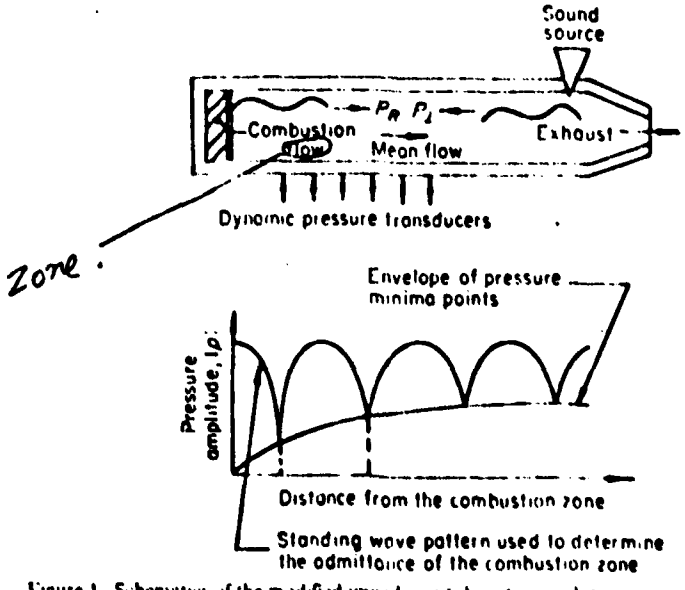

Figure 1 Schematics of the modified impedance tube set-up and its associated wave structure

Due to the high temperatures of the [illegible] hardware limitations, it is [illegible] tube to measure the standing wave structure. Instead, the structure of the impedance tube standing wave is measured by using several pressure transducers that are located at several pre-selected locations along the walls of the impedance tube. The measured acoustic pressure data are then used to determine the wave structure in the impedance tube and the admittance of the localized combustion process. In what follows the theoretical foundation for the high temperature impedance tube will be described in detail.

2. CONSERVATION EQUATIONS

In this section the analytical procedure and numerical methods that have been developed to determine the unknown admittances of surfaces exposed to high temperature conditions and combustion processes, such as the surface of a burning solid propellant sample, are discussed. Specifically, the analytical procedure and numerical methods developed to utilize acoustic pressure measurements at a discrete number of locations in the determination of the structure of the standing wave and the unknown admittance at one end of the impedance tube, with account being taken of the presence of an axial steady temperature gradient and an axial mean flow gradient along the tube, and gas-phase losses, are discussed.

To deduce the required standing wave structure from the measurements, one needs to obtain solutions of the conservation equations that describe the behavior of small amplitude disturbances in a long and narrow tube containing a high temperature mean flow resulting in a temperature gradient along the tube. The solutions needed are obtained in what follows here on the basis of certain assumptions: (1) the combustion process is concentrated at the surface of the test sample in the tube; (2) the gas in the tube is perfect and consists of a single species; (3) the fluctuating part of the heat transfer to the wall is negligible; (4) both the steady and unsteady flows are one dimensional; (5) the amplitudes of the waves are sufficiently small so that all non-linear terms involving products of these quantities may be neglected; (6) the acoustic gas phase losses in the flow field (e.g., due to presence of particles) can be accounted for in the conservation equations by introducing an overall bulk loss coefficient or gas phase loss coefficient which is proportional to the local oscillatory velocity. Under these assumptions, the flow in the impedance tube can be described by the following system of conservation equations [1]:

continuity: $$\partial\rho/\partial t + \partial(\rho u)/\partial x = 0, \tag{1}$$

momentum: $$\partial(\rho u)/\partial t + \partial(\rho u^2)/\partial x = -\partial p/\partial x - F, \tag{2}$$

energy: $$\rho T(\partial s/\partial t + u\,\partial s/\partial x) = C_v Q/R, \tag{3}$$

state: $$p = \rho RT, \tag{4}$$

where ρ is the density, u the axial velocity, p the pressure, T the absolute temperature, s the entropy, t the time, x the axial co-ordinate, F the retarding force per unit volume due to gas phase losses, Q the heat gain or loss per unit volume, R the specific gas constant and C_v the specific heat at constant volume.

To obtain the needed solutions, each of the dependent variables is assumed to consist of a sum of a steady state quantity (to be denoted by a superposed bar) and a time dependent small amplitude perturbation (to be denoted by a prime). These expressions are then substituted into the above conservation equations which are then separated into

corresponding [illegible] and unsteady conservation. The resulting steady state conservation equations can be expressed in the following forms, in which the mean retarding force $\bar{F}$ has been neglected:

$$\frac{d\bar{p}}{dx} = \frac{\bar{m}^2 R\bar{\rho}}{\bar{m}^2 R\bar{T} - \bar{p}^2}\frac{d\bar{T}}{dx}, \qquad \frac{d\bar{\rho}}{dx} = \frac{1}{R\bar{T}}\left(\frac{d\bar{p}}{dx} - \frac{\bar{p}}{\bar{T}}\frac{d\bar{T}}{dx}\right). \tag{5, 6}$$

$$\frac{d\bar{u}}{dx} = -\frac{\bar{m}}{\bar{\rho}^2}\frac{d\bar{\rho}}{dx} = -\frac{mR\bar{T}}{\bar{p}}\left(\frac{d\bar{p}}{dx} - \frac{\bar{p}}{\bar{T}}\frac{d\bar{T}}{dx}\right). \tag{7}$$

Here $\bar{m}$ is the steady state mass flow rate of combustion products per unit area that in the case of a burning solid propellant would equal $\bar{\rho}_s\bar{r}$, where $\bar{\rho}_s$ is the propellant density and $\bar{r}$ the steady state propellant burning rate.

Linearizing the corresponding unsteady conservation equations, assuming that the solutions are periodic in time, and solving for the space derivatives of the perturbations, one obtains the following system of wave equations [1]:

$$\frac{dZ_i}{dx} = \sum_{j=1}^{3} A_{ij} Z_j, \qquad i = 1, 2, 3, \tag{8}$$

where Z_1, Z_2 and Z_3, respectively, represent u', p' and ρ' and the coefficients A_{ij} are

$$A_{11} = \{\bar{u}\bar{\rho}\, d\bar{u}/dx - i\omega\bar{u}\bar{\rho} + G\bar{u}\}/\{\bar{\rho}(\bar{c}^2 - \bar{u}^2)\}, \tag{9}$$

$$A_{12} = \{(\bar{u}\bar{c}^2/\bar{p})\, d\bar{\rho}/dx - i\omega\}/\{\bar{\rho}(\bar{c}^2 - \bar{u}^2)\}, \tag{10}$$

$$A_{13} = -(1/\bar{\rho})\, d\bar{u}/dx - \{(\bar{c}^2\bar{u}/\bar{\rho})\, d\bar{\rho}/dx\}/\{\bar{\rho}(\bar{c}^2 - \bar{u}^2)\}, \tag{11}$$

$$A_{21} = -\{i\omega\bar{\rho} + \bar{\rho}\, d\bar{u}/dx + G + (u^2\bar{\rho}\, d\bar{u}/dx - \bar{u}\, d\bar{p}/dx + i\omega\bar{u}^2\bar{\rho})\}/(\bar{c}^2 - \bar{u}^2), \tag{12}$$

$$A_{22} = -\bar{u}\{(\bar{c}^2\bar{u}/\bar{\rho})\, d\bar{\rho}/dx - i\omega\}/(\bar{c}^2 - \bar{u}^2), \tag{13}$$

$$A_{23} = \bar{u}\{(\bar{c}^2\bar{u}/\bar{\rho})\, d\bar{\rho}/dx\}/(\bar{c}^2 - \bar{u}^2), \tag{14}$$

$$A_{31} = -(1/\bar{u})\{d\bar{p}/dx + [u\rho\, d\bar{u}/dx - d\bar{p}/dx + i\omega\bar{u}\bar{\rho} + G\bar{u}]/(\bar{c}^2 - \bar{u}^2)\}, \tag{15}$$

$$A_{32} = -(1/\bar{u})\{(u\bar{c}^2/\bar{p})\, d\bar{\rho}/dx - i\omega\}/(\bar{c}^2 - \bar{u}^2), \tag{16}$$

$$A_{33} = (1/\bar{u})[-i\omega + \{(\bar{c}^2\bar{u}/\bar{\rho})\, d\bar{\rho}/dx\}/(\bar{c}^2 - \bar{u}^2)], \tag{17}$$

where $\bar{c} = (\gamma\bar{p}/\bar{\rho})^{1/2}$, $G = F'/u'$ (e.g., gas phase loss coefficient), and γ is the specific heats ratio. The above system of equations represented by equations (8) can be considerably simplified when the magnitude of the mean flow $\bar{u}$ is very small. For this case the oscillatory flow equations become

$$du'/dx = i\omega p'/\bar{\rho}\bar{c}^2, \tag{18}$$

$$dp'/dx = -(i\omega\bar{\rho} + G)u', \tag{19}$$

$$\rho' = (p'/\bar{c}^2) + (iu'/\omega)\, d\bar{\rho}/dx. \tag{20}$$

Examination of equations (18) through (20) shows that in this case the oscillatory density is decoupled from the system of differential equations. Therefore, equations (18) and (19) can be solved to determine the oscillatory velocity and pressure, and these solutions together with equation (20) can be used to determine the unknown density perturbation.

Since the solutions of the systems of wave equations for the cases $\bar{u} = 0$ and $\bar{u} = \bar{u}(x) \neq 0$ are similar, the method of solution for these two cases can be illustrated by discussing the general case, when $\bar{u} \neq 0$, described by equations (8). To solve equations (8), the coefficients A_{ij} must be evaluated. Inspection of equations (9) through (17) reveals that

these coefficients is a knowledge of the steady state solutions of equations (5) through (7) and the value of the gas phase loss coefficient G. Inspection of equations (5) through (7) also shows that the needed steady state solutions can be determined from these equations once the temperature distribution $\bar{T}(x)$ and the value of $\bar{p}(x)$ at some x_0 location (i.e., the "initial" point for the integration) are known.

Temperature measurements along the impedance tube could, in principle, be used to provide the needed axial steady temperature distribution. However, measured temperature data [1] indicate the presence of a radial temperature gradient along the length of the tube. Therefore, the question comes up regarding the "best" radial location to be used for the measurement of a bulk axial temperature distribution that is consistent with the one dimensional wave propagation model used in the present analysis. Since it is difficult to locate such a radial position in the impedance tube, a *different approach* for the determination of the average or bulk axial temperature distribution has been developed. By using energy conservation considerations, it is shown in references [1] and [6] that the axial steady state temperature distribution in the impedance tube is given by the following expression:

$$\bar{T}(x) = T_w(x) + (T_c - T_w(0))\, e^{-x\Lambda}, \tag{21}$$

where

$$\Lambda = C\{1 + T_w(x)/\bar{T}(x)\}^n, \qquad n = 0{\cdot}68, \tag{22}$$

and the unknown constant C needs to be determined from experimental data. In the study described here this constant has been determined from measured oscillatory pressure data by applying a non-linear regression technique, as will be discussed below. The value of C thus determined is the one that results in the "best" fit between the measured and computed impedance tube wave structures. To complete the set of needed input data, the mean pressure $\bar{p}(x)$ can be measured at some initial location $x = x_0$ in the impedance tube and the steady state mass flow rate $\bar{m}$ either determined from known data or determined experimentally. For example, in solid propellant studies the steady state mass flow rate $\bar{m}$ is obtained from the relation $\bar{m} = \rho_s \bar{r}$, where $\bar{r}$ is determined from measured propellant sample thickness and its burning time, and the density ρ_s is determined by weighing a known volume of the propellant sample. The remaining input quantities, such as the flame temperature T_c, the gas constant R and the specific heat ratio γ, are obtained from data in the literature. Finally, the wall temperature distribution $T_w(x)$ can be obtained from measured wall temperature data. With these data available, equations (5) through (7) can be solved to determine the axial distribution of all the steady state variables.

Equations (8) are a system of three linear, homogeneous coupled first-order ordinary differential equations, and they could be treated as an initial value problem once the dependent variables u', p' and ρ' were known at any x location in the impedance tube. With these values used as initial conditions, equations (8) can be integrated from the initial location toward the combustion zone, to determine the values of the dependent variables u', p' and ρ' at that location. Once determined, these quantities can be used to determine the unknown admittance and the entropy perturbation of the combustion process.

3. DETERMINATION OF THE INITIAL CONDITIONS

Unfortunately, accurate measurements of Z_1 and Z_3 (i.e., u' and ρ') are extremely difficult if not impossible at this time. Hence, one must resort to the use of a different analytical technique for the solution of equations (8). Due to the linearity of equations (8),

-10

the needed initial value data on Z_1 and Z_3 can be replaced by measurements of Z_2 (i.e., p') at two additional axial locations. The mathematical technique that makes the use of measured Z data in the solution of the system of equations is based on the "transmission matrix" concept [7].

Equations (8) can be written in the following matrix form:

$$\{Z'\}_x = [A]_x\{Z\}_x. \tag{23}$$

where the subscript x represents the location at which the elements of the matrix are evaluated. In terms of the backward transmission matrix $[T]$, $\{Z\}$ can be written as

$$\{Z\}_x = [T]_x\{Z\}_{x_0}. \tag{24}$$

Equation (24) indicates that once the transmission matrix $[T]_x$ and $\{Z\}_{x_0}$ are known, $\{Z\}_x$ can be evaluated. To determine $[T]_x$ and $\{Z\}_{x_0}$, one can use equation (24) to obtain the following expression for $\{Z\}_{x_0}$:

$$\{Z\}_{x_0} = [T]_x^{-1}\{Z\}_x. \tag{25}$$

Now, differentiating equation (24) with respect to x and using equation (25) yields the following expression for $\{Z'\}_x$:

$$\{Z'\}_x = [T']_x[T]_x^{-1}\{Z\}_x. \tag{26}$$

Comparing equations (23) and (26), one gets

$$[A]_x\{Z\}_x = [T']_x[T]_x^{-1}\{Z\}_x. \tag{27}$$

Since $\{Z\}_x$ is an arbitrary matrix, it can be eliminated from both sides of equation (27) to give

$$[T']_x = [A]_x[T]_x. \tag{28}$$

The matrix $[T]_x$ can be determined from the integration of equation (28), once $[T]_{x_0}$ is known. By letting x go to x_0 in equation (24) one obtains $[T]_{x_0} = I$, the identity matrix. From equation (24) it follows that

$$Z_{x_1} = [T]_{x_1}\{Z\}_{x_0}, \qquad Z_{x_2} = [T]_{x_2}\{Z\}_{x_0}. \tag{29, 30}$$

Using equations (29) and (30) to obtain expressions for the elements $(Z_2)_{x_1}$ and $(Z_2)_{x_2}$ leads to the derivation of two algebraic equations involving $(Z_1)_{x_0}$ and $(Z_3)_{x_0}$. These algebraic equations can then be solved for $(Z_1)_{x_0}$ and $(Z_3)_{x_0}$, since Z_2 is known at x_0, x_1 and x_2 from experimental data. Thus, by making use of $\{Z\}_{x_0}$ and $[T]_x$, $\{Z\}_x$ can be evaluated from equation (24).

4. NON-LINEAR REGRESSION TECHNIQUE

According to the above discussion any three accurate pressure measurements together with a known axial temperature profile and a bulk loss coefficient can be used to determine the unknown admittance of the combustion process. There are no limitations on the magnitudes of steady or unsteady variables in the evaluation of exact initial conditions at the combustion surface. However, errors in experimental measurements result in errors in the computed admittance values. These errors can be minimized by increasing the number of acoustic pressure measurements and utilizing a non-linear regression technique in the data reduction [8].

Let E_i be a quantity measured at x_i, $i = 1, 2, \ldots, n$ and T_i the corresponding theoretically calculated quantity evaluated at the same location x_i. In the present problem, the experimentally measured quantity is the acoustic pressure Z_2 which is measured at various x_i locations. Non-linear regression consists of finding values of u', p' and ρ' at $x = x_0$, (i.e., values of Z_{01}, Z_{02} and Z_{03}) which give the best fit between the theoretically predicted acoustic pressure distributions, obtained from the solution of the differential equations (23), and the experimentally measured acoustic pressures. This is accomplished by computing the values of u', p' and ρ' at $x = x_0$ which minimize the root-mean-square deviation between the theoretically predicted acoustic pressure distribution and the experimental data. The calculated optimum values of u', p' and ρ' at $x = x_0$ can then be used to obtain optimum values of the combustion process admittance and response factor. To find the minimum root-mean-square deviation, the following function F is minimized:

$$F = \sum_{i=1}^{n} (E_i - T_i)^2. \tag{31}$$

If a minimum of F exists, then the gradient of F vanishes at the minimum: that is, $\partial F/\partial Z_{0_1} = \partial F/\partial Z_{0_2} = \partial F/\partial Z_{0_3} = 0$, or

$$\frac{\partial F}{\partial Z_{0_k}} = -2 \sum_{i=1}^{n} \left[(E_i - T_i) \frac{\partial T_i}{\partial Z_{0_k}} \right] = 0, \qquad \text{for} \quad k = 1, 2, 3. \tag{32}$$

Equation (32) represents a set of three non-linear equations for the unknowns Z_{0_1}, Z_{0_2} and Z_{0_3} as T_i and $\partial T_i/\partial Z_{0_k}$ are both functions of Z_{0_k}. A Newton Raphson iterative scheme is used to obtain a solution of equation (32), by utilizing a linearized version of this equation which involves the expansion of T_i in a first-order Taylor series with respect to the parameters Z_{0_1}, Z_{0_2} and Z_{0_3}. The resulting system of linear algebraic equations can be expressed in the following form:

$$\sum_{i=1}^{n} (E_i - T_i^m) \frac{\partial T}{\partial Z_{0_k}}\bigg|_{(i,m)} = \sum_{j=1}^{3} \left[(Z_{0_j}^{m+1} - Z_{0_j}^m) \sum_{i=1}^{n} \frac{\partial T}{\partial Z_{0_j}}\bigg|_{(i,m)} \frac{\partial T}{\partial Z_{0_k}}\bigg|_{(i,m)} \right], \qquad k = 1, 2, 3, \tag{33}$$

where m represents the mth iteration.

For compactness, equation (33) can now be rewritten in matrix form, by making the definitions

$$b_k^m = \sum_{i=1}^{n} (E_i - T_i^m) \frac{\partial T}{\partial Z_{0_k}}\bigg|_{(i,m)}, \qquad a_{kj}^m = a_{jk}^m = \sum_{i=1}^{n} \frac{\partial T}{\partial Z_{0_j}}\bigg|_{(i,m)} \frac{\partial T}{\partial Z_{0_k}}\bigg|_{(i,m)},$$

$$B^m \equiv \begin{Bmatrix} b_1^m \\ b_2^m \\ b_3^m \end{Bmatrix}, \qquad A^m = \begin{bmatrix} a_{11}^m & a_{12}^m & a_{13}^m \\ a_{21}^m & a_{22}^m & a_{23}^m \\ a_{31}^m & a_{32}^m & a_{33}^m \end{bmatrix}, \qquad Z_0^m = \begin{Bmatrix} Z_{0_1}^m \\ Z_{0_2}^m \\ Z_{0_3}^m \end{Bmatrix}.$$

In terms of these quantities equation (33) can be expressed as $A^m(Z_0^{m+1} - Z_0^m) = B^m$, or, equivalently,

$$Z_0^{m+1} = Z_0^m + (A^m)^{-1} B^m. \tag{34}$$

Equation (31) is a linear equation for the unknown Z_0^{m+1} and it can be readily solved once the elements of A^m and B^m are computed. The computation of these elements requires the

determination of the derivatives $(\partial T_i/\partial Z_{0_k})_{(l,m)}$ in the present study these derivatives are computed numerically by utilizing the following finite difference formula:

$$\left.\frac{\partial T_i}{\partial Z_{0_k}}\right|_{(l,m)} = \frac{T_i(Z^m_{0_1}, \ldots, Z^m_{0_k}(1+\varepsilon), \ldots) - T_i^m}{\varepsilon Z^m_{0_k}}, \tag{35}$$

where ε is a small number. Thus, to solve for the elements of the matrices A^m and B^m of equation (34), it is necessary to compute T_i four times for each iteration by solving equations (23). The first solution is obtained at Z^m_0 and the remaining solutions of T_i are obtained by varying each of three parameters by a small amount $\varepsilon Z^m_{0_k}$ in succession.

The non-linear regression technique can also be used to determine the values of the heat transfer parameter C (i.e., see equations (21, 22)) and the gas phase loss coefficient G. In this case the function F in equation (31) is partially differentiated with respect to C and G, now represented by Z_{0_1} and Z_{0_2} respectively, and the derivatives are equated to zero. Then all the steps involved in the procedure leading from equation (32) to equation (35) are repeated to evaluate the optimum values of C and G.

In the actual computational scheme, the function F in equation (31) is expressed either by using the real and imaginary parts of the oscillatory pressures, which can be computed from the measured amplitudes and phases, or by utilizing pressure amplitudes only [1]. Accordingly, the following functions F have been used:

$$F = \sum_{i=1}^{n} [(p'_{r,c} - p'_r)^2 + (p'_{i,e} - p'_i)^2], \tag{36}$$

or

$$F = \sum_{i=1}^{n} (p'_{a,e} - p'_a)^2, \tag{37}$$

where the subscripts r, i and a, respectively, represent the real part, imaginary part and the amplitude of a complex quantity and the subscript e refers to experimental quantities. The numerical solution of equation (23) gives the real and imaginary parts of the oscillatory pressures at locations in the impedance tube where these values are determined experimentally. Therefore, the derivatives of these variables with respect to u'_0, p'_0 and ρ'_0 (i.e., $\partial p'_r/\partial Z_{0_k}$ and $\partial p'_i/\partial Z_{0_k}$) can be readily computed and used in the non-linear regression scheme where both the amplitude and phase of the oscillatory pressures are needed to compute the admittances. In the second scheme, where only the pressure amplitudes are used to compute the admittances, the derivatives $\partial p'_a/\partial Z_{0_k}$ are obtained by using $\partial p'_r/\partial Z_{0_k}$ and $\partial p'_i/\partial Z_{0_k}$ computed in the first scheme. With the real and imaginary parts of u'_0, p'_0 and ρ'_0 represented by Z_{0_k}, $k = 1, 2, \ldots, 6$, the derivatives of pressure amplitude p'_a are given by

$$\frac{\partial p'_a}{\partial Z_{0_k}} = \frac{\partial \sqrt{(p'^2_r + p'^2_i)}}{\partial Z_{0_k}} = \frac{1}{p'_a}\left(p'_r \frac{\partial p'_r}{\partial Z_{0_k}} + p'_i \frac{\partial p'_i}{\partial Z_{0_k}}\right). \tag{38}$$

Once these derivatives are computed the non-linear regression can be used to minimize the error between theoretically computed and experimentally measured pressure amplitudes.

5. COMPUTATIONAL SCHEME TO MINIMIZE THE ERROR

The non-linear regression is used to find the values of u'_0, p'_0 and ρ'_0 at the combustion zone which give the best fit between the theoretically predicted acoustic pressure distribution and the corresponding experimentally measured acoustic pressures. A similar

non-linear regression procedure is also used to obtain the constants C [illegible] these two non-linear regression operations are coupled, they must be solved together to obtain the combustion zone admittance. The manner in which this is done can be briefly explained as follows.

(1) Initially, arbitrary values of C and G are chosen, and, with three measured pressures used together with the "transmission matrix" scheme, a set of "initial" values for u'_0, p'_0 and ρ'_0 at the combustion process is computed.
(2) The non-linear regression scheme is then used to obtain the values of u'_0, p'_0 and and ρ'_0 which minimize the root-mean-square deviation between the theoretically predicted data and the experimentally measured data for the chosen values of C and G.
(3) Then the values of C and G are recomputed while keeping (and using) the determined (in Step (2)) "optimum" values of u'_0, p'_0, and ρ'_0 constant.
(4) Steps (2) and (3) are repeated until u'_0, p'_0, ρ'_0, C and G converge to a given set of values.

6. ILLUSTRATIONS OF COMPUTATIONAL SCHEME

To check the accuracy of the data reduction schemes discussed in the last section, computations were performed for a number of hypothetical cases for which the exact values of C, G, u'_0, p'_0 and ρ'_0 were assumed to be known. With these values used as initial conditions, the conservation equations (i.e., equations (8)) describing the oscillatory flow field in the impedance tube were solved to determine the "exact" wave structure in the hypothetical impedance tube. The axial distributions of the steady state variables needed for the solution of equations (8) were computed from equations (5), (6), (7), (21) and (22). In these equations different forms of wall temperature distributions were used with a fixed flame temperature, T_f of 3780°R. Solution of equation (5) indicated that the steady state pressure variation was almost negligible. Different values of $\bar{m}$ were used (see equations (5) through (7)) in this analysis such that the maximum values of $\bar{u}$ at $x = 0$ varied from 0 to 200 ft/s. The specific heat ratio γ and the specific gas constant, R, were assumed to be 1·28 and 2480 ft-lbf/slug°R, respectively.

A number of oscillatory pressure data at different axial locations along the tube were taken from the solution of equations (8) and were perturbed from their exact values. These deviations represent the expected errors in the measured acoustic pressure data. These modified pressure data were then fed into the developed data reduction programs in an effort to determine the error in the admittance computation resulting from the artificially introduced experimental inaccuracies. Careful examination of the results obtained from the various hypothetical cases investigated indicates that the heat transfer parameter C converges rapidly to its correct value, whereas the gas phase loss coefficient G converges slowly. Therefore, to obtain an accurate value of G the tolerance limit must be kept as small as possible and the errors in the input pressure data should not be too large. Two sets of such computations are presented below. In these two cases the wall temperature was assumed to be constant (i.e., $T_w = 810$°R) and the mean flow velocity $\bar{u}$ was kept zero.

Case 1. In this case the gas phase loss in the impedance tube was assumed to be zero and, with use of known values of C, u'_0, p'_0 and ρ'_0, equations (8) were solved to determine the corresponding hypothetical standing wave structure in the tube. Then, an arbitrary initial value of C was chosen and input pressure data, obtained by modifying the computed "exact" pressure data at a discrete number of points, were used to recompute the wave structure and the desired value of C. The recomputed and "exact" wave

structures are shown in Figures 2 and 3, and Table 1 provides a comparison between the "exact" and the computed values [illegible] Figure 4 shows excellent agreeme[illegible] distributions. Therefore, this technique can be used to obtain axial temperature distribution in any pipe with high temperature flow situations where direct temperature measurements are difficult.

Case 2. In this case equations (8) were solved for a situation where the gas phase loss was assumed to be present in the impedance tube and the constant G was assigned a specific value. Then, with use of the assumed values of C, G, u'_0, p'_0 and ρ'_0, equations (8) were solved to determine the hypothetical "exact" acoustic pressure wave structure in the impedance tube. As was done in Case 1 above, assumed values of C and G and perturbed "exact" pressure data were used to recompute the wave structure and the values of C and G. For brevity, the results presented herein are for the case where $\alpha Y = 0.1$ and they are presented in Figures 5 through 7 and in Table 2. It should be pointed out, however, that similar results were also obtained for wide ranges of both positive and negative values of the real part of the admittance. In one of the two computational schemes used to determine the variables at the combustion zone, the gas phase loss coefficient was kept zero. In this case (i.e., Plot B in Figures 5 and 6) the recomputed and "exact" wave structures are not in good agreement, particularly at and near pressure minima, and there are considerable discrepancies between the computed and exact values of u'_0, p'_0, ρ'_0 and the admittance Y. In the second case, the determination of the bulk loss coefficient G was also included in the data reduction scheme which now resulted in good agreement between the two wave structures (i.e., between plots A and C in Figures 5 and 6) and the variables u'_0, p'_0, ρ'_0 and Y. However, Figure 7 shows excellent agreement between the exact and both the recomputed temperature distributions (i.e., between A, B and C in Figure 7) because the axial steady state temperature distribution depends only on the axial wave length variation of the standing wave and does not depend on the magnitude of oscillatory pressure.

Since the primary objective of this study was to determine whether the non-linear regression technique developed could handle situations in which a gas phase loss is present in the flow, the data reported in Case 2 describes a situation in which only small errors were introduced into the "exact" pressure data that was used to generate the input pressure points needed for the data reduction procedure. However, additional, related hypothetical cases in which the input pressure data contained relatively large errors were also investigated in the course of this study and they produced good agreements between the "exact" and recomputed wave structures and between the assumed and recomputed values of u'_0, ρ'_0, p'_0, C, G and Y. It has also been observed in these studies that the quality of the computed results improves when the number of input pressure points increases and when the input pressure data describe the wave structure over a tube length that includes at least two minimum points.

Examination of Figures 2 through 7 and Tables 1 and 2 indicate very good agreement between the assumed and computed values of u'_0, p'_0, ρ'_0, C, G and the admittance Y. This good agreement suggests that the data reduction procedures developed as part of this research effort can indeed be used to determine unknown admittance values in high temperature impedance tube experiments without much loss of accuracy. The applications of the experimental procedures developed in this paper in the determination of the admittances of combustion processes are described elsewhere [1, 2].

Reference [1] describes the application of this technique for the measurement of burning solid propellant admittances. Some of the measured admittance values showed considerable amount of scatter. The observed scatter in the admittance values was

233-10

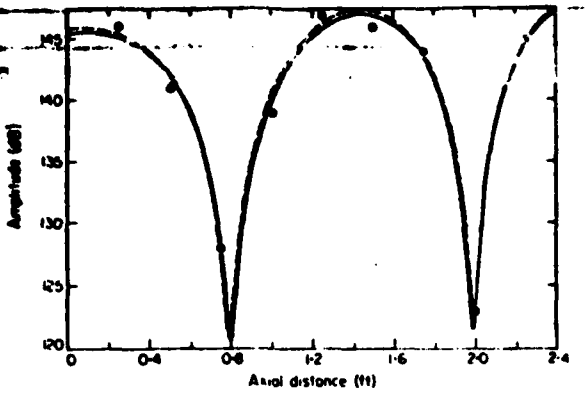

Figure 2. Exact, recomputed and input pressure amplitude data used to check the developed data reduction procedure. $Y_s = -0.05$, $G = 0$, chamber pressure = 15.7 psi, excitation frequency = 1000 Hz; ——, exact structure; – – – –, structure recomputed by using pressure amplitudes and phases; – · – ·, structure recomputed by using pressure amplitudes only; ●, "perturbed" input pressure amplitude data.

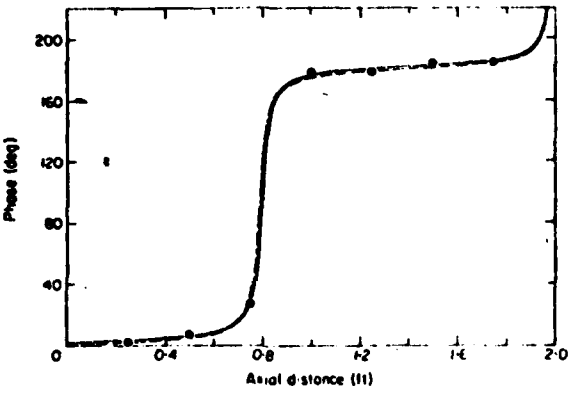

Figure 3. Exact, recomputed and input pressure phase data used to check the developed data reduction procedure. $Y_s = -0.05$, $G = 0$, chamber pressure = 15.7 psi, excitation frequency = 1000 Hz; ——, exact structure; – – –, structure recomputed by using pressure amplitudes and phases; · · · · ·, structure recomputed by using pressure amplitudes only; ●, "perturbed" input pressure amplitude data.

Phase

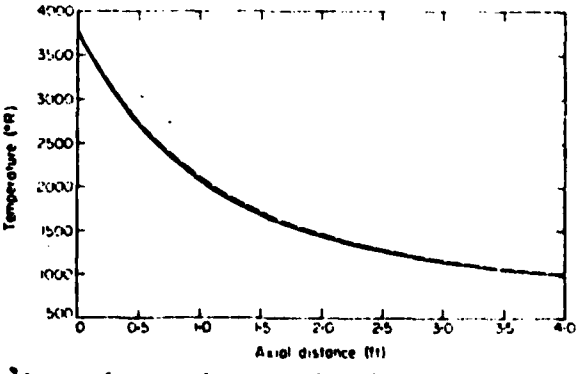

Figure 4. Axial distribution of exact and recomputed steady state temperature in the impedance tube. ~~$Y_s = -0.05$, $G = 0$, chamber pressure = 15.7 psi, excitation frequency = 1000 Hz~~; ——, exact structure; – – –, structure recomputed by using pressure amplitudes and phases; · · · · ·, structure recomputed by using pressure amplitudes only; ~~●, "perturbed" input pressure amplitude data~~.

233-11

TABLE 1

Comparison between correct values and [illegible] technique

Chamber pressure = 15·7 psi
Frequency of excitation = 1000 Hz

Parameters		Correct values	Computed using amplitude and phase	Computed using amplitude only	Initial guess
Real part of admittance, Y_r		−0·05	−0·049757	−0·052565	
Imaginary part of admittance, Y_i		0·15	0·1236	0·1232	
Heat transfer parameter, C (ft)		0·943	0·972	0·973	2·0
Pressure at combustion zone p'_0	Amplitude (dB)	145·436	145·815	145·818	
	Phase (deg)	230·2	229·9	228·6	
Velocity at combustion zone u'_0	Amplitude (ft/s)	1·48	1·301	1·308	
	Phase (deg)	−21·4	−18·17	−18·27	
Density at combustion zone ρ'_0	Amplitude (slug/ft^3)	$0·612 \times 10^{-6}$	$0·6472 \times 10^{-6}$	$0·6477 \times 10^{-6}$	
	Phase (deg)	229·0	228·7	227·4	

TABLE 2

Data computed with gas phase loss, by using non-linear regression for a positive real admittance

Chamber pressure = 300 psi
Frequency of excitation = 1000 Hz

Parameters		Correct values	Computed values using amplitude and phase: Assuming zero loss	Computed values using amplitude and phase: Loss coefficient and heat transfer parameter computed simultaneously
Real part of admittance, Y_r		0·1	0·055532	0·10147
Imaginary part of admittance, Y_i		0·15	0·13315	0·1362
Bulk loss coefficient, G (lbf s/ft^4)		1·5	0·0	1·556
Heat transfer parameter, C (ft)		1·0	1·024	1·021
Pressure at combustion zone p'_0	Amplitude (dB)	145·4357	145·4	145·5
	Phase (deg)	230·1944	229·9	230·1
Velocity at combustion zone u'_0	Amplitude (ft/s)	0·088204	0·07068	0·08356
	Phase (deg)	−75·496	−62·76	−76·54
Density at combustion zone ρ'_0	Amplitude (slug/ft^3)	$0·6143 \times 10^{-6}$	$0·6197 \times 10^{-7}$	$0·6219 \times 10^{-6}$
	Phase (deg)	232·4994	231·1	232·4

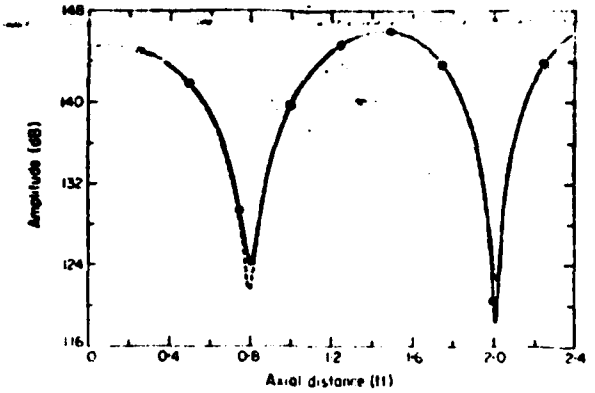

Figure 5. Exact, recomputed and input pressure amplitude data used to check the developed data reduction procedure; $Y_s = 0.1$, $G = 1.5$, chamber pressure = 300 psi, excitation frequency = 1000 Hz; ——, exact structure (A); – – –, recomputed structure when overall bulk loss coefficient was kept zero (B); – · – · –, recomputed structure when overall bulk loss was considered to be present (C); ●, "perturbed" input pressure amplitude data.

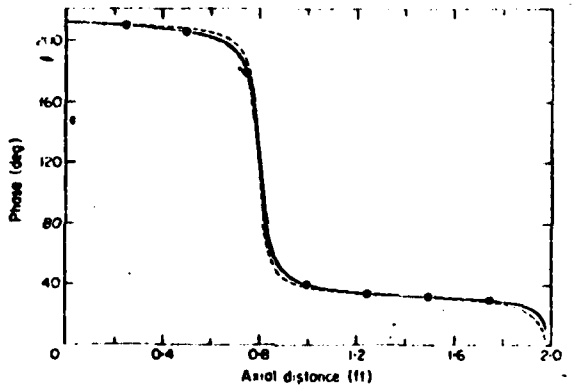

Figure 6. Exact, recomputed and input pressure phase data used to check the developed data reduction procedure; $Y_s = 0.1$, $G = 1.5$, chamber pressure = 300 psi, excitation frequency = 1000 Hz; ——, exact structure (A); – – –, recomputed structure when overall bulk loss coefficient was kept zero (B); – · – · –, recomputed structure when overall bulk loss was considered to be present (C); ●, "perturbed" input pressure phase data.

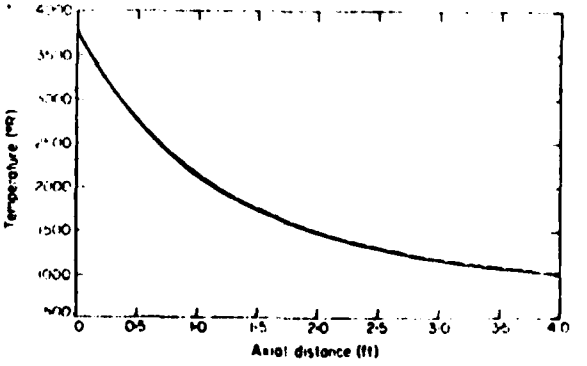

Figure 7. Axial distribution of exact and recomputed steady state temperature in the impedance tube; ——, exact structure (A); – – –, recomputed structure when overall bulk loss coefficient was kept zero (B); – · – · –, recomputed structure when overall bulk loss was considered to be present (C).

possibly due to some experimental difficulties, discussed in reference [1]. Those difficulties were the [illegible] duration [illegible] number of [illegible] describe the standing wave in the impedance tube. However, in a parallel study [2] where these shortcomings were overcome with a steady burning, longer test duration and large number of pressure measurement points covering two or more pressure minima to describe the standing wave, the admittance values obtained showed very little scatter and they agree very well with the theory. In this study [2] the admittances of reactive gaseous rocket injectors were measured by using the modified impedance tube technique.

REFERENCES

1. M. SALIKUDDIN 1978 *Ph.D. Thesis, School of Aerospace Engineering, Georgia Institute of Technology, Atlanta, Georgia.* Application of impedance tube technique in the measurement of burning solid propellant admittances.
2. B. A. JANARDAN, B. R. DANIEL, W. A. BELL and B. T. ZINN 1977 *Presented at the Spring Meeting Central States Section, The Combustion Institute Lewis Research Center,* 28–30 *March.* Measurements of reactive gaseous rocket injector response factors.
3. W. E. LAWRIE 1959 *W.A.D.C., Technical Report No.* 58-460. Development of sound absorbing materials for noise suppressors. Part I: Development of equipment for evaluating acoustical and durability properties of sound absorbing materials at elevated temperatures.
4. D. R. A. CHRISTIE 1976 *Journal of Sound and Vibration* **46**, 347–355. Measurement of the acoustic properties of a sound absorbing material at high temperatures.
5. R. A. SCOTT 1946 *Proceedings of the Physical Society* **58**, 253–254. An apparatus for accurate measurement of the acoustic impedance of sound absorbing materials.
6. D. R. BLETZ 1957 *Jet Propulsion.* A simple equation for rapid estimation of rocket nozzle convective heat transfer coefficients. 41, 1171 - 1179
7. S. RUBIN 1967 *Journal of the Acoustical Society of America* ~~4, 000–000~~. Review of mechanical impedance and transmission matrix concept.
8. R. C. PFAHL, JR. and B. J. MITCHEL 1970 *American Institute of Aeronautics and Astronautics Journal* ~~8, 000–000~~. Nonlinear regression methods for simultaneous property measurement.

1046-1052

EXPERIMENTAL DETERMINATION OF SOLID PROPELLANT ADMITTANCES BY THE IMPEDANCE TUBE METHOD*

J. D. Baum**, B. R. Daniel# and B. T. Zinn##
School of Aerospace Engineering
Georgia Institute of Technology
Atlanta, Georgia

INTRODUCTION

This paper describes recent advances made in a research program, sponsored by AFOSR, that is concerned with the application of the modified impedance tube technique in the measurement of the admittances and response functions of burning solid propellants. This data is needed to evaluate the relative driving characteristics of various solid propellants and as an input data for combustion instability analysis of solid rocket motors. To date, most response function measurements were performed utilizing the T-burner technique[1]. However, due to difficulties associated with the interpretation of T-burner data, additional experimental techniques, such as the rotating valve[2] and the impedance tube[3,4], have recently been used to measure propellant response functions.

A schematic of the modified impedance tube is shown in Fig. 1. The tested solid propellant disc is placed at one end of the tube and a combination of an acoustic driver and an exhaust valve is placed at the opposite end. Performing a test consists of turning on the acoustic driver to excite a standing wave of a predetermined frequency in the tube and the ignition and burn out of the tested solid propellant sample. During the test, heat losses to the tube walls and the presence of waves moving in both directions result in an axially varying steady temperature profile and a standing acoustic wave in the tube, as shown in Fig. 2. It can be shown that the characteristics of the standing wave are dependent, among other things, upon the boundary conditions at the burning propellant surface that are described by specifying the admittance at the propellant surface. It can be shown[5] that the magnitude and sign of the real part of the admittance are directly related to the magnitude and direction of acoustic energy flow at the combustion zone. When the real part of the admittance is positive, acoustic energy is flowing from the combustion zone into the tube and the propellant is said to be driving. When this occurs, disturbances in the gas phase are amplified by the combustion process at the propellant surface.

In the impedance tube experiment, the relationship between the admittance of the burning solid propellant surface and the impedance tube wave structure is utilized to determine the admittance at the propellant surface. This is accomplished by measuring the resulting acoustic wave structure and relating it

---

* Research Supported under AFOSR Grant 73-2571
** Graduate Research Assistant
# Senior Research Engineer
Regents' Professor

to the unknown admittance by utilizing the solutions of the impedance tube wave equations.

Fifteen pressure transducers are placed at predetermined locations along the tube walls to measure the acoustic pressure amplitudes and phases. The data acquired at different instances during the test period are input into a newly developed data reduction scheme that determines the admittances and response functions at the burning solid propellant surface. This paper describes recent efforts that were concerned with: (1) the improvement of the data acquisition system; and (2) the development of a new data reduction scheme.

IMPROVED DATA ACQUISITION SYSTEM

During the past several months, efforts have been made to improve the accuracy of the measured data. The efforts included: (1) increasing the accuracy and the dynamic range of the measured acoustic data and (2) increasing the number of pressure transducers utilized in the determination of the acoustic wave structure in the impedance tube. A combination of sixteen piezoelectric and condenser type pressure transducers were utilized. To acquire the pressure amplitude and phase data measured by the ten piezoelectric pressure transducers, a minicomputer data acquisition system is utilized. This system consists of a Hewlett Packard 2100S minicomputer with an HP 7901 disc system and a Preston GMAD-1 analog-to-digital convector. By passing the signals measured by the pressure transducers through low pass filters, the D.C. component is filtered out and the A.C. component is amplified to levels below the A-to-D input voltage limitation. The software utilized for data acquisition via this system has been rewritten to include direct memory access, resulting in an increase of the maximum transfer rate to the minicomputer from 40,000 words per second to 600,000 words per second.

In addition, theoretical studies of the characteristics of the standing wave structure have indicated that the accuracy of the measured admittances depends upon the ability to accurately measure the difference between the maxima and minima of the standing wave amplitudes. To acquire such a capability, the transducer calibration procedure has been modified. Transducers located near the pressure minima are calibrated to cover the range 110-155 dB while transducers located near pressure maxima are calibrated to cover the 120-165 dB range, as shown in Fig. 3. This procedural results in a measurement system capable of measuring a 110-165 dB range that is needed to obtain the desired experimental accuracy.

Previous analytical studies had indicated that reliable determination of the admittance of a burning solid propellant require the determination of the standing wave structure through a distance covering at least two standing wave minima. This is illustrated in Fig. 4 which describes a hypothetical, theoretically predicted standing wave in an impedance tube for a given admittance value and different values of the gas phase loss parameter G that is representative of the acoustic energy loss in the gas phase. Fig. 4 shows that pressure amplitudes corresponding to two different values of G coincide along a distance measured from the propellant sample (i.e., $x = 0$) through the first pressure minimum, but they "separate out" as the second minimum point is approached. This clearly indicates that for an accurate measurement of the bulk loss parameter G, and hence the admittance of the tested solid propellant, the standing wave structure has to be measured through a distance covering at least

two standing wave pressure minima. To accomplish this, the number of pressure transducers has been increased from ten to fifteen. A typical distribution of the pressure transducers along the tube is shown in Fig. 5. It is worth noting that the more accurate piezoelectric pressure transducers are located near pressure minima where the greatest experimental accuracy is required.

IMPROVED DATA REDUCTION PROCEDURE

Earlier in this program, the impedance tube wave equations, shown in Fig. 6, were utilized in an iterative solution procedure to determine in the unknown admittance at the propellant surface and the parameters G and C that respectively described the gas phase losses and the steady state temperature distribution. Subsequently, this procedure was improved by eliminating the need to numerically iterate while determining the unknown propellant admittance. The latter change resulted in considerable savings in computer time.

More recently, the accuracy of the determined unknowns has been improved by redefining the error function F whose minimization results in the determination of the needed unknowns. This improvement is outlined in Fig. 7 where both old and newly defined error functions are shown. When the previous error function was utilized, errors near pressure amplitude maxima completely dominated the behavior of the error function with errors near minima point having little influence upon the behavior of F. It shows in Fig. 7 that when the previous definition of F was used, a 1 dB error near a maximum point resulted in a "contribution" to F that is 1000 times larger than a corresponding contribution from a 1 db error near a minimum point. Also shown in Fig. 7 is the newly defined error function F where a "weighting" procedure is used to eliminate the discussed uneven contributions to F of different measurement locations.

RESULTS

Considering the complexity of the propellant admittance measurement technique, the repeatability of the experimental data was of much concern. The repeatability achieved is demonstrated in Fig. 8 showing the time evolution of pressure amplitudes measured at distances of 2.0 and 11.75 inches from the propellant surface in two different tests conducted with an A-13 propellant. Examination of this figure indicates remarkable similarity in the time variation of the amplitudes and excellent agreement between the computed values of the admittance and the bulk gas phase loss G.

Typical admittance and gas phase loss data obtained during tests conducted with the composite propellants A-13 and A-14, at 300 psig chamber pressure are presented in Figures 9 through 13. Figures 9 and 10 show the time variations of the real and imaginary parts of the admittance Y and the bulk gas phase loss G during tests conducted with A-13 and A-14 propellants. It is noted that the real part of the admittance Y_R varies little with time while energy losses in the gas phase vary significantly with time. These figures demonstrate the ability of the impedance tube technique to simultaneously measure the time variation of acoustic energy gains and losses inside the tube during a test. Figures 11 and 12 describe the frequency dependence of the real part of the admittance Y_R and the bulk gas phase loss parameter G obtained from experiments conducted with A-13 and A-14 propellants. The Y_R curves indicate that this quantity peaks at around 650 Hz for A-13 propellant and at around 1000 Hz for the A-14 propellant.

A comparison between values of the real part of the response function $R_b^{(r)}$, for the A-13 propellant, obtained by the impedance tube technique, the T-burner[1], and the microwave technique[6] is shown in Fig. 13. Good agreement is demonstrated at frequencies below 450 Hz while at frequencies above 450 Hz the results differ significantly. The reasons for these discrepancies are yet to be resolved.

CONCLUSIONS

Significant improvements have been achieved in the data acquisition and data reduction procedures, as demonstrated by the results provided in this paper. It has been shown that the real part of the admittance Y_R remains constant during the steady state burn period while gas phase losses may vary significantly during the same time period. Reproducibility of the measured quantities has been established as well as the capability of this experimental technique to measure gas phase losses in the impedance tube simultaneously with the measurement of the burning solid propellant surface admittance.

REFERENCES

1. "T-Burner Manual," Prepared by the Committee on Standardization of Combustion Instability Measurement in the T-Burner by the ICRIG Working Group on Solid Propellant Combustion, Chemical Propulsion Information Agency Publication No. 191(1969).

2. Brown, R. S., Erickson, J. E., and Babcock, W. R., "Combustion Instability Study of Solid Propellant," AFRPL-TR-73-42. June 1973.

3. Zinn, B. T., Salikuddin, M., Daniel, B. R. and Bell, W. A., "Solid Propellant Admittance Measurement by the Driven Tube Method," AFOSR-TR-73-2571, August 1975.

4. Zinn, B. T., Salikuddin, M., Daniel, B. R., and Bell, W. A., "Solid Propellant Admittance Measurement by the Driven Tube Method," AFOSR-TR-73-2571, August 1978.

5. Perry, E. H., "Investigation of the T-Burner and its Role in Combustion Instability Studies," Ph.D. Thesis, Daniel and Florence Guggenheim Jet Propulsion Center, California Institute of Technology, Pasadena, California, May 1970.

6. Strand, L. D., Magiwala, K. R., and McNamara, R. P., "Microwave Measurement of Solid Propellant Pressure-Coupled Response Function," AIAA Paper 79-1211, Presented at the AIAA/SAE 15th Joint Propulsion Conference, Las Vegas, Nevada, June 18-20, 1978.

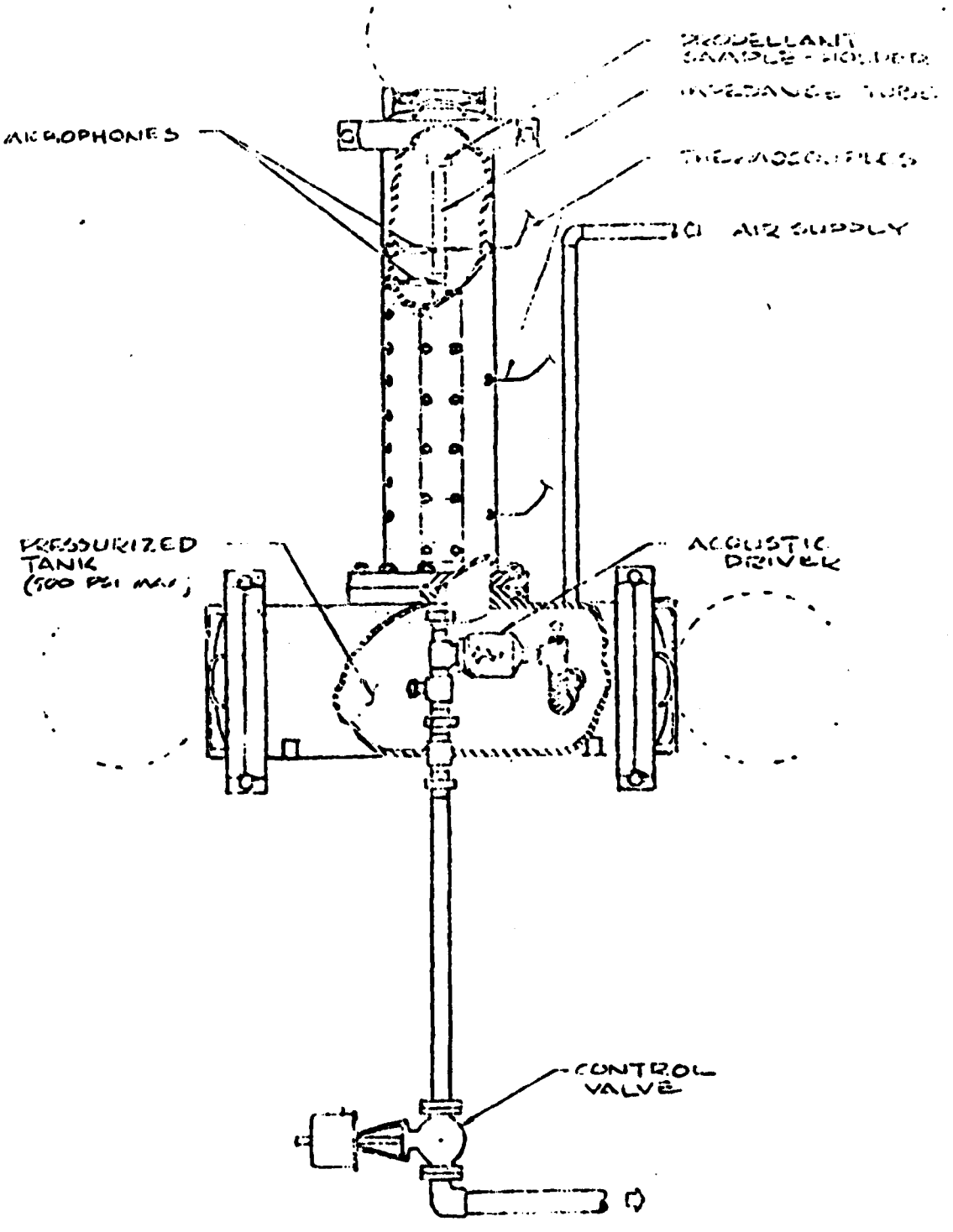

Fig. 1. Schematic Diagram of Pressurized Driven Burner Facility.

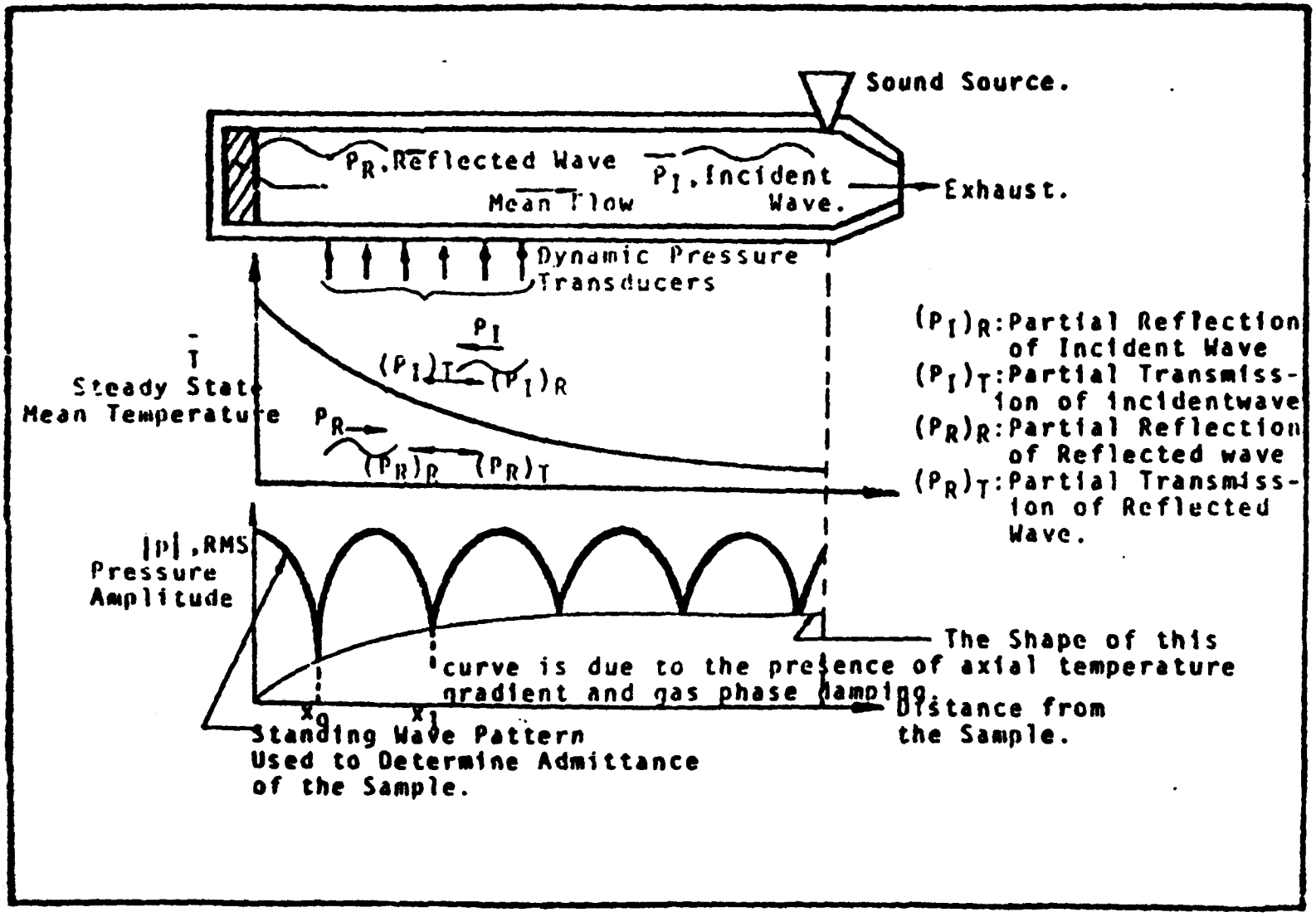

Fig. 2. An Impedance Tube, a Typical Axial Steady State Temperature Distribution and a Typical Standing Wave Pattern.

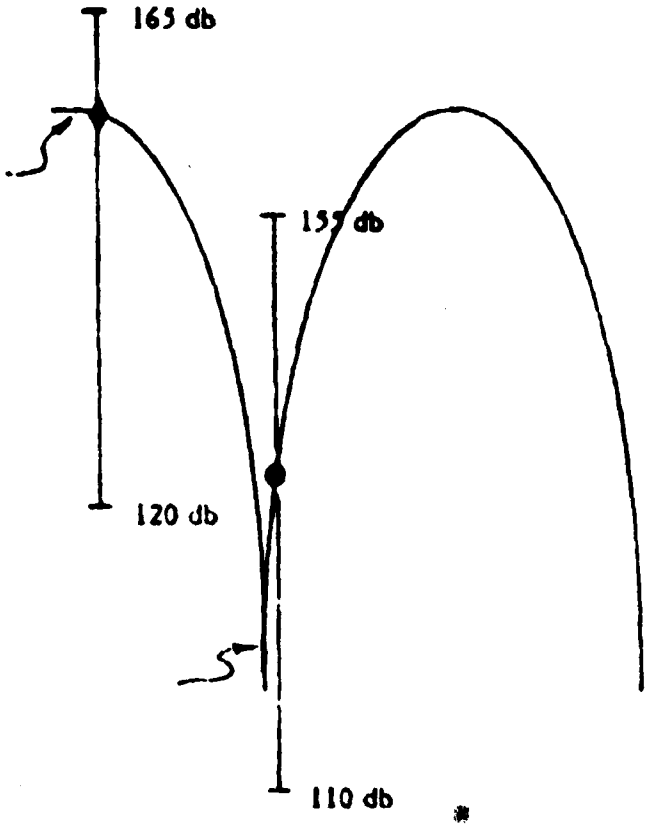

Fig. 3. New Calibration Procedure for Pressure Transducers.

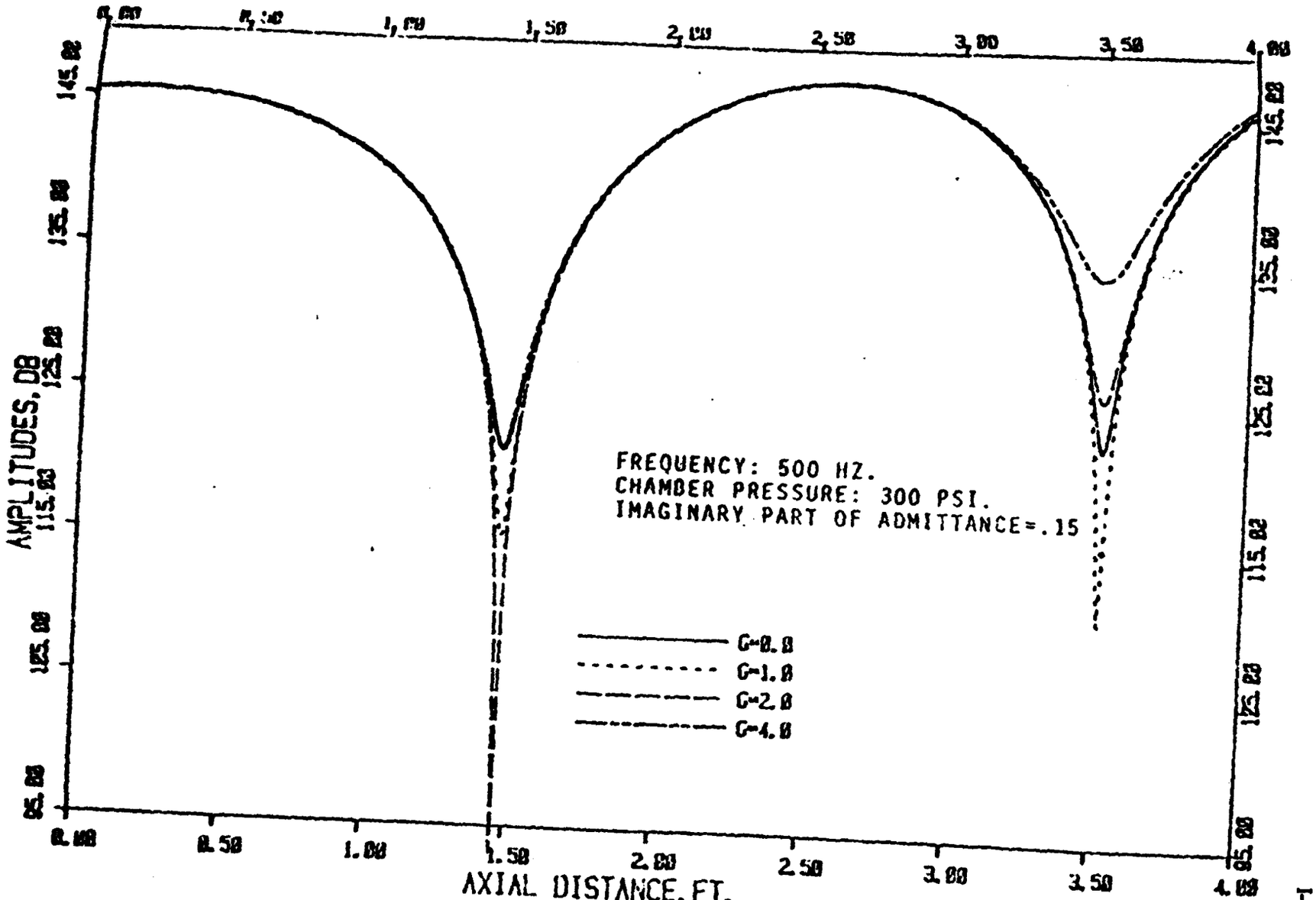

Fig. 4. Axial Variation of Pressure Amplitude.

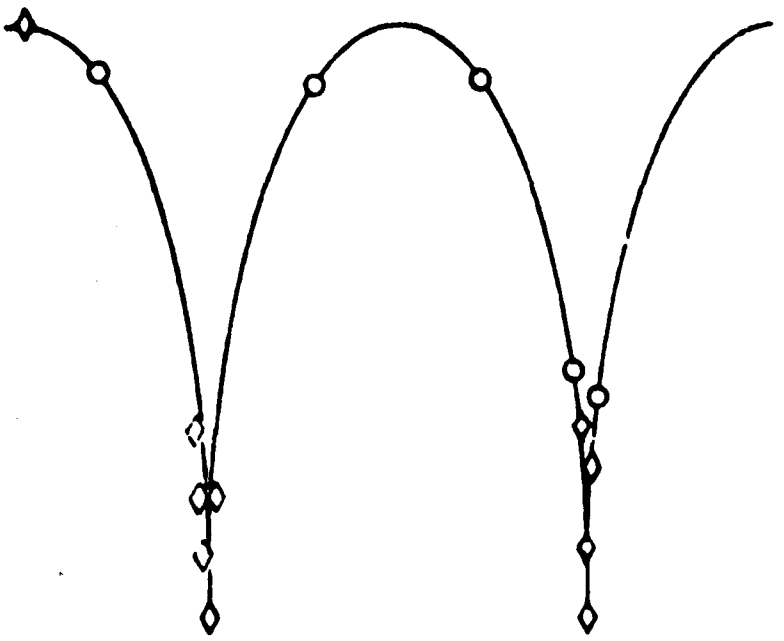

◊ - PIEZOELECTRIC TRANSDUCER

○ - PHOTOCON TRANSDUCER

Fig. 5. Axial Distribution of Pressure Transducers.

CONTINUITY

$$i\omega\rho' + \frac{d}{dx}\left[\bar{\rho}u' + \rho'\bar{u}\right] = 0$$

MOMENTUM

$$\rho'\left[i\omega u' + \frac{d}{dx}(\bar{u}u')\right] + \bar{u}\rho'\frac{d\bar{u}}{dx} = -\frac{dp'}{dx} \underbrace{- Cu'}_{\substack{\text{Gas Phase} \\ \text{Damping}}}$$

ENERGY

$$i\omega p' + u'\frac{d\bar{p}}{dx} + \bar{u}\frac{dp'}{dx} = \bar{c}^2\left[i\omega\rho' + u'\frac{d\bar{\rho}}{dx} + \bar{u}\frac{d\rho'}{dx} + \bar{u}\frac{p'}{p}\frac{d\bar{\rho}}{dx} - \bar{u}\frac{\rho'}{\rho}\frac{d\bar{\rho}}{dx}\right]$$

In obtaining a solution the above equations are recast in the following form

$$\frac{d\rho'}{dx} = f_1 \quad ; \quad \frac{dp'}{dx} = f_2 \quad ; \quad \frac{du'}{dx} = f_3$$

Where f_1, f_2 and f_3 are functions of u', ρ', p', C, C and ω.

Fig. 6. Impedance Tube Wave Equations.

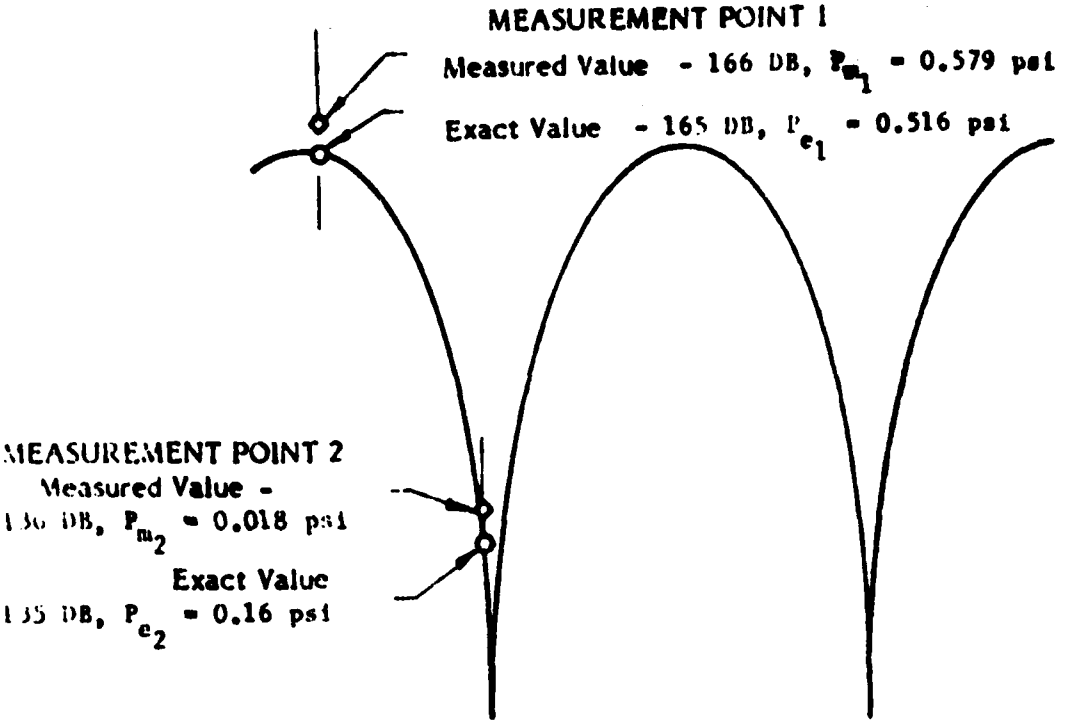

PREVIOUS DEFINITION OF THE ERROR FUNCTION

$$F = \sum_{i=1}^{n} (P'_{exp_i} - P'_{th_i})^2 \qquad \text{where } P'_{exp_i}, P'_{th_i} \text{ are in psi}$$

POINT 1 : $F_1 = (P_{m_1} - P_{e_1})^2 = (0.063)^2 = 0.396 \times 10^{-2}\ (psi)^2$

POINT 2 : $F_2 = (P_{m_2} - P_{e_2})^2 = (0.002)^2 = 0.396 \times 10^{-5}\ (psi)^2$

THUS $\dfrac{F_1}{F_2} = 1000$

TO EQUALLY WEIGH ALL MEASUREMENT POINTS, THE ERROR FUNCTION HAS BEEN REDEFINED AS FOLLOWS:

$$F = \sum_{i=1}^{n} \left[(P'_{exp_i} - P'_{th_i}) \frac{P'_{exp_1}}{P'_{exp_i}} \right]^2$$

POINT 1 : $F_1 = \left[(P_{m_1} - P_{e_1}) \dfrac{P_{m_1}}{P_{m_1}} \right]^2 = (0.063)^2 = 0.396 \times 10^{-2} (psi)^2$

POINT 2 : $F_2 = \left[(P_{m_2} - P_{e_2})^2 \dfrac{P_{m_1}}{P_{m_2}} \right]^2 = (0.063)^2 = 0.396 \times 10^{-2} (psi)^2$

and $\dfrac{F_1}{F_2} = 1$

40

F: Modified Data Reduction Scheme.

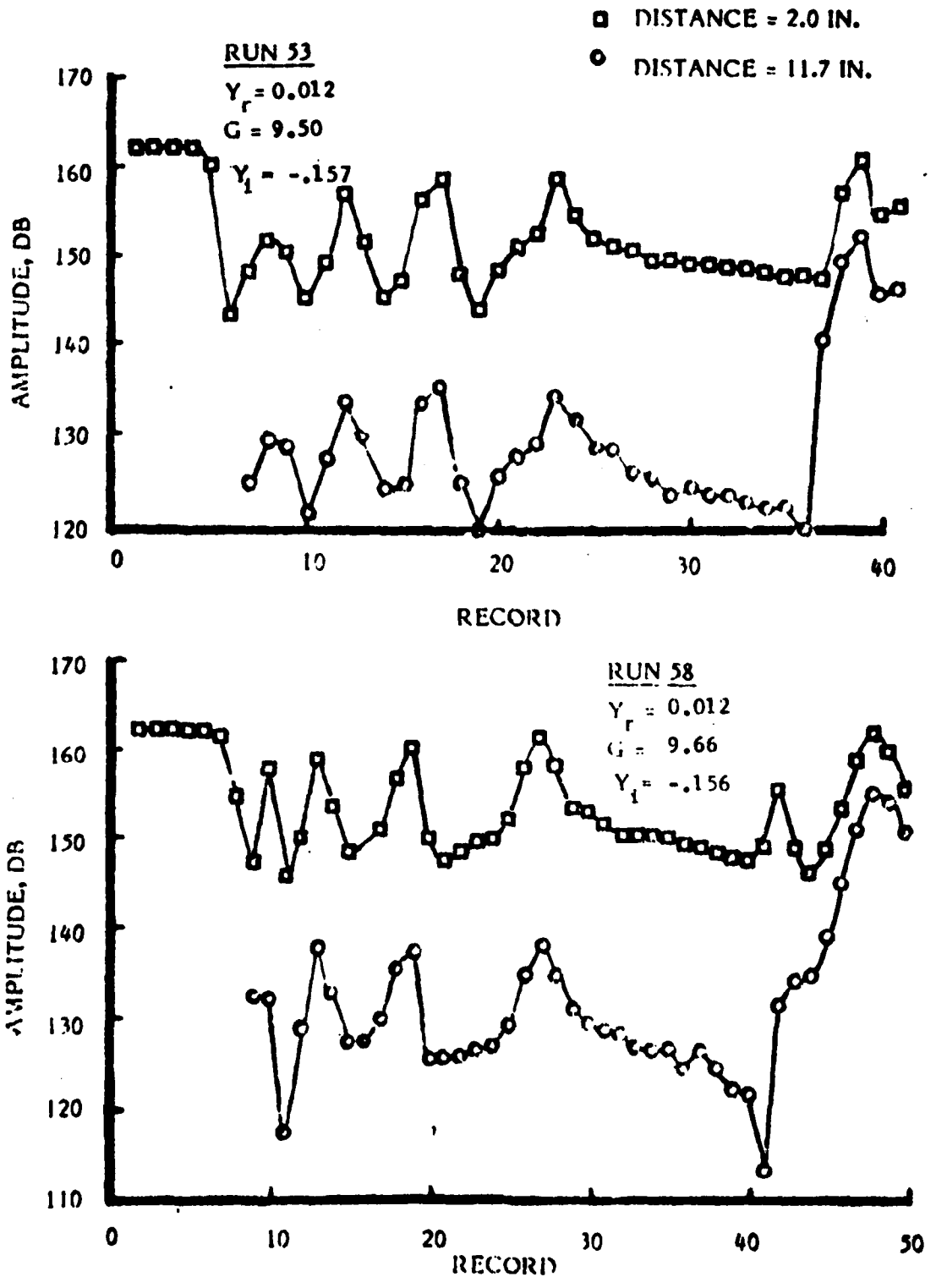

Fig. 8. REPEAT RUNS, A-13, 675 HZ 300 PSIG

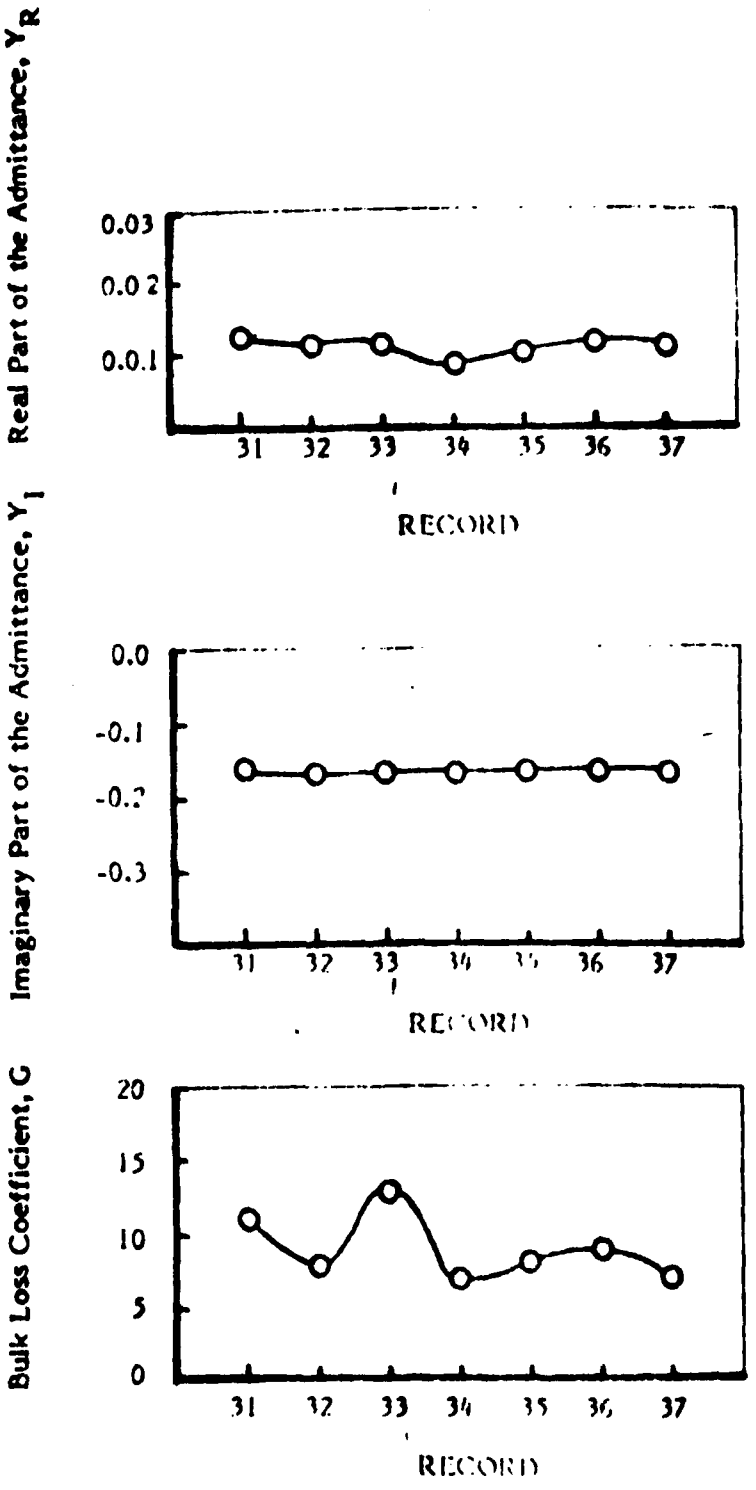

Fig. 9. TYPICAL DATA MEASURED DURING A GIVEN RUN
A-13 Propellant, 725 Hz, P = 300 psig

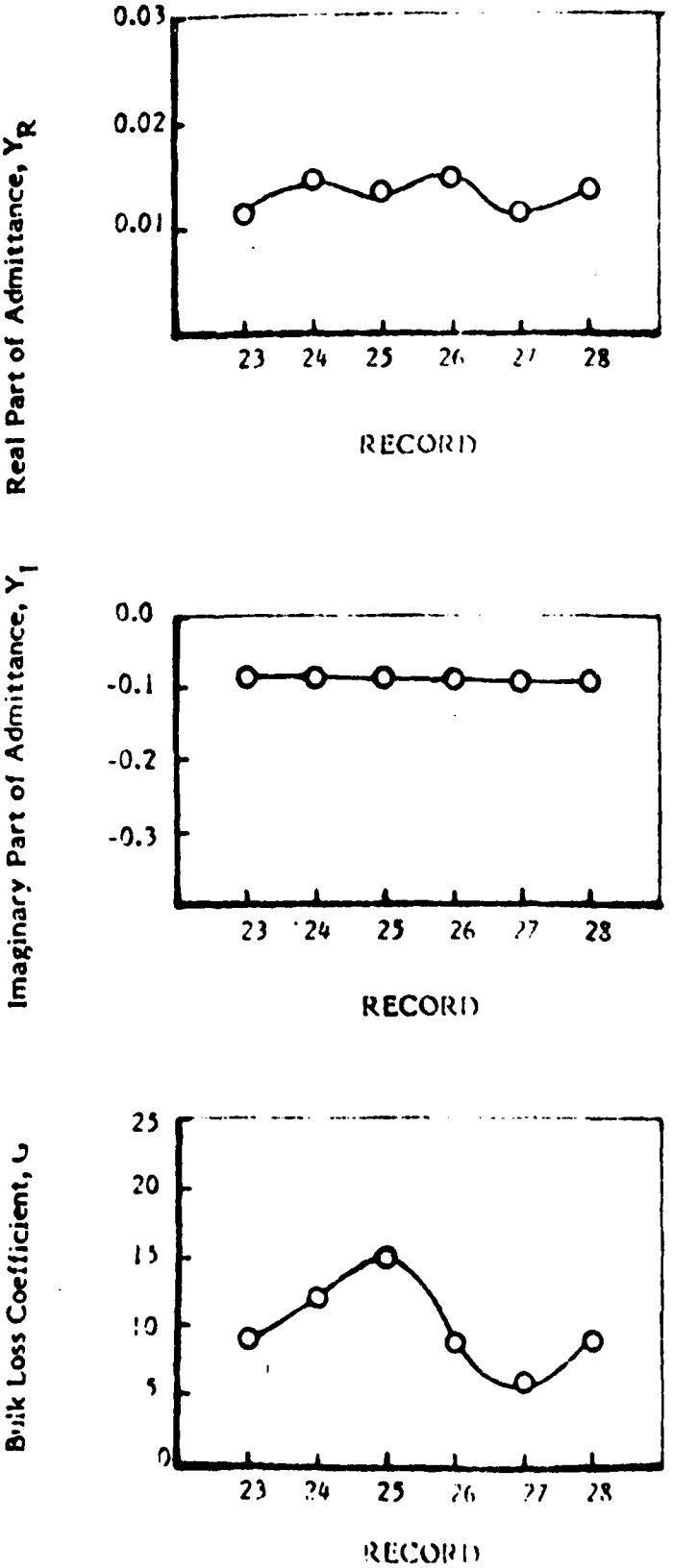

Fig. 10. TYPICAL DATA MEASURED DURING A GIVEN RUN
A-14 Propellant, f = 675 Hz, P = 300 psig

AD-A083 764 GEORGIA INST OF TECH ATLANTA SCHOOL OF AEROSPACE ENG--ETC F/G 21/8.2
ROCKET RESEARCH AT GEORGIA TECH.(U)
NOV 79 E W PRICE, W C STRAHLE, B T ZINN F49620-78-C-0003
UNCLASSIFIED AFOSR-TR-80-0305 NL

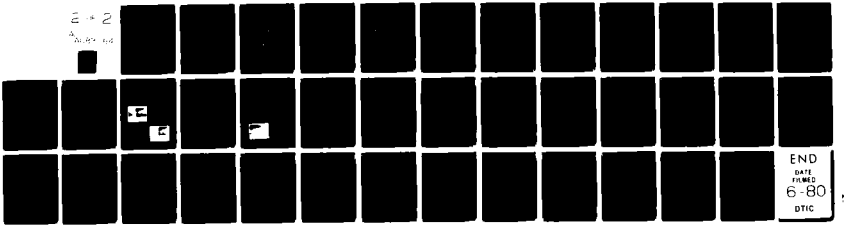

END
DATE FILMED
6-80
DTIC

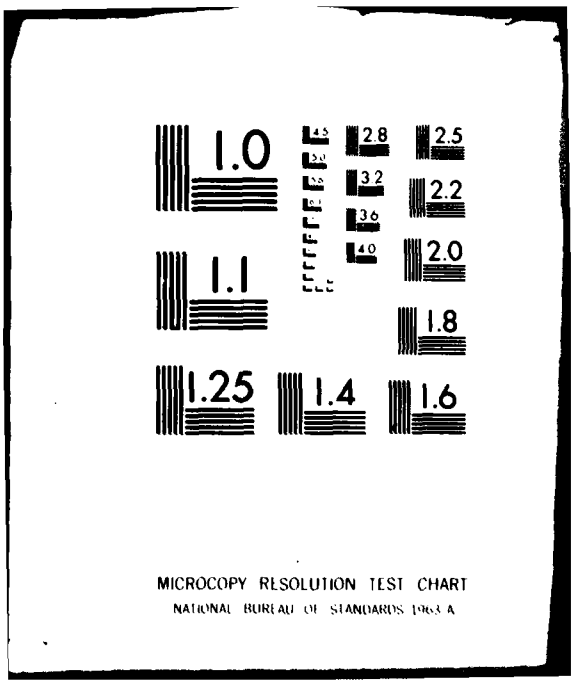
1.0
1.1
1.25
1.4
1.6
1.8
2.0
2.2
2.5
2.8
3.2
3.6
4.0
MICROCOPY RESOLUTION TEST CHART
NATIONAL BUREAU OF STANDARDS 1963 A

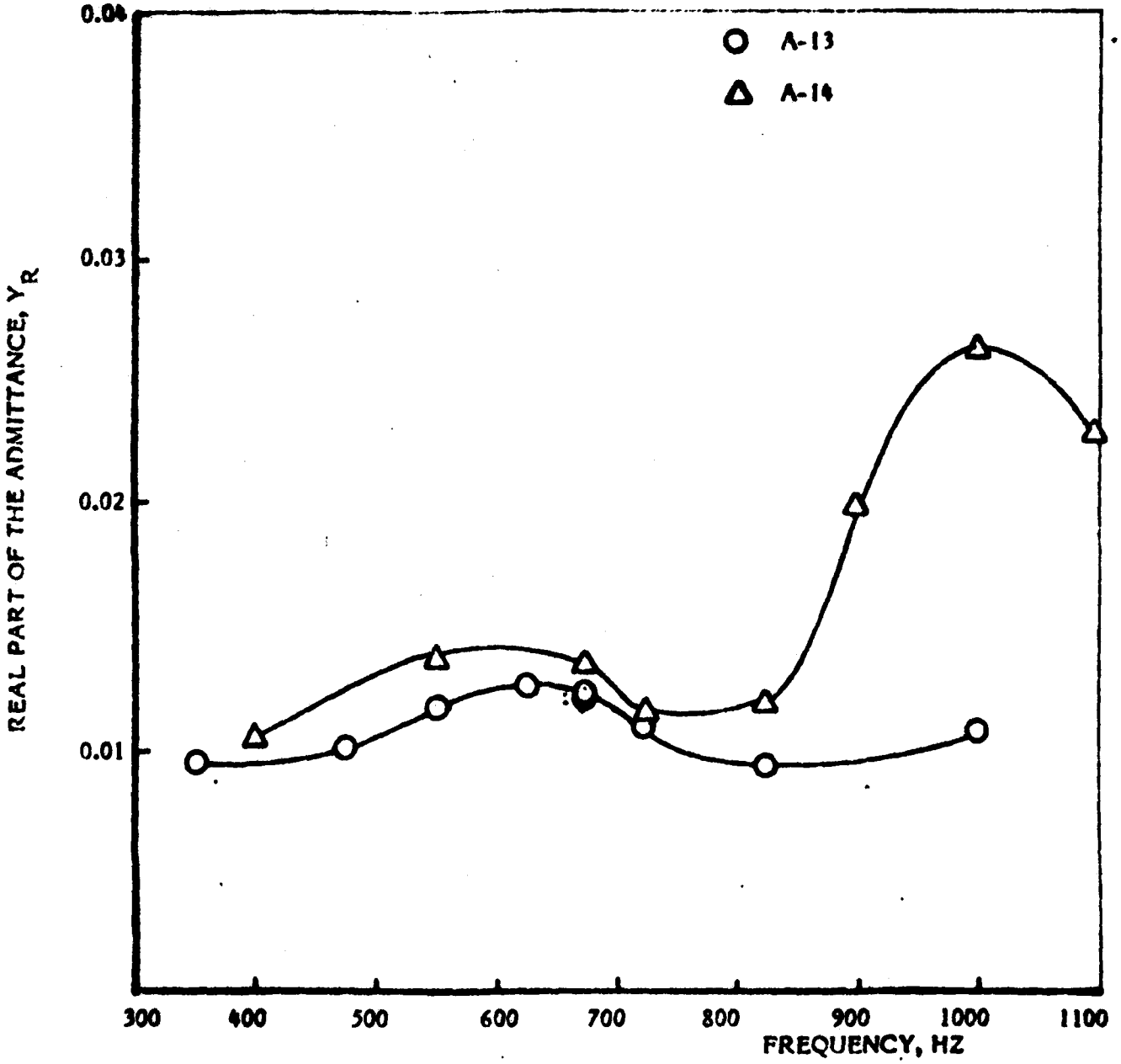

Fig. 11. Real Part of the Admittance vs. Frequency A-13 and A-14 Propellants 300 psig.

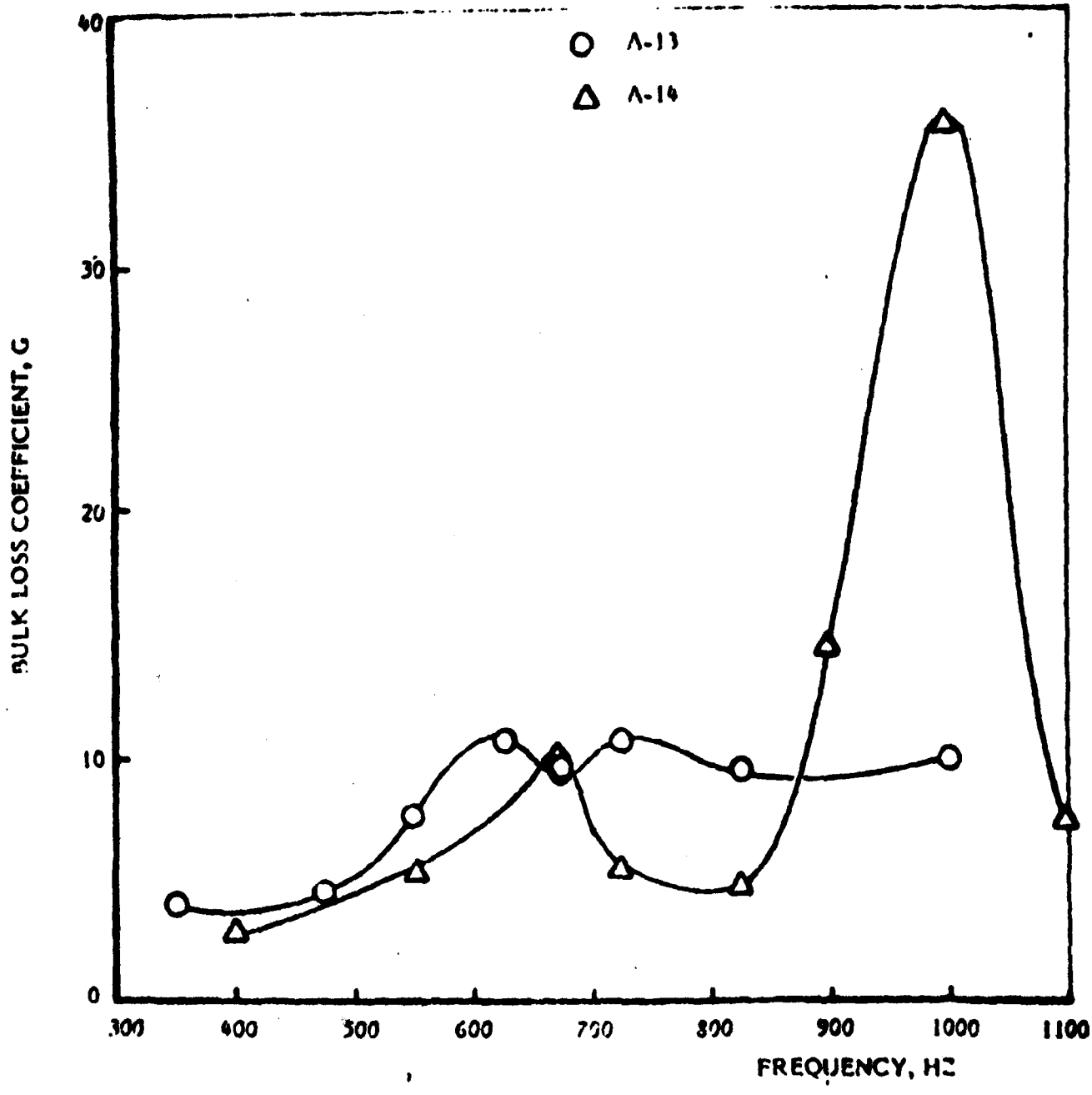

Fig. 12. BULK LOSS COEFFICIENT VS. FREQUENCY
A-13 and A-14 Propellants, 300 psig

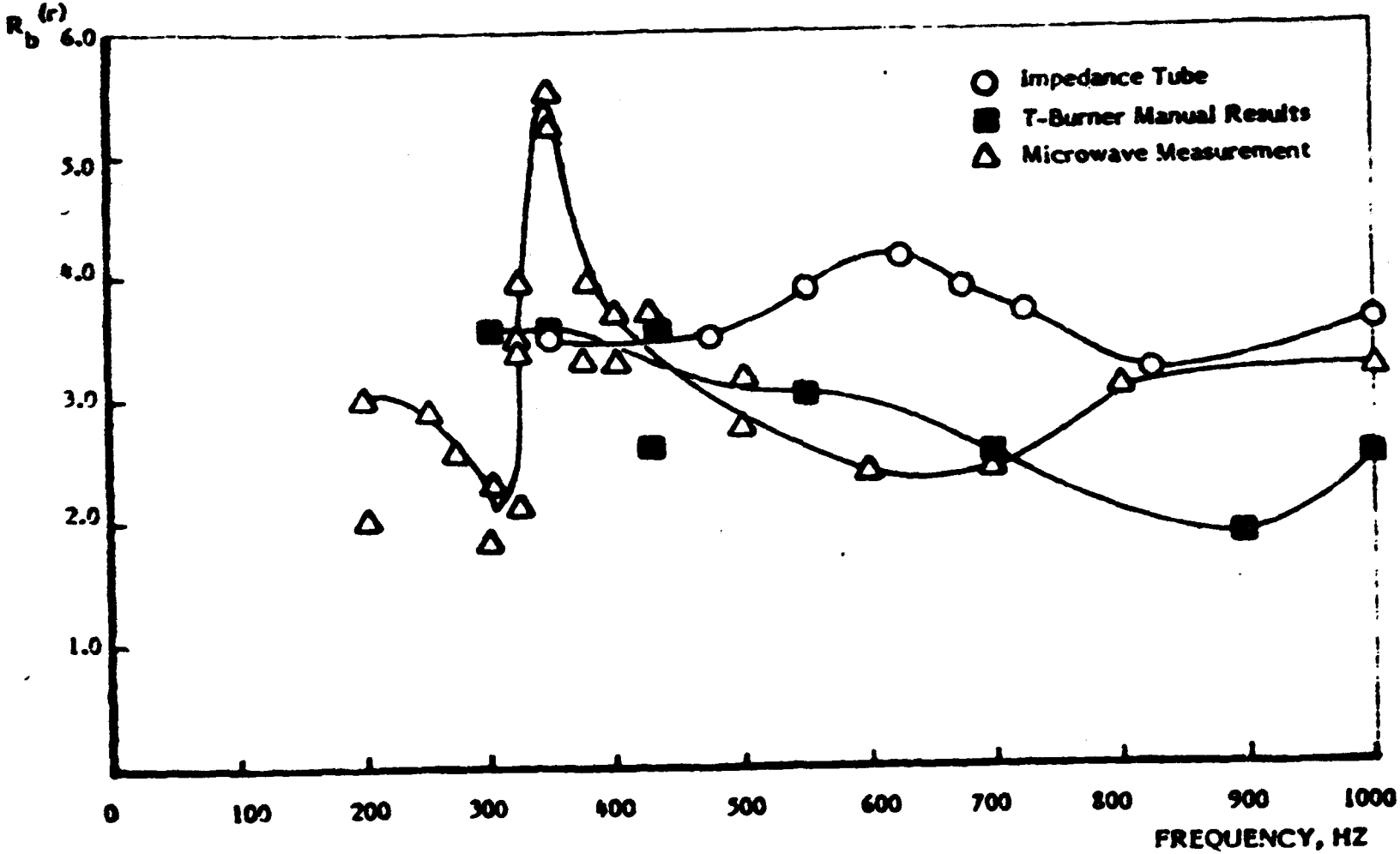

Fig. 13. REAL COMPONENT OF RESPONSE FUNCTION VS. FREQUENCY FOR A-13 PROPELLANT.
COMPARISON BETWEEN DIFFERENT TECHNIQUES.
2MPa(300 psia) NOMINAL PRESSURE.

DETERMINATION OF SOLID PROPELLANT ADMITTANCES BY THE IMPEDANCE TUBE METHOD*

J. D. Baum**, B. R. Daniel# and B. T. Zinn##
School of Aerospace Engineering
Georgia Institute of Technology
Atlanta, Georgia

Abstract

This paper describes the adaptation of the impedance tube technique for the measurement of solid propellant admittances and response functions. These quantities are needed for combustion stability analysis of solid rocket motors. The experimental set up consists of a tube with a disc of solid propellant sample placed at one end and a combination of an exhaust valve and an acoustic driver placed at the other end. Performing a test consists of turning on the acoustic driver to excite a standing wave of a predetermined frequency in the tube, ignition and burnout of the solid propellant sample. During a test, acoustic pressure data is measured by fifteen pressure transducers distributed along a distance that includes, at least, two standing wave pressure minima. The data is transferred via a fast analog-to-digital convertor to a mini computer system for immediate storage and later analysis. The measured acoustic pressure amplitude and phase data are input into a newly developed data reduction procedure that is based upon the solution of the impedance tube wave equations, for the determination of the admittance and response function of the tested solid propellant sample and the acoustic energy losses in the gas phase. The paper presents results obtained in a series of tests conducted with an A-14 propellant. The paper demonstrates the capability of the developed experimental technique to simultaneously determine the acoustic characteristics of the flow inside the impedance tube and the admittance of the burning solid propellant for the duration of the experiment.

Nomenclature

A_{ij}	coefficients defined in Ref. 7
C	a constant defined in Eq. 8
$\bar{c}$	velocity of sound, in/sec.
c_p	specific heat at constant pressure, BTU/Lbm,$^\circ$R
c_v	specific heat at constant volume, BTU/Lbm,$^\circ$R
E	error function defined in Eq. 14 (Lbf/in^2)^2
F	losses due to viscosity and gas phase damping, Lbm/in^{3}sec
G	gas phase bulk loss coefficient
I	identity matrix
M	Mach number, dimensionless
m	mass flow rate per unit cross sectional area, Lbm/in^2
p	pressure, Lbf/in^2
Q	volumetric heat source
R	specific gas constant Lbf-ft/slug$^\circ$R , also solid propellant response function, dimensionless
r	burning rate, in/sec
s	entropy, BTU/Lbm$^\circ$R
T	temperature, $^\circ$R ; also Transmission matrix defined in Eq. 10
T_{w_o}	wall temperature at x = 0, $^\circ$R
u	axial velocity, in/sec
Y	specific admittance, dimensionless
Z	variable used to represent oscillatory quantities (defined in Eq. 6)
ρ_s	density of solid propellant, Lbm/in^3
ρ	density, Lbm/in^3

Superscripts

$(\bar{\ })$	variable describing a steady state quantity
$(\ )'$	variable describing a perturbation quantity

Subscripts

$(\ )_b$	quantity evaluated at the propellant surface
$(\ )_w$	quantity evaluated at the wall
$(\ )_R$	real part of a complex quantity
$(\ )_I$	imaginary part of a complex quantity

Introduction

This paper describes recent advances made in the application of the modified impedance tube technique in the measurement of solid propellant admittances and response functions. The solid propellant admittance, defined as the complex ratio of the velocity perturbation normal to the propellant surface and the pressure perturbation evaluated at the proepllant surface, is a measure of the amplification (or attenuation) sustained by a gas phase disturbance upon interaction with the combustion process at the solid propellant surface. Consequently, the admittances of solid propellants are used to evaluate the relative driving characteristics of various solid propellants. In addition, since the stability of a solid rocket depends upon the energy balance between various processes that contribute to the combustor disturbance attenuation or amplification, the ability to determine quantitatively the admittance of the burning solid propellant is of utmost importance for the development of a capability for designing stable rocket motors. The development of an experimental technique capable of measuring the admittance and response functions of burning solid propellants under conditions simulating those experienced by unstable solid rockets is the main objective of the research work described in this paper.

To date, most response function measurements were performed utilizing the self excited T-burner technique[1]. When weakly driving and aluminized propellants failed to generate the desired oscillations in the T-burner, the variable area T-burner[2] and the pulsed T-burner[3] were developed. However, due to difficulties associated with the interpretation of T-burner data, additional experimental techniques such as the rotating valve[4], microwave[5] and the impedance tube[6,7] have recently been developed for the measurement of burning solid propellant response functions. Comparisons of the data generated by these various experimental techniques would hopefully result in accurate solid propellant response function data.

A schematic of the modified impedance tube is shown in Fig. 1. The tested solid propellant disc is placed at one end of the tube and a combination of an acoustic driver and

* Research Supported under AFOSR Grant 73-2571
** Graduate Research Assistant
# Senior Research Engineer
Regents' Professor

an exhaust valve is placed at the opposite end. Performing a test consists of turning on the acoustic driver to excite a standing wave of a predetermined frequency in the tube and the ignition and burn out of the tested solid propellant sample. During the test, heat losses to the tube walls and the presence of waves moving in both directions result in an axially varying steady temperature profile and a standing acoustic wave in the tube. It can be shown that the characteristics of the resulting standing wave are dependant, among other things, upon the boundary conditions at the burning propellant surface that can be described* by specifying the propellant surface admittance. It can also be shown[6] that the magnitude and sign of the real part of the admittance are directly related to the magnitude and direction of acoustic energy flow at the burning propellant surface. When the real part of the admittance is positive, acoustic energy is flowing from the combustion zone into the impedance tube and the propellant is said to be driving. When this occurs, disturbances in the gas phase are amplified by the combustion process at the propellant surface.

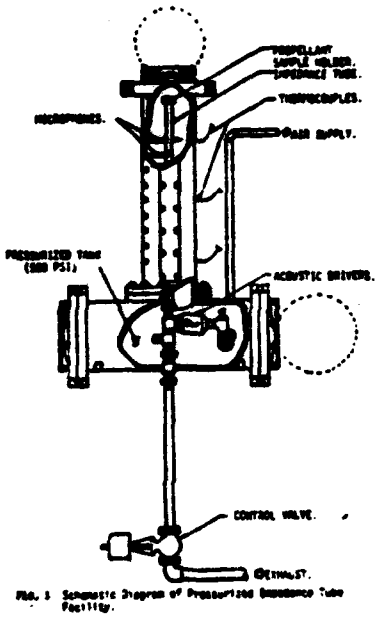

Fig. 1 Schematic Diagram of Pressurized Impedance Tube Facility

In the impedance tube experiment, the relationship between the admittance at the burning solid propellant surface and the impedance tube wave structure is utilized to determine the admittance at the propellant surface. This is accomplished by measuring the resulting acoustic wave structure and relating it to the unknown admittance by utilizing the solutions of the impedance tube wave equations.

During a test, fifteen pressure transducers are placed at predetermined locations along the tube walls to measure the acoustic pressure amplitudes and phases. The data acquired at different instances during the test period are input into a newly developed data reduction scheme that determines the admittance and response function at the burning solid propellant surface. This paper describes recent efforts that were concerned with improvement of the data acquisition system and the development of a new data reduction scheme. In addition, results obtained in tests conducted with a composite solid propellant (i.e., A-14) are presented and discussed.

* Under isentropic conditions, otherwise the entropy perturbation of the surface is also needed.

Improved Data Reduction Procedure

A new data reduction procedure that utilizes acoustic pressure amplitude and phase data measured at discrete points along the wall of the impedance tube for the determination of the admittance of the tested solid propellant, is outlined in this section. To develop the needed data reduction scheme, the assumptions introduced in Ref. (7) for describing the impedance tube flow are utilized. Under these assumptions, the flow inside the tube can be described by the following set of one dimensional conservation equations:

$$\text{Continuity} \qquad \frac{\partial \rho}{\partial t} + \frac{\partial}{\partial x}(\rho u) = 0 \tag{1}$$

$$\text{Momentum} \qquad \frac{\partial}{\partial t}(\rho u) + \frac{\partial}{\partial x}(\rho u^2) = -\frac{\partial p}{\partial x} - F \tag{2}$$

$$\text{Energy} \qquad \rho T\left(\frac{\partial s}{\partial t} + u\frac{\partial s}{\partial x}\right) = c_{vR}\frac{Q}{} \tag{3}$$

$$\text{State} \qquad p = \rho R T \tag{4}$$

First and second laws of thermodynamics:

$$ds = c_p \frac{dT}{T} - R\frac{dp}{p} \tag{5}$$

Next, each of the following dependent variables is expressed as a sum of a steady state solution and a time dependent perturbation (e.g., $p(x,t)=p(x)+p'(x,t)$) and these expressions are substituted into Eqs. (1) through (5). Separating the resulting equations into the corresponding steady state and unsteady systems of equations, linearizing the unsteady equations assuming that the solutions are periodic in time (i.e., $p'(x,t)=p'(x)e^{i\omega t}$), as is the case in the impedance tube experiment), using the relation $F' = Gu'$ (where G is a constant) yield a system of linear wave equations that can be expressed in the following form

$$\frac{dZ_i}{dx} = \sum_{j=1}^{3} A_{ij} Z_j \qquad i=1,2,3. \tag{6}$$

Where Z_1, Z_2 and Z_3 respectively represent u', p' and ρ'. The coefficients A_{ij} depend upon the corresponding steady state solutions and the acoustic energy gas phase loss that is specified by a parameter G. Expression for the coefficients A_{ij} are given in Ref. 7.

Before proceeding with the solution of Eqs. (6), a comment regarding the determination of the steady state solution is in order. Analysis of the corresponding steady state conservation equations shows that once the behavior of one of the dependent variables is known, the remaining dependent variables could be determined by utilizing the steady state conservation equations. Experiments and related analytical studies[7] conducted earlier under this investigation had shown that a steady state temperature distribution that is consistent with the one dimensional description of the wave propagation problem in the impedance tube is provided by the following expression:

$$T(x) = T_w(x) + (T_c - T_w(o))e^{-x/\Lambda} \tag{7}$$

yields a unique set of initial conditions u', p' and ρ' at the burning propellant surface (i.e., x = 0) that minimizes the error function E.

Determination of the Propellant Admittance

The following procedure has been utilized in the determination of the unknown propellant admittance from the measured acoustic pressure data:

(1) Initially, arbitrary values of G and C are assumed. Next, $[A]_x$ is evaluated. Equations (12) are then integrated forward utilizing a fourth-order Runga-Kutta method to evaluate $[T]_x$

(2) Utilizing the calculated $[T]_x$ and the set of acoustic pressure measurements P_{ex}, the values of u', p' and ρ' are evaluated at the propellant surface by utilizing Eq. (21).

(3) $[Z]_x$ is calculated, utilizing Eq. (10).

(4) E is calculated, utilizing Eq. (15).

(5) The above calculated error function E represents its minimum for a given set of the parameters C, G that appear in the matrix $[A]_x$. To minimize the error function E with respect to G and C, Muller's iteration technique has been utilized. This technique provides a rapid method for alternately iterating on the parameters G and C until the minimum of E, for which $\frac{\partial E}{\partial G} = \frac{\partial E}{\partial C} = 0$, is reached.* The admittance and the response function of the burning solid propellant, the gas phase acoustic energy losses and the axial distribution of the acoustic velocity, density and entropy are evaluated for the minimizing set of $\{Z\}_{x_0}$, G and C.

Improved Data Acquisition Procedure

During the past several months, efforts have been made to improve the accuracy of the measured data. The efforts included: (1) increasing the accuracy and the dynamic range of the measured acoustic data and (2) increasing the number of pressure transducers utilized in the determination of the acoustic wave structure in the impedance tube. A combination of fifteen piezoelectric and condenser type pressure transducers were utilized. To acquire the pressure amplitude and phase data measured by the ten piezoelectric pressure transducers, a minicomputer data acquisition system is utilized. This system consists of a Hewlett Packard 2100S minicomputer with an HP 7901 disc system and a Preston GMAD-I analog-to-digital convertor. By passing the signals measured by the pressure transducers through high pass filters, the d.c. component is filtered out and the a.c. component is amplified to levels below the A-to-D input voltage limitation. The software utilized for data acquisition via this system has been rewritten to include direct memory access, resulting in an increase of the maximum transfer rate to the minicomputer from 40,000 words per second to 600,000 words per second.

In addition, theoretical studies of the characteristics of the standing wave structure have indicated that the accuracy of the measured admittances depends upon the ability to accurately measure the difference between the maxima and minima of the standing wave amplitudes. To acquire such a capability, the transducer calibration procedure has been modified. Tranducers located near the pressure minima are calibrated to cover the range 110-135 dB while transducers located near pressure maxima are calibrated to cover the 120-165 dB range, as shown in Fig. 2. This procedural results in a measurement system capable of measuring a 110-165 dB range that is needed to obtain the desired experimental accuracy.

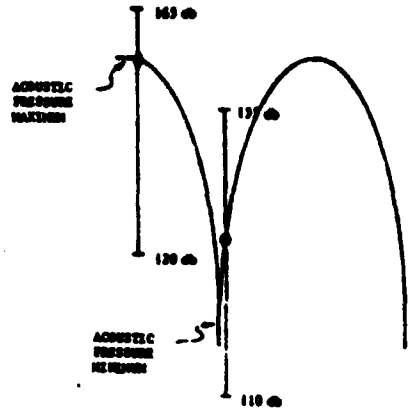

FIG. 2. CALIBRATION RANGES FOR VARIOUS PRESSURE TRANSDUCERS.

Previous analytical studies had indicated that reliable determination of the admittance of a burning solid propellant requires the determination of the standing wave structure through a distance covering at least two standing wave minima. This is illustrated in Fig. 3 which describes a hypothetical, theoretically predicted, standing wave in an impedance tube for a given admittance value and different values of the gas phase loss parameter G that is representative of the acoustic energy losses in the gas phase. Figure 3 shows that pressure amplitudes corresponding to two different values of G coincide along a distance measured from the propellant sample (i.e., x = 0) through the first pressure minimum, but they "separate out" as the second minimum point is approached. This clearly indicates that for an accurate measurement of the bulk loss parameter G, and hence the admittance of the tested solid propellant, the standing wave structure has to be measured through a distance covering at least two standing wave pressure minima. To accomplish this, the number of pressure transducers has been increased from ten to fifteen. A typical distribution of the pressure transducers along the tube is shown in Fig. 4. It is worth noting that the more accurate piezoelectric pressure

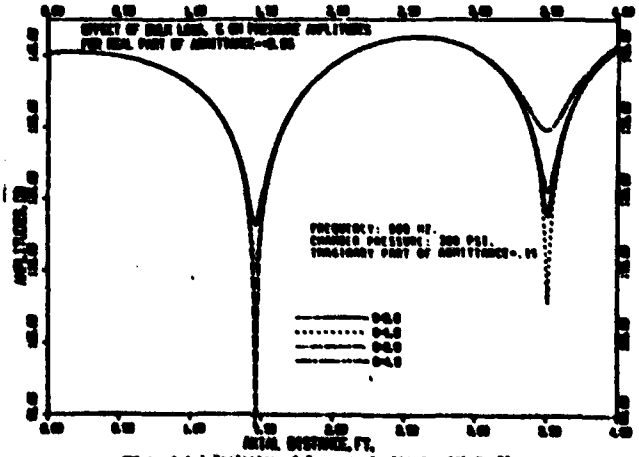

FIG. 3. Axial Variation of Pressure Amplitude with the Flow.

* The quantity $\{Z\}_{x_0}$ is calculated at every one of these iteration steps.

transducers are located near pressure minima where the greatest experimental accuracy is required.

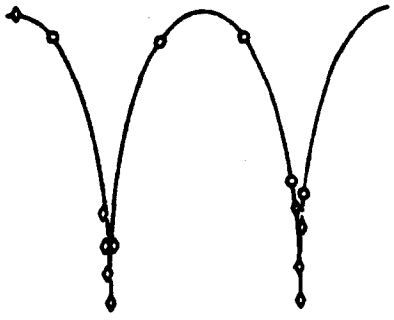

◊ - PIEZOELECTRIC TRANSDUCER

○ - PHOTOCON TRANSDUCER

FIG. 4. A TYPICAL AXIAL DISTRIBUTION OF THE PRESSURE TRANSDUCER.

Typical Results

Considering the complexity of the propellant admittance measurement technique, the repeatability of the experimental data was of much concern. The repeatability achieved is demonstrated in Fig. 5 showing the time evolution of the pressure amplitudes measured at distances of 2.0 and 11.75 inches from the propellant surface in two different tests conducted with an A-13 propellant. Examination of this figure indicates remarkable similarity in the time evolution of the amplitudes and excellent agreement between the computed values of Y and G.

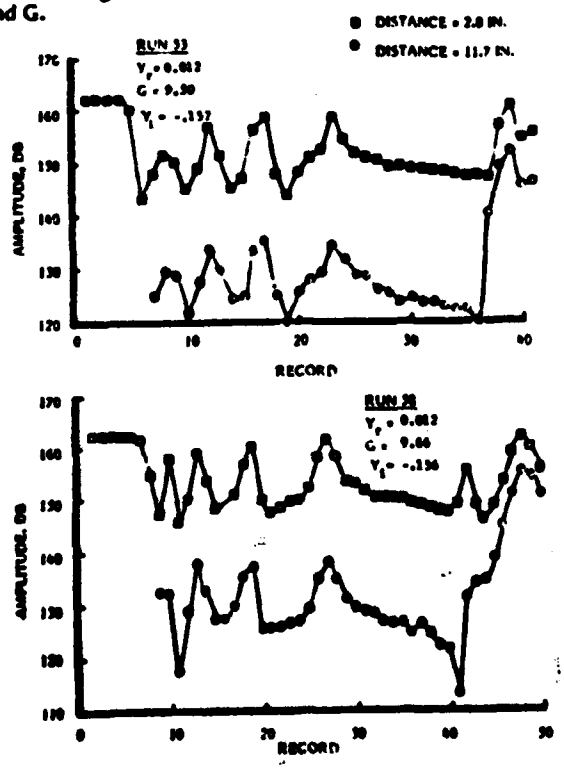

FIG. 5. REPEAT RUNS, A-13, 675 HZ 500 PSIG

Typical admittance and gas phase loss data obtained during tests conducted with the an A-14 composite solid propellant at 300 psig chamber pressure are presented in Figs. 6 through 8 where the abscissa "Record", corresponds to time. Figure 6 shows the time variation of the real and imaginary parts of the admittance Y and the bulk gas phase loss coefficient G during a test conducted with an A-14 propellant at the frequency of 675 Hz. It is noted that the real part of the admittance Y_R varies little with time while energy losses in the gas phase vary significantly with time. These figures demonstrate the ability of the impedance tube technique to simultaneously measure the time variation of acoustic energy gains and

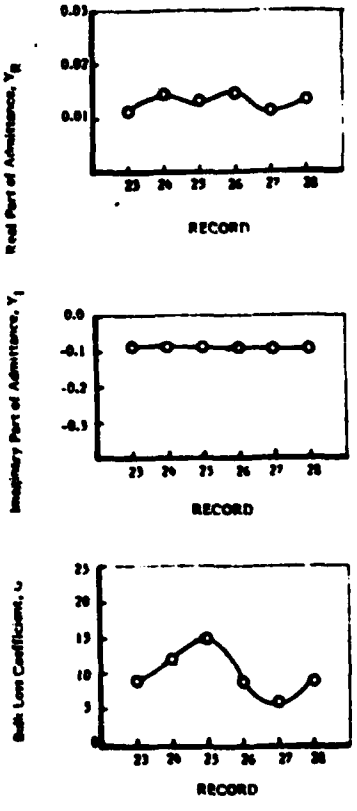

FIG. 6. TYPICAL DATA MEASURED DURING A GIVEN RUN
A-14 Propellant, f = 675 Hz, P = 300 psig.

losses inside the tube during a test. Figures 7 and 8 describe the frequency dependence of the real part of the admittance Y_R and the bulk gas phase loss parameter G obtained from experiments conducted with an A-14 propellant. The Y_R curve indicate that this quantity peaks at around 1000 Hz.

Figures 9 through 14 provide comparisons between the predicted (based upon the determined values of the propellant admittance and the parameters G and C) impedance tube wave structure (i.e., amplitude and phase) and the measured acoustic pressure data at three different instances during a test conducted with an A-14 propellant at the frequency of 625 Hz and chamber pressure of 300 psig.

These figures demonstrate the dependence of the impedance wave structure upon the gas phase losses, which are described by the parameter G which increases in magnitude from 5 to 15 during the test period covered by

these figures. The effect of the change in G becomes particularly apparent when one examines Figs. 12 and 14 that show the manner in which the slope of the phase-space curve changes near the second minima point as the value of G increased from 10 to 15 between two instants of time. Yet, while the values of G change with time the calculated values for the real part of the admittance Y_R remain virtually the same, indicating an almost constant addition of acoustic energy to the gas phase by the burning propellant. Finally, it is important to note the excellent agreement shown in Figs. 9 through 14 between the calculated wave structure (based upon the determined values of the propellant admittance, G and C) and the measured experimental; agreement that provide further support to the applicability of the developed experimental technique.

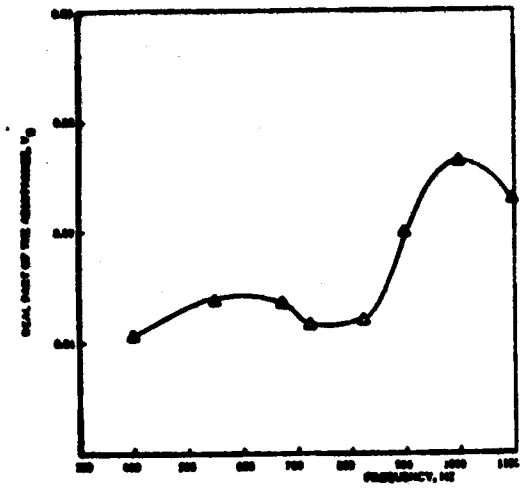

FIG. 7. REAL PART OF THE ADMITTANCE VS. FREQUENCY FOR AN A-14 PROPELLANT, 500 psig.

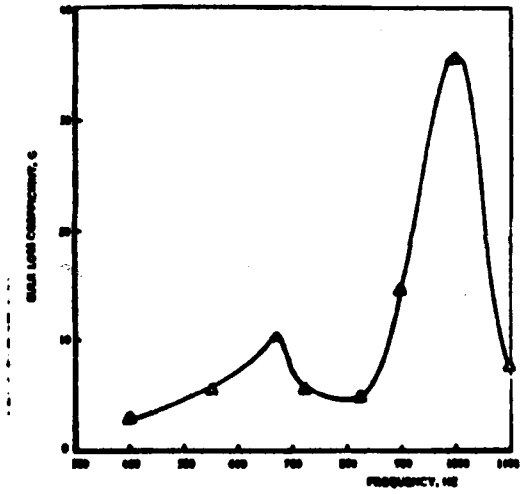

FIG. 8. GAIN LOSS COEFFICIENT VS. FREQUENCY FOR AN A-14 PROPELLANT, 500 psig.

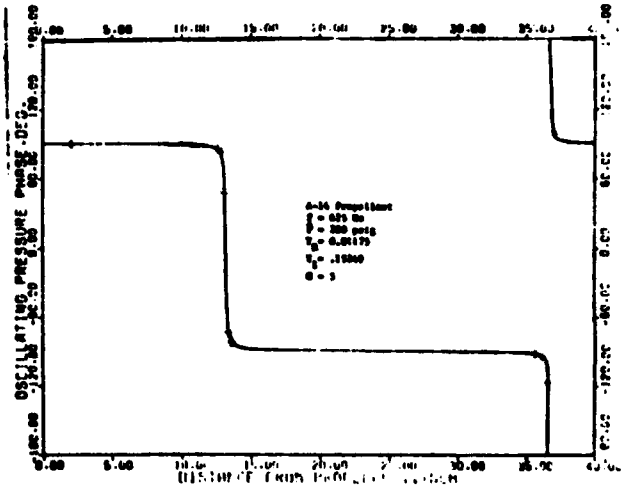

FIG. 10. AXIAL VARIATION OF PRESSURE PHASE: A COMPARISON BETWEEN EXPERIMENTAL AND THEORETICALLY CALCULATED VALUES FOR RECORD POINT 26.

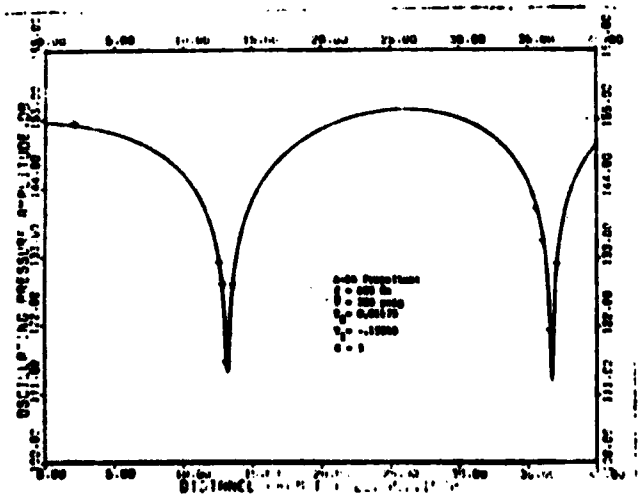

FIG. 9. AXIAL VARIATION OF PRESSURE AMPLITUDE: A COMPARISON BETWEEN EXPERIMENTAL AND THEORETICAL CALCULATED VALUES FOR RECORD POINT 26.

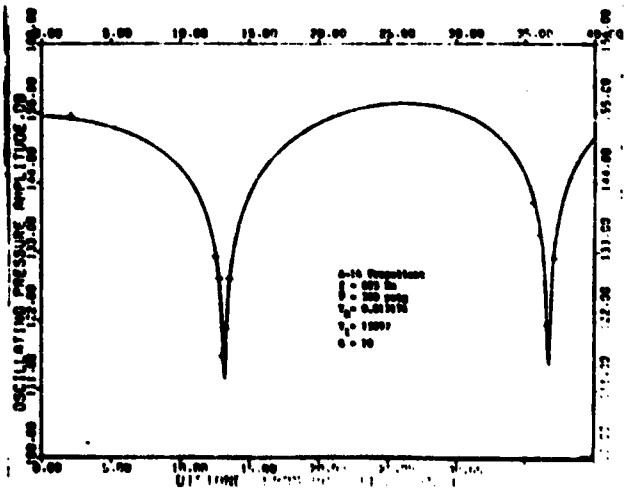

FIG. 11. AXIAL VARIATION OF PRESSURE AMPLITUDE: A COMPARISON BETWEEN EXPERIMENTAL AND THEORETICALLY CALCULATED VALUES FOR RECORD POINT 26.

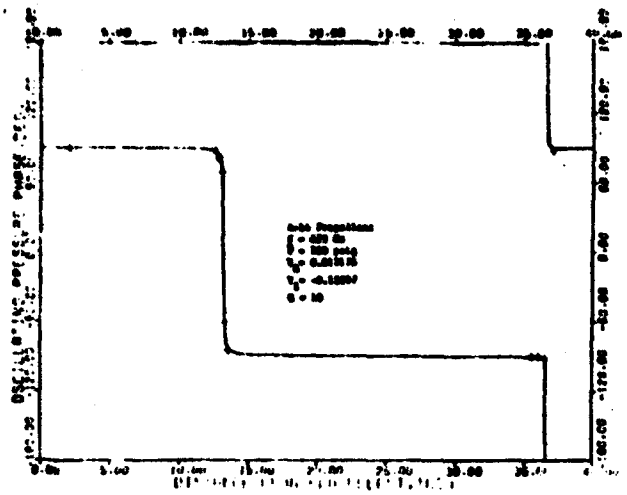

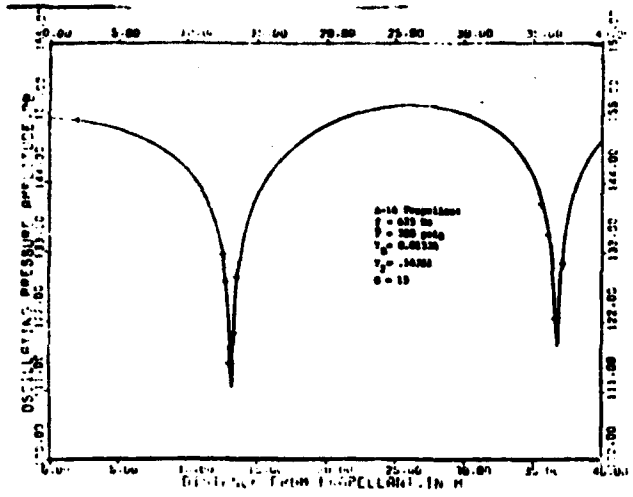

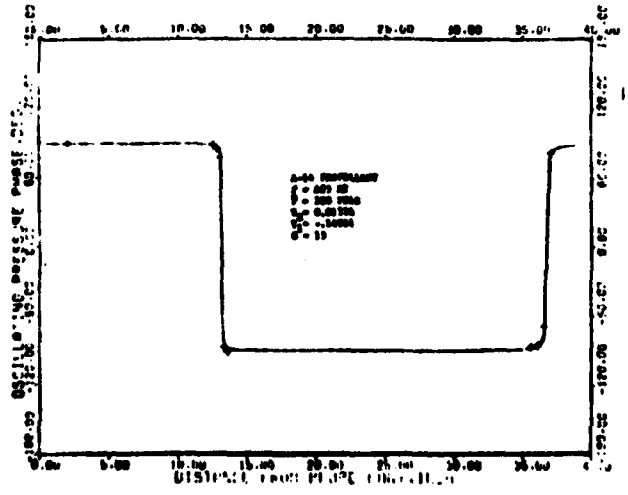

Conclusions

Significant improvements have been achieved in the data acquisition and data reduction procedures in the solid propellant impedance tube experiment, as demonstrated by the results provided in this paper. It has been shown that the real part of the burning propellant admittance Y_R remains constant during the steady state burn period while gas phase losses may very significantly during the same time period. Reproducibility of the measured quantities has been established as well as the capability of this experimental technique to measure gas phase losses in the impedance tube simultaneously with the measurement of the burning solid propellant surface admittance. Finally, it has been shown that the determined propellant admittance and gas phase losses result in impedance tube wave structures that are in excellent agreement with the measured acoustic pressure data.

References

1. "T-Burner Manual," Prepared by the Committee on Standarization of Combustion Instability Measurement in the T-Burner by the ICRIG Working Group on Solid Propellant Combustion, Chemical Propulsion Information Agency Publication No. 191 (1969).

2. Derr, R. L., "Development and Evaluation of the Variable-Area T-Burner," AFRPL-TR-72-97. Lockheed Propulsion Co. Redland, Calif.

3. Oberg, C. L., Ryan, N. W., and Baer, A. D., "A Pulsed T-Burner Technique," AIAA Journal, Vol. 6, No. 5, May 1968, pp.920-921.

4. Brown, R. S., Erickson, J. E., and Babcock, W. R., "Combustion Instability Study of Solid Propellants", AFRPL-TR-73-42, June 1973.

5. Strand, L. D., Magiwala, K.R., and McNamara, R. P., "Microwave Measurement of Solid Propellant Pressure-Coupled Response Function," AIAA Paper 79-1211, Presented at the AIAA/SAE 15th Joint Propulsion Conference, Las Vegas, Nevada, Jun 18-20, 1978.

6. Zinn, B. T., Salikuddin, M., Daniel, B. R. and Bell, W. A., "Solid Propellant Admittance Measurement by the Driven Tube Method," AFOSR-TR-73-2571, August 1975.

7. Salikuddin, M., and Zinn, B. T., "Adaptation of the Impedance Tube Technique for the Measurement of Combustion Process Admittances", AIAA Paper 79-0167, Presented at the 17th Aerospace Sciences Meeting, New Orleans, La, January 15-17, 1979.

8. Perry, E. H., "Investigation of the T-Burner and it's Role in Combustion Instability Studies," Ph.D. Thesis, Daniel and Florence Guggenheim Jet Propulsion Center, California Institute of Technology, Pasadena, California, May 1970.

9. Rubin, S., "Review of Mechanical Impedance and Transmission Matrix Concept," J. of Acoustical Society of America, Vol. 4, No. 5, May 1967.

10. Baum, J. D., "Experimental Determination of the Admittances of Solid Propellants by the Impedance Tube Method," Ph.D. Thesis, School of Aerospace Engineering, Georgia Institute of Technology, Atlanta, Georgia. To be Published.

APPENDIX II-A

MACH 3 HYDROGEN EXTERNAL/BASE BURNING

Douglas H. Neale, Sr. Research Engineer
James E. Hubbartt, Professor*
Warren C. Strahle, Regents' Professor*
School of Aerospace Engineering, Georgia Institute of Technology
Atlanta, Georgia

Abstract

Experimental studies of base pressure manipulation for an axisymmetric model at Mach 3 with simulated and actual external/base burning are described. Early work using contoured test section walls and cold gas base region injection is reviewed to demonstrate wake detail and length scale changes under the influence of simulated external/base burning. Tests with actual combustion of radially and axially injected hydrogen are then reported. Outstanding performance values with significant base drag reduction is shown for injection and burning directly in the near-wake (base burning). Current attempts at radial injection and burning in the free stream (external burning) have not yet succeeded. These tests, however, have defined an envelope within which external burning, if feasible, will presently be achieved.

Nomenclature

A_b	=	model base area
I	=	injection flow parameter (Figure 8)
I_{sp}	=	specific impulse (Figure 8)
M	=	Mach number
$\hat{M}$	=	molecular weight
$\dot{m}_{Bleed}$	=	injection mass flow
p	=	static pressure
p_1	=	free stream static pressure
p_o	=	total pressure (Pitot)
p_{o1}	=	free stream total pressure
p_b	=	base pressure
p_{bo}	=	undisturbed base pressure
R	=	model radius
RSP	=	rear stagnation point
T_o	=	stagnation temperature
T_{o1}	=	free stream stagnation temperature
V_1	=	free stream velocity
ρ_1	=	free stream density
γ	=	ratio of specific heats

Introduction

The application of burning, either in the near wake (base) or in the free stream adjacent to the near wake (external), can provide significant base drag reduction for projectiles operating at airbreathing altitudes. The coupling of attractive performance values with hardware simplicity makes this a particularly interesting propulsion concept.

The feasibility of external/base burning for propulsion in which the subsonic near-wake transmits elevated downstream pressures to the projectile base has been established. At present, however, no analytical model exists which adequately treats the complex base flows that result from combustion in and near the wake. A major contribution in understanding these flows, establishing and optimizing performance criteria and providing direction for theory can be supplied experimentally through detailed pressure and temperature measurements in the wake region for various modes of external/base combustion. Current studies in the School of Aerospace Engineering at Georgia Tech seek to provide this information.

A versatile experimental facility has been established for both simulation and actual combustion testing of axisymmetric external/base burning configurations at Mach 3 with a 5.72 cm dia. model in a 15.2 cm dia. test section (Reynolds number based on model diameter = 3.0×10^6). The blow-down facility is shown in Figures 1 and 2. The hollow cylindrical model is mounted in

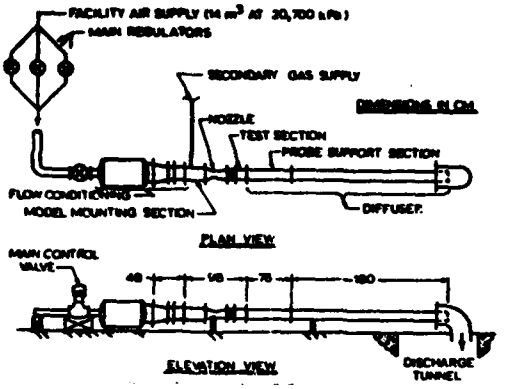

Figure 1. External/Base Burning Test Facility Schematic.

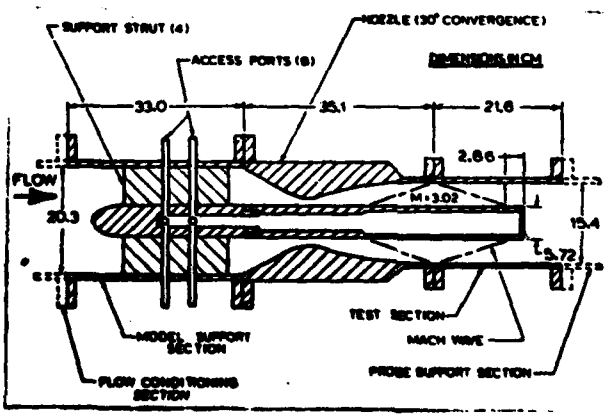

Figure 2. External/Base Burning Test Section Schematic.

* Members, AIAA

the subsonic flow, passes through the nozzle throat and terminates in the plexiglass test section. Gases for base region injection are brought in through four of the eight support strut access ports. The remaining four ports are used to bring model surface static pressure tubes to the external data acquisition system. Detailed pressure and temperature wake measurements are made with computer controlled traverses of probes introduced through the constant-area diffuser downstream of the test section. Run times range from 4-7 minutes depending on the stagnation pressure selected. Tunnel flow is not heated and stagnation temperatures drift downward from ambient to approximately-20°C during a typical test.

Program Review

The initial phase of the present comprehensive experimental study involved simulation of various external/base burning modes. These results have been reported previously and will be summarized here briefly to emphasize important findings and to trace program evolution.[1,2]

First, measurements were made to provide undisturbed Mach 3 axisymmetric base flow detail for theoretical model comparisons. Typical results are shown in Figures 3 and 4 in which radial and axial Mach number and pressure profiles are presented. These measurements reveal presence of a base recirculation region, wake thickness variation, streamline curvature, base pressure and near-wake length as defined by the location of M = 1 on the centerline.

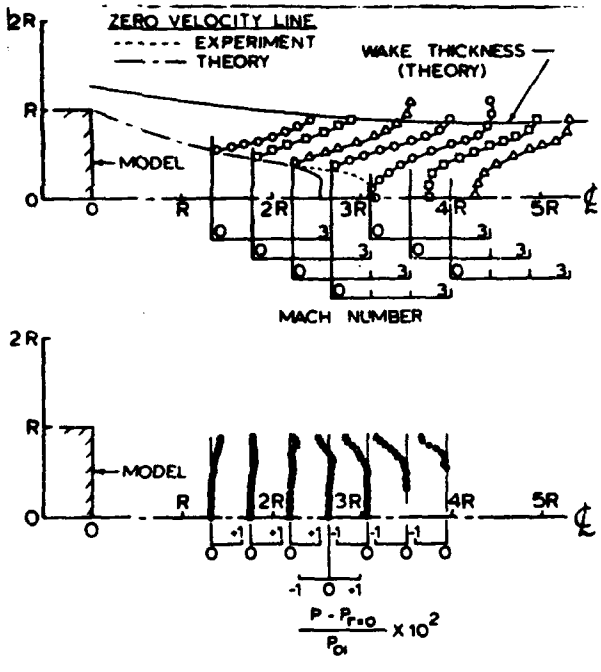

Figure 3. Near Wake Radial Mach Number and Static Pressure Distributions (Zero External Compression).

Second, tests with simulated axisymmetric external burning were completed using contoured test section walls. The wall contours were designed to focus compression fields on the wake representing a reasonable fixed total heat addition applied in the free stream over three successively shorter heating lengths (Compression Sections I, II and III). One additional test section (IV) was fabricated to show the effects of discrete burning for comparison with the equivalent axisymmetric case (II). Each test section was translated relative to the model base to investigate the importance of disturbance location. Figure 5 shows base pressure elevation to free stream values and above for most cases with an optimum axial position depending on the simulated heating severity. Base pressure rise is reduced if disturbances are applied discretely rather than axisymmetrically. Nevertheless, for all cases examined, base pressure was still boosted sufficiently to eliminate base drag. The effect of axisymmetric external compression on near-wake length scales is shown in Figure 6. Wake lengths are strongly controlled by external disturbance location as reflected by changes in the position of the rear stagnation and M = 1 points on the centerline. In addition, wake lengths decrease with increasing compression severity for a given axial location.

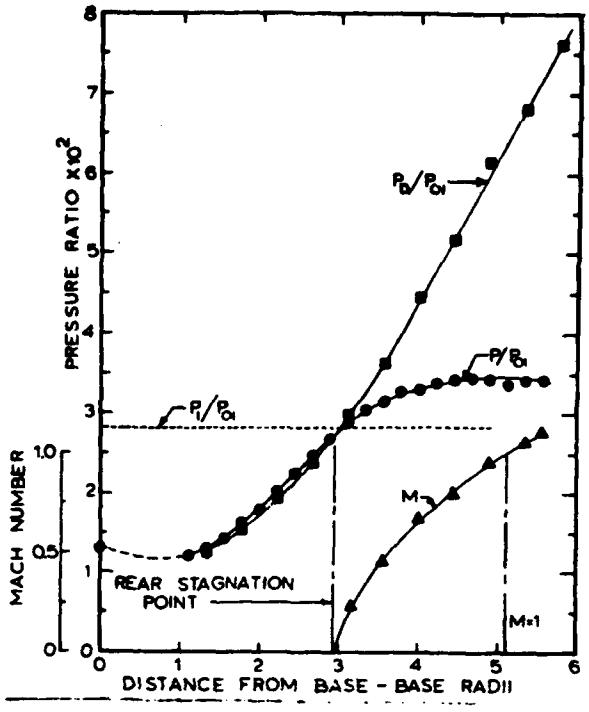

Figure 4. Near Wake Centerline Pressure and Mach Number Distributions (Zero External Compression).

Further simulation studies of discrete external burning were completed using solid pegs to model the blockage effects of radial fuel injection jets (no external compression). Figure 7 compares wake centerline structure for this case with the original clean base data. The disturbances generated by the pegs result in a mild decrease in base pressure and a significant shortening of the near-wake.

The third segment of testing involved simulation of base burning with cold gas injection into the near-wake region. The model was fitted with a porous sintered-metal base plate for uniform injection and tests were run with

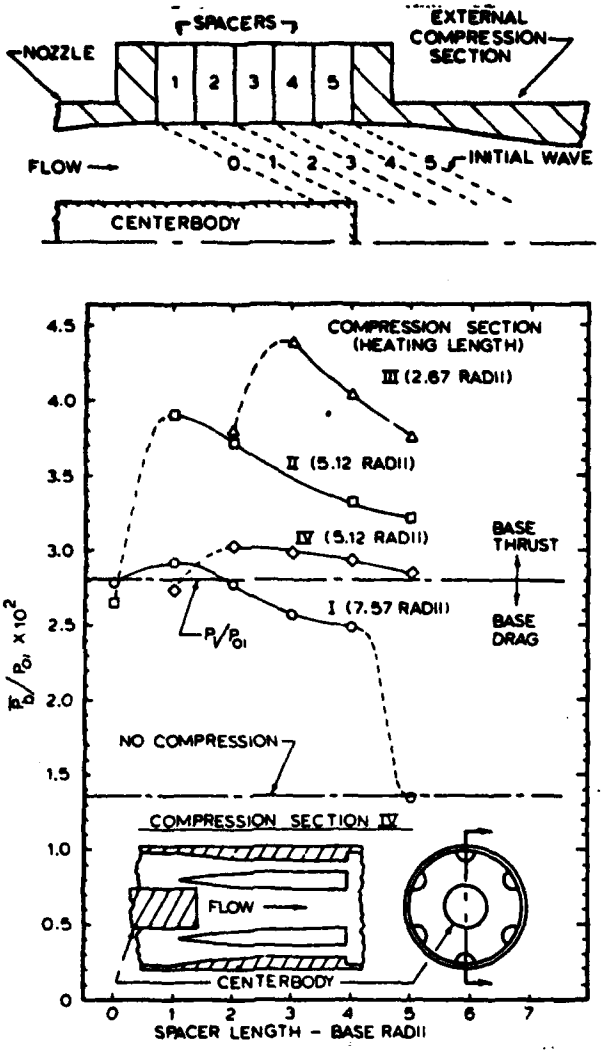

Figure 5. Base Pressure Manipulation with Axisymmetric and Discrete External Compression.

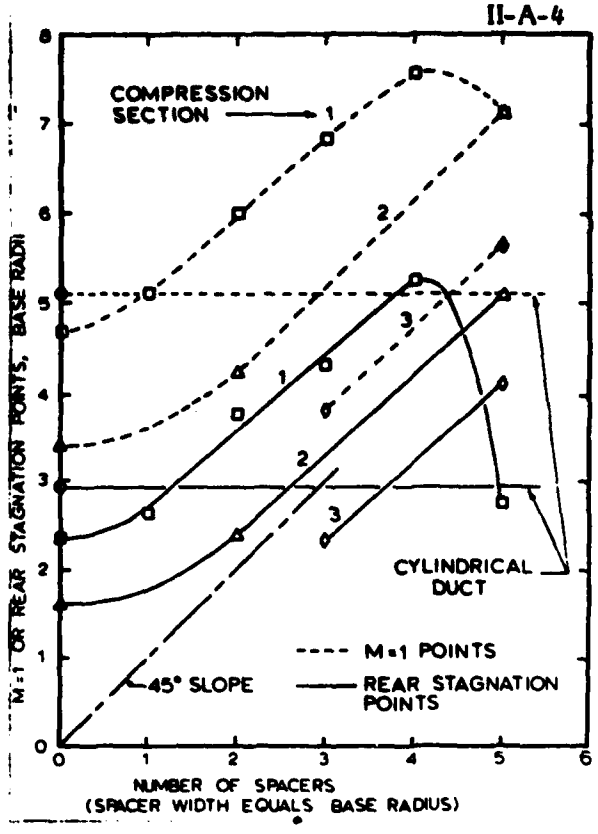

Figure 6. Effects of External Compression Strength and Location on Near Wake Length Scales.

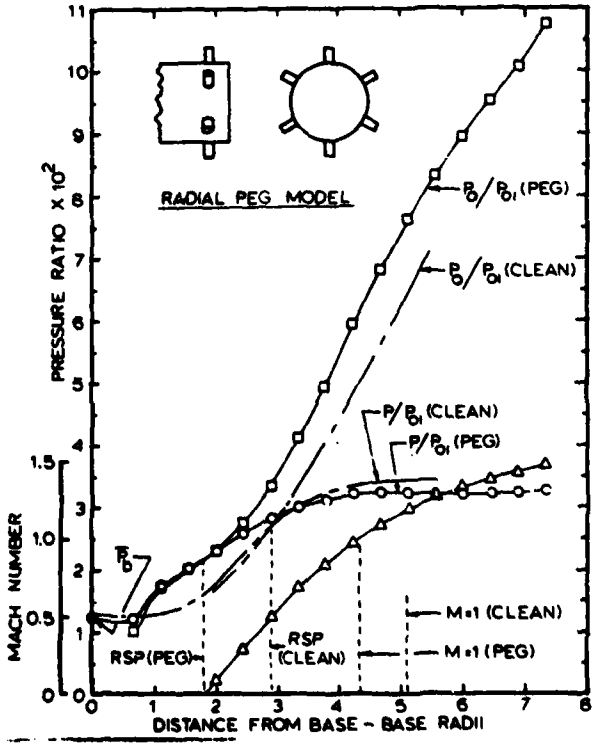

Figure 7. Comparison of Centerline Pitot Pressure, Static Pressure and Mach Number Distributions for the Peg and Clean Base.

three gases displaying a range of molecular weights. Base pressure elevation and performance values for nitrogen (air), helium and hydrogen are presented in Figure 8 showing the expected gains with decreasing molecular weight (increased volumetric flow). Figure 9 gives a successful correlation of base pressure rise with injection rate parameter modified by a factor involving molecular weight and specific heat ratio of the injected gas[3]. Figure 10 gives typical static pressure and Mach number distributions in the near wake for a moderate air injection rate. A recirculation region persists for this case, although the region has been axially displaced with base bleed. Tests at higher injection rates revealed that the recirculation bubble can be completely blown away.

The final phase of non-combustion work combined simulated axisymmetric external compression with cold gas base bleed. Wake length and base pressure alterations for a range of base injection parameter values with and without external compression are shown in Figure 11. Without compression, base pressures rise modestly and wake lengths increase significantly with increasing base bleed. When

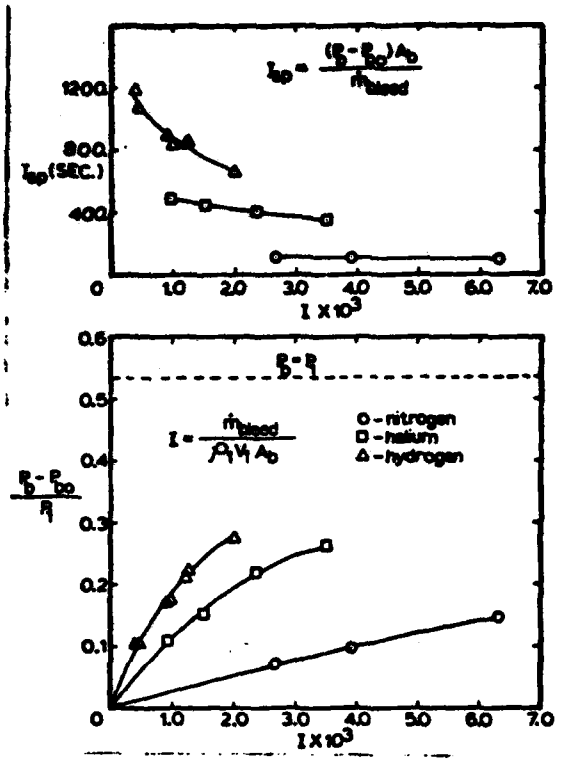

Figure 8. Base Pressure Rise and Performance for Alternate Cold Gas Base Bleed.

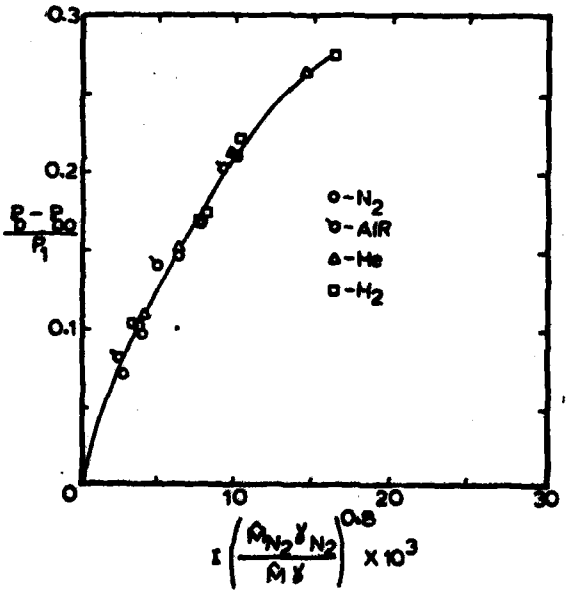

Figure 9. Base Pressure Rise Correlation for Cold Gas Base Injection.

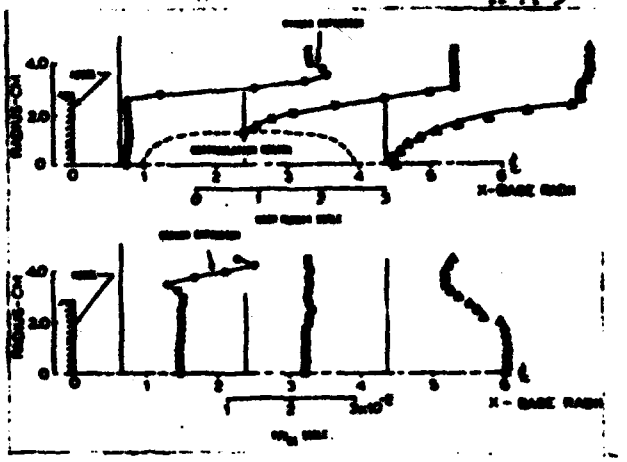

Figure 10. Typical Near-Wake Mach Number and Static Pressure Profiles with Base Injection (I = .010).

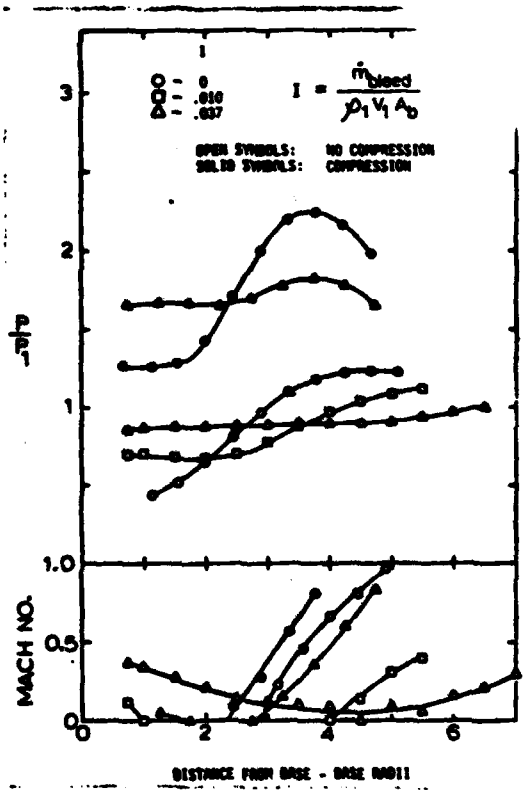

Figure 11. Wake Detail and Length Scale Changes for Cold Gas Bleed with and without External Compression.

external compression is imposed (Compression Section II) along with base bleed, base pressure is further elevated suggesting the possible additiveness of the two effects. The imposition of external compression, however, strongly controls wake length such that there is little difference between the length with zero bleed and zero compression and the length with high bleed (I = .037) and compression.

Current Work

After completion of external/base burning simulation studies, the facility was modified for controlled base region injection and burning of hydrogen. Initial tests were designed to evaluate performance and detail wake structure for hydrogen base burning with injection directly into the near-wake through a porous base plate. The tunnel was operated at 930 kpa (135 psia) simulating Mach 3 flight at approximately 10,700 m (35,000 ft). However, since tunnel heating is not available, the resulting stagnation temperature is approximately 330°C (600°F) below the corresponding Mach 3, 10,700 m value. Under these severe conditions, attempts at base region ignition with a 6000 volt A.C. spark source were unsuccessful. As an alternative to more powerful spark sources, a pyrotechnic compound paste was employed to achieve ignition. The paste was coated on the surface of an "L" shaped cylindrical igniter probe introduced to the tunnel downstream of the test section. The active portion of the igniter was located along the wake centerline from two to five model radii downstream of the base. Paste firing was initiated with an embedded hot nichrome filament. A typical firing is shown in Figure 12.

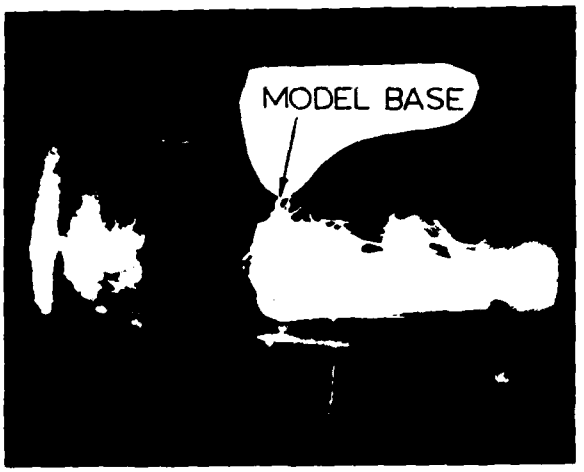

Figure 12. Pyrotechnic Igniter Firing in Near-Wake with Hydrogen Base Bleed.

Early tests with burning revealed instability and flameout upon removal of the igniter probe. The problem was overcome by installing four tabs of catalytic platinum gauze on the base plate. The final igniter configuration utilizing a consummable base mounted sting is shown in the top panel of Figure 13.

Typical operation with hydrogen base burning at Mach 3 is shown in Figure 14. For injection rates greater than $I \approx 4.0 \times 10^{-4}$ the visible combustion region extends four to five model diameters downstream of the base plane while remaining attached to the base. For lower injection flows the luminous region diminishes rapidly in size and intensity and is closely confined to the base. Observation of igniter flare particle paths and pitot-static pressure measurements with burning indicate that, even at high injection rates, a recirculation region persists in the wake. Temperature measurements in the wake with platinum-platinum, 10% rhodium thermocouples show that combustion exists throughout the visible conical region. These measurements show further that burning extends into the shear layer. Temperatures approaching the thermocouple useful limit of 1600°C were only encountered within two or three model radii of the base for even the highest injection rates attempted. This value is significantly below the stoichiometric flame temperature for hydrogen and indicates the lean nature of the wake.

The performance of hydrogen base burning at Mach 3 is shown in Figure 15 for the range of flows and configurations investigated. The lower portion of Figure 15 shows that base pressure rises with increased hydrogen injection and approaches free stream static pressure (near-elimination of base drag). The diminishing returns of increased injection, however, are reflected by the rapid decline of specific impulse values shown in the upper portion of the figure. Nevertheless, a significant reduction

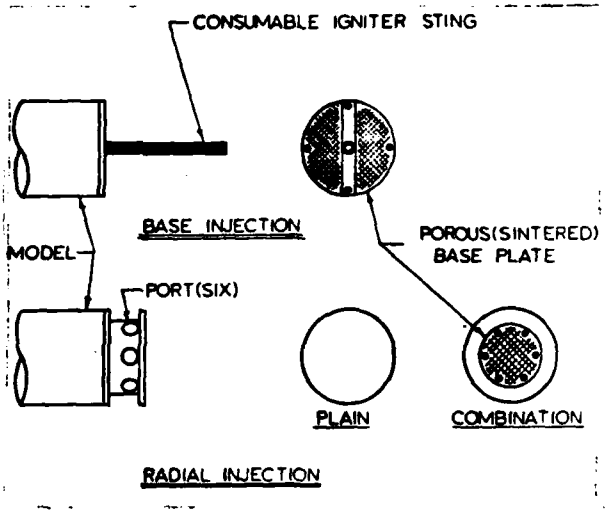

Figure 13. External/Base Burning Injection Configurations.

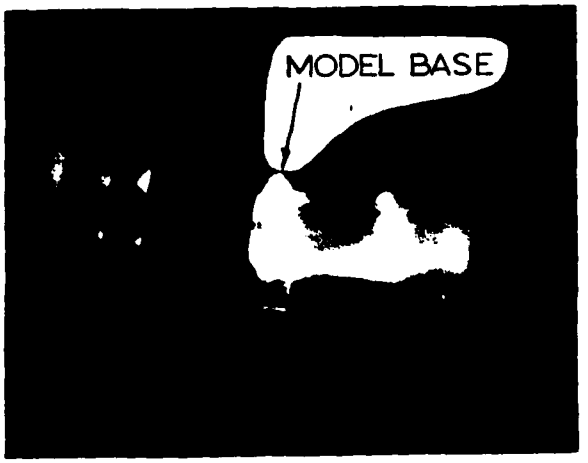

Figure 14. Hydrogen Base Burning at Mach 3.

in base drag at impressive values of I_{sp} have been demonstrated. For example, these tests show an 80% reduction in base drag with I_{sp} = 5000 sec. and a 50% reduction with I_{sp} = 12000 sec. For comparison, Figure 16 presents Mach 3 performance for a hydrogen burning ramjet with various inlet designs. It is clear that base burning is strongly competitive with ramjet operation for this application.

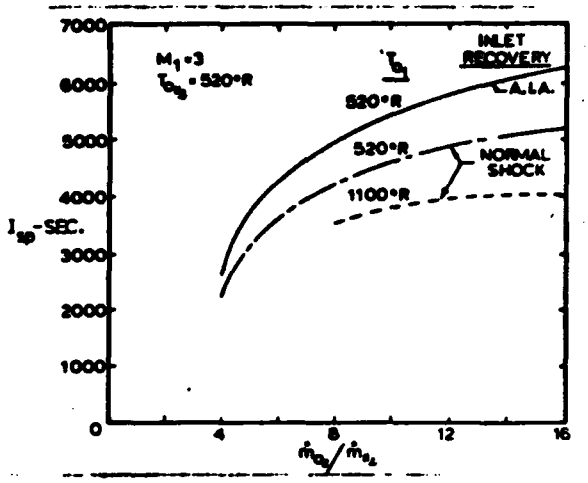

Figure 16. Mach 3 Ramjet Performance.

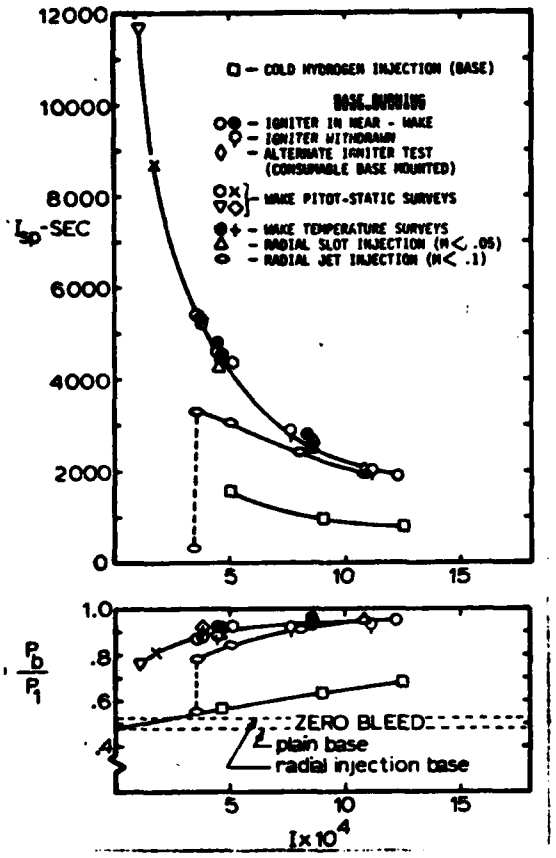

Figure 15. Base Burning Performance at Mach 3.

Further base pressure studies were completed by combining base burning with two cases of simulated axisymmetric external burning and one case of simulated discrete external burning (use of contoured test sections from original experiments). The first two panels (left to right) in Figure 17 show that the combined effect of simultaneous base and simulated external burning is very nearly the sum of the individual contributions. The third panel reinforces this finding for an alternate test section. In all three cases the base pressure was boosted above free stream static pressure yielding a condition of base thrust. Panel three, in fact, shows an instance in which the base thrust is sufficiently high to eliminate all drag on a well designed vehicle.

The last panel in Figure 17 shows results using simulated discrete external burning (equivalent to axisymmetric Compression Section II). Once again, the measured base pressure with base burning and compression is very close to the simple sum of the individual experimental values. Comparison of panels three and four confirm earlier findings that the application of external burning in discrete plumes diminishes the base pressure boost obtained with axisymmetric burning; however, a condition of base thrust is still demonstrated for this case.

Tests with radial injection of hydrogen for attempted "pure " external burning were next attempted. A modified base configuration using six equally spaced injection ports recessed in an annular channel was used for these studies (Figure 13). The channel design was included to provide a cavity in which favorable mixing and residence times would exist for ignition and sustained burning. As with the base burning tests, a pyrotechnic compound served as the source of ignition. The channel was lined with the compound and flared with a hot nichrome filament. Platinum gauze was used as a catalyst in the channel but not in the base region.

Initial tests were performed with subsonic injection through six, 9.5 mm orifices yielding jet velocities ranging from 50-170 m/sec ($I = 3\text{-}11 \times 10^{-4}$). Ignition was readily achieved for $I \geq 4 \times 10^{-4}$ with burning apparent both confined within the channel and in the wake as shown in Figure 18 (wake burning outlined). Reduction of hydrogen flow resulted in progressively weaker burning (decreasing luminosity) in the base region with wake combustion terminating abruptly at $I \approx 3.25 \times 10^{-4}$. Burning in the channel persisted, however, for even lower flows and was made evident by the continued glow of the platinum gauze. Base burning probably could have been extended to lower injection rates by using platinum mounted on the base, but such efforts were not pursued.

Performance values for "external" burning with subsonic discrete jet radial injection of hydrogen are included in Figure 15. As might be expected from test observations, this mode of operation more resembles base burning with direct injection rather than external burning with radial injection and discrete plume combustion in the free stream. The loss of wake burning is shown clearly in the precipitous drop in base pressure and corresponding I_{sp}. With burning in the channel alone, the base pressure is very nearly the same as for the radial injection model configuration with zero hydrogen flow. Since burning in the channel provides a negligible improvement in base pressure, its primary value must be considered as that of a possible flameholder for the radially injected stream at some sacrifice in I_{sp}. Base pressure and I_{sp} values for both the base and subsonic radial injection modes converge at the

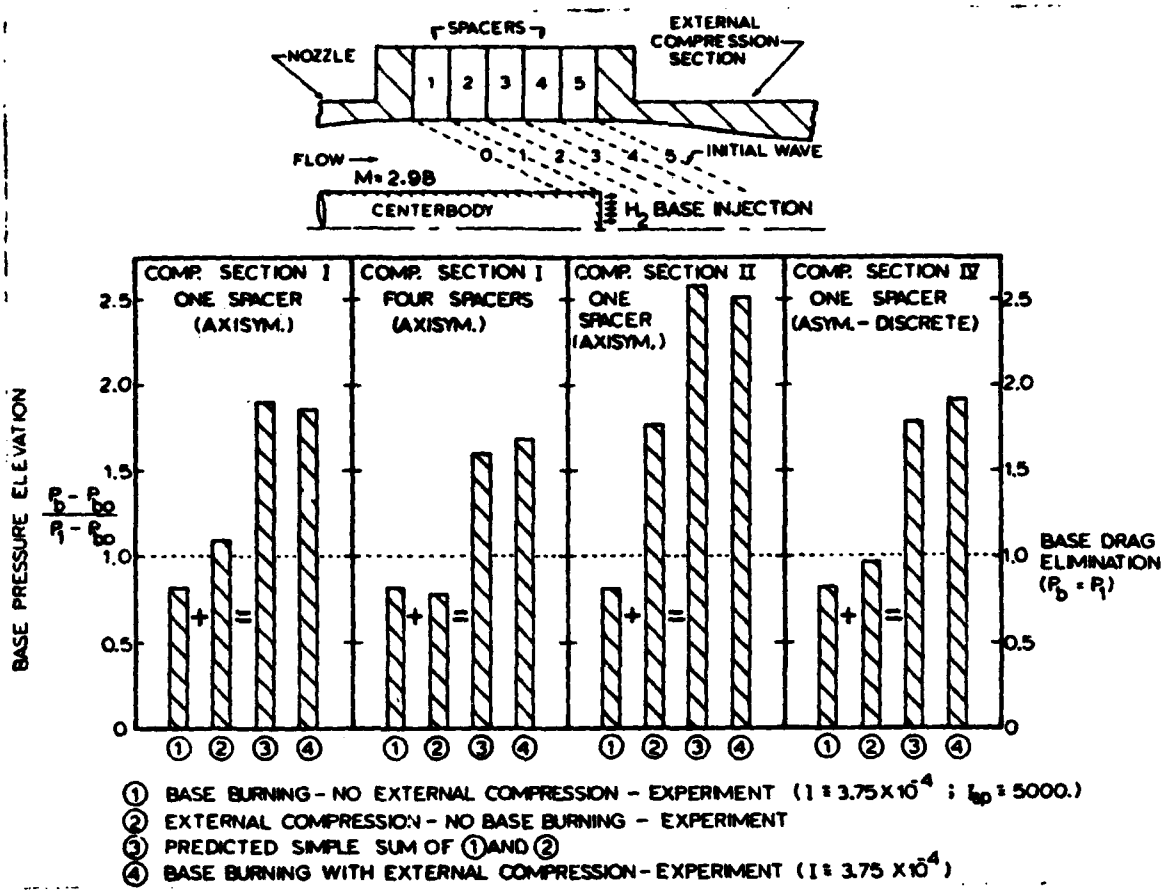

Figure 17. Mach 3 Hydrogen Base Burning withSimulated External Burning.

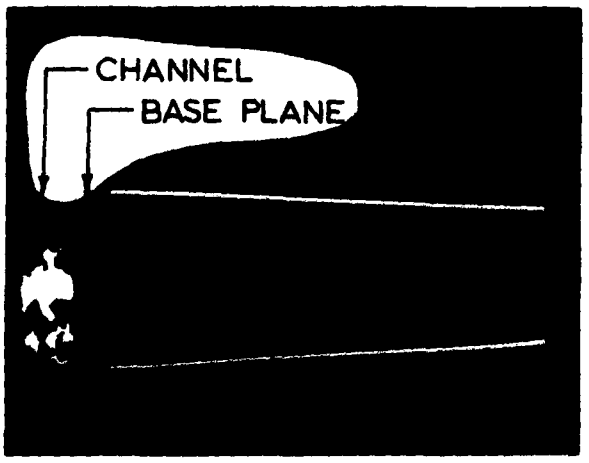

Figure 18. External/Base Burning of Hydrogen at Mach 3 with Subsonic Radial Injection.

higher injection rates. This convergence suggests that, with larger flows, increasing percentages of the radially injected hydrogen escape the channel and are entrained and burned in the near-wake region.

The results of the subsonic radial injection tests indicate that, in order to have some chance for true external burning, significant free stream penetration with the fuel jets must be achieved. To that end, the original orifices were plugged and re-drilled to 1mm dia. for choked operation at flows comparable to those used in the previous subsonic injection tests. Platinum gauze tabs were fastened to the base as well as in the channel. Attempts to ignite at $I = 8 \times 10^{-4}$ and 11×10^{-4} (jet Mach numbers, based on cavity to free-stream pressure ratio, of 2.14 and 2.42 respectively) were repeatedly unsuccessful. Local jet burning was observed within the groove during the pyrotechnic flare; however, once the source of ignition was removed, all burning ceased. Unlike earlier tests with subsonic injection, no combustion was initiated in the wake region. It is apparent that the higher injection velocity used to obtain free stream penetration for potential external burning resulted in channel conditions unfavorable for sustaining an ignition source. In addition, the absence of base combustion indicates either that the high velocity injection has altered the mechanism by which channel ignition begets base ignition or that the increased free-stream jet penetration has significantly reduced hydrogen entrainment in the wake. The need for testing

radial injection velocities between the extremes just described is evident. These tests, in which orifice diameters are enlarged incrementally to provide the desired velocity range while maintaining comparable hydrogen flows, are in progress. Included in these tests are attempts at igniter firings in the base region as well as in the channel to ascertain the presence of hydrogen in the wake.

Concurrent with tests varying radial injection Mach number are those in which supplemental base bleed is introduced. The original radial injection base has been modified for these experiments as shown in Figure 13. One test series with this configuration using only channel ignition has been completed. Hydrogen injection was split approximately 60% - 40% in favor of base injection with attempted ignition at $I = 10.9 \times 10^{-4}$ (based on total hydrogen flow). This condition resulted in a radial jet Mach number of 2.07 and sufficient hydrogen base bleed, as determined from original base burning tests, to assure wake combustion. Sustained channel burning was achieved for this case but base burning was not initiated. Total hydrogen injection was decreased in steps to $I = 3.67 \times 10^{-4}$ (M = 1.50) with no loss in channel burning. Base pressure remained nearly constant throughout the range and was only about 20% higher than for this identical base configuration with zero injection. These results confirm the earlier suggestions that the higher radial injection rates tend to destroy the mechanism which induces wake ignition from channel ignition and that channel burning has little effect on base pressure. It is probable that most of the modest base pressure rise shown is attributable to the hydrogen bleed directly into the base region. The most significant result of this test series, however, is the lack of sustained burning in the radial jets away from the channel confines even though a continuous, stable source of ignition is present.

The experiments performed to this time have defined the limits within which external burning with hydrogen can be obtained with the present facility. At one extreme, low subsonic radial injection results in an essentially base burning condition. At the other extreme, injection at Mach numbers exceeding about 2.1 renders maintenance of a flame holding region impossible for this configuration. If true external burning is to be achieved, it will exist within the envelope of injection Mach numbers and mass flows under current examination.

Summary and Conclusions

Tests with axial injection and burning of hydrogen in the near-wake have shown that significant base drag reduction and excellent performance can be combined. Drag reductions of 80% and 50% have been demonstrated for specific impulse values of 5000 sec and 12000 sec respectively. Near-elimination of base drag appears to be an upper limit for this mode of external burning, however, and can only be achieved with heavy penalties in I_{sp}.

Pure external burning with radial injection and combustion in the free stream offers the hope of generating base thrust by elevating wake pressures above free stream levels. Tests with low radial injection velocities (M < 0.1) result in no appreciable free stream jet penetration. Hydrogen is apparently swept into the wake and burns as though it has been injected directly through the base. Accordingly, this mode performs similarly to but less efficiently than the direct base burning mode. Radial injection with comparable mass flows through choked nozzles to increase jet penetration has not yet yielded true external burning. Flameholder combustion for jet Mach numbers greater than about 2.1 cannot be sustained. Successful flameholder operation has been demonstrated for jet Mach numbers from 1.5 to 2.1, but propagation of combustion into the free stream is not evident. Operation in this mode gives base pressures only slightly higher from those with no injection at all.

Current tests exploring jet injection Mach numbers between the extremes so far investigated should reveal whether or not pure external burning is feasible. These tests are being run with base as well as flameholder ignition to ascertain the presence of combustible mixtures in the wake. In addition, cases are being examined in which direct base bleed is combined with radial injection to verify and supplement the results already in hand.

Bibliography

1. Neale, D. H., Hubbartt, J. E., Strahle, W. C. and Wilson, W. W., "Effects of External Compression on an Axisymmetric Turbulent Near Wake", AIAA Journal, Vol. 16, No. 9, September, 1978.

2. Neale, D. H., Hubbartt, J. E. and Strahle, W. C., "Effects of Axial and Radial Air Injection on the Near Wake with and Without External Compression", Technical Note, AIAA Journal, Vol. 17, No. 3, March, 1979.

3. Freeman, L. M. and Korkegi, R.H., "Projectile Aft-Body Drag Reduction by Combined Boat-Tailing and Base Blowing", AFAPL-TR-75-112, February, 1976.

APPENDIX IV-A

TURBULENCE GENERATED PRESSURE FLUCTUATIONS IN A ROCKET-LIKE CAVITY

Warren C. Strahle* and Douglas H. Neale†

Georgia Institute of Technology
Atlanta, Georgia 30332

Abstract

Theoretical acoustics applied to the pipe flow turbulence problem in a configuration which was experimentally investigated yields an analytical formula for random pressure fluctuations generated by the turbulence. In order to calculate the pressure fluctuations, it is found that certain spatial correlations of the fluctuation in the square of the axial velocity are needed. These are measured by hot film anemometry, as are the pressure fluctuations, in a fully developed pipe flow and the theory is shown to be semi-quantitative; a lower bound to the pressure fluctuation emerges. Application to the problem of pressure fluctuation in rocket motors and attendant vibration are indicated.

Nomenclature

A	=	pipe cross section area
a	=	pipe radius
c	=	speed of sound
f	=	quantity defined by Eq. (9)
g	=	Green's function for H
g_w	=	Green's function for plane wave acoustics problem
H	=	Bernoulli enthalpy
J_m	=	Bessel function of order m
ℓ	=	duct length
n	=	outward unit normal vector
p	=	pressure
S_{ij}	=	cross spectral density between signal i and signal j
s_{mn}	=	Eigenvalue in the problem for H
s	=	entropy
t	=	time
t_o	=	sample time in Fourier transform
$\underline{u}$	=	vortical velocity vector
V	=	volume
$\underline{v}$	=	velocity vector
$\underline{w}$	=	potential velocity vector
x_i	=	Cartesian coordinate in i^{th} direction
x	=	distance along duct
x_o	=	distance along duct
β	=	quantity defined by Eq. (10)
δ	=	Dirac delta function
ρ	=	density
ω	=	radian frequency
φ	=	velocity potential

Subscripts

t	=	transverse part
oo	=	plane approximation
cor	=	correlation scale
∞	=	value at infinity in the potential field
ω	=	Fourier transform
1	=	x-direction

Supercripts

′	=	fluctuation
–	=	mean or ensemble average

Introduction

Pressure fluctuations inside of a rocket motor cavity are one source of motor vibrations. Typically, the broad band random pressure fluctuations which are normally considered reasonable to tolerate are of the order of 1% rms magnitude when compared with the mean chamber pressure. Depending upon the frequency content of this background noise in the pressure, however, this 1% level can cause vibration troubles. Especially if the excitation frequencies overlap a longitudinal mode frequency of the chamber cavity, strong longitudinal resonances may occur with attendant thrust fluctuations. Such fluctuations in thrust can be more than the 1% level of the pressure fluctuations because the pressure field is spatially variant and differentially acts on the head and aft ends of the cavity. This kind of problem is currently believed to exist in one large system.(1)

There are several potential sources for the background pressure fluctuations, and many of these have been considered in Ref. (2). However, the results of Ref. (2) contain an ambiguity in interpretation due to the simplified theory employed, and it is desireable to use a more accurate theory to treat the problem. The approach here is to look at the problem of turbulence induced pressure fluctuations, both theoretically and experimentally, with a view towards prediction of the pressure fluctuation level in rocket motors, due to the turbulence field. There will necessarily be left out, at this point, other potential sources of vibration such as combustion noise.(2)

The approach here is to first look at a relatively well characterized turbulence field, that of pipe flow, encountering a rocket-like flow termination, that of a choked deLaval nozzle. The purpose is to see the accuracy with which the pressure fluctuation levels may be predicted by theory, given appropriate measurements of the turbulence field. If satisfactory answers may be obtained, the theory may be applied to rocket motors as further information becomes available on the rocket motor turbulence field, as given, for example,

by the computations of Ref. (3). For the moment, however, this may be regarded as a fundamental investigation of turbulence generated pressure fluctuations in a given type of interior flow problem.

Analysis

Consider the configuration of Fig. 1, where a pipe flow is terminated by a choked nozzle and is also the configuration in the experimental results to follow. Except very near the walls the inlet flow is nearly potential; there follows a transition to turbulent flow and finally a fully developed purely vortical turbulent pipe flow. In the fully developed turbulent region it is the mean flow which is purely vortical, but superimposed is a turbulent fluctuation which has pressure fluctuations associated with it. The calculation of the pressure field is the issue here.

Consider the formulation of the conservation equations as given by Yates and Sandri.[4]

$$\frac{D}{Dt}\left(\frac{\partial\varphi}{\partial t}+\frac{|\nabla\varphi|^2}{2}\right)-a^2\nabla^2\varphi=\frac{DH}{Dt}-T\frac{Ds}{Dt} \tag{1}$$

$$\nabla^2 H=-\frac{\partial^2 u_i u_j}{\partial x_i \partial x_j}-\frac{\partial^2}{\partial x_i \partial x_j}\left(u_j\frac{\partial\varphi}{\partial x_i}\right)-\frac{\partial}{\partial x_j}\left(\frac{\partial u_j}{\partial x_i}\frac{\partial\varphi}{\partial x_j}\right)+\frac{\partial}{\partial x_i}\left(T\frac{\partial s}{\partial x_i}\right) \tag{2}$$

$$\underset{\rightarrow}{v}=\underset{\rightarrow}{w}+\underset{\rightarrow}{u}\qquad \underset{\rightarrow}{w}=\nabla\varphi\qquad \nabla\cdot\underset{\rightarrow}{u}=0 \tag{3}$$

$$\frac{Ds}{Dt}=0 \tag{4}$$

$$s=s(p,h)=s_o=0=\ln\frac{h}{h_o}-\frac{\gamma-1}{\gamma}\ln\frac{p}{p_o} \tag{5}$$

In the above, all effects of transport phenomena are neglected so that when considering fluctuations it is understood that the frequency domain under consideration is that of the energy containing eddies of the turbulent flow. A companion equation to Eq. (2) has been omitted; it is the vorticity conservation equation. H is the Bernoulli enthalpy given by

$$H=h+\frac{\partial\varphi}{\partial t}+\frac{|\nabla\varphi|^2}{2} \tag{6}$$

and plays a fundamental role in the generation of noise in Eq. (1). In the potential flow region of the pipe flow $\nabla^2 H = 0$ and $H = H_\infty$, a constant. In the fully developed pipe flow region such a relation does not hold, but Eq. (2), using the consequence of Eq. (4), becomes

$$\nabla^2 H = - \frac{\partial^2 u_i u_j}{\partial x_i \partial x_j} - \frac{\partial^2 \left(u_j \frac{\partial \varphi}{\partial x_i} \right)}{\partial x_i \partial x_j} - \frac{\partial}{\partial x_j} \left(\frac{\partial u_i}{\partial x_i} \frac{\partial \varphi}{\partial x_j} \right) \tag{7}$$

It will be assumed that the majority of the experimental configuration is filled with the fully developed pipe flow so that Eq. (7) is to be solved.

It is assumed that the potential velocities are much less than the vortical velocities, which may be verified after the fact, so that Eq. (7) becomes

$$\nabla^2 H = - \frac{\partial^2 (u_i u_j)}{\partial x_i \partial x_j} \equiv - f(x_i, t) \tag{8}$$

The genesis of Eq. (2) is the momentum equation

$$\nabla H = \nabla \left(\frac{|\nabla \varphi|^2}{2} \right) - \frac{\partial \underset{\rightarrow}{u}}{\partial t} - \underset{\rightarrow}{v} \cdot \nabla \underset{\rightarrow}{v} \tag{9}$$

which is zero on the walls of the tube because all velocities must vanish. At the head end of the tube $\nabla H = 0$ since the flow is a potential flow. At the nozzle end, however, more care is required. What is needed to solve Eq. (8) is the boundary condition $\nabla H \cdot \underset{\rightarrow}{n}$ on all boundaries of the flow region.

Splitting the velocity into its mean plus fluctuating components and noting that at the nozzle end $\overline{\nabla \varphi} = 0$ and $\underset{\rightarrow}{\overline{v}} = u_1 (r)$, the $x_1 = x$ component of Eq. (9) becomes

$$\nabla H \cdot \underset{\rightarrow}{i} = - \frac{\partial u_1}{\partial t} - \underset{\rightarrow}{u} \cdot \nabla u_1 \equiv \beta \tag{10}$$

In Eq. (10) the fluctuations in the potential field have been neglected as compared with those in the vortical (turbulence) field.

Now it is presumed tht the vortical field is known or can be measured so that the right hand sides of Eqs. (8) and (10) are known. The solution may be written in terms of the Green's function for the Poisson equation

$$\nabla^2 g(x_i, x_{o_i}) = - \delta(x_i - x_{o_i}) \tag{11}$$

$\nabla g \cdot \underset{\rightarrow}{n} = 0$ on the side wall and exit plane

$g = 0$ at the entrance plane

Manuscript
Page No. 5

whereby

$$H - H_\infty = \int_V g(x_i, x_{o_i})\, f(x_{o_i})\, dV + \int_{A_e} g\, \beta\, d\, A \qquad (12)$$

The Green's function may be constructed by standard methods and is given by

$$g = \sum_{m,n=0}^{\infty} F_{mn}(x, x_{o_i})\, J_m(s_{mn} r) \begin{matrix} \cos m\theta \\ \sin m\theta \end{matrix} \qquad (13)$$

where F_{mn} satisfies

$$\frac{d^2}{dx^2} F_{mn} - s_{mn}^2 F = - \frac{\Theta(\theta_o)\, J_m(s_{mn} r_o)\, \delta(x-x_0)}{\pi\, a^2\, \Lambda_{mn}}$$

$$\Lambda_{mn} = \frac{1}{\epsilon_m}\left[1 - \left(\frac{m^2}{s_{mn} a}\right)^2\right] J_m^2 (s_{mn} a)$$

$\epsilon = 1$ if $m = 0$
$= 2$ if $m \geq 1$

and s_{mn} is determined by

$$s_{mn}\, J_m'(s_{mn} a) = 0$$

The term in the solution with m = n = 0 has only an axial dependence and corresponds to cross section averages of quantities. Emphasizing this,

$$g = g_{oo} + g_t \qquad H - H_\infty = H_{oo} + H_t - H_\infty$$

where the t subscript denotes the part which is due to transverse dimensions of the duct.

The crucial step is now taken to ignore the higher terms in g other than g_{oo}. It will be argued later that this will yield a lower bound on the pressure generated by the turbulence. Constructing g_{oo} from Eqs. (14), it is found

$$g(x,x_o) = g_{oo} = - \frac{x}{\pi a^2} \qquad x_o \geq x$$

$$g(x,x_o) = g_{oo} = - \frac{x_o}{\pi a^2} \qquad x_o \leq x$$

The fluctuation in H, $H' = H_{oo} - H_{\infty}$, is then constructed from Eq. (12) after considerable manipulation and noting that $\nabla \cdot \underline{u} = 0$. The result is

$$H' = \frac{1}{A} \int dA \, (u_1 u_1)' \tag{15}$$

This result, remarkable in its simplicity, says that Bernoulli enthalpy fluctuations are merely created by the fluctuations in the square of the axial velocity components.

Now moving to construction of the unsteady potential field, it is readily shown that for low Mach number, which is assumed, and sufficiently small fluctuations in the potential field, which has already been assumed, Eq. (1) reduces to

$$\frac{\partial^2 \varphi'}{\partial t^2} - \bar{c}^2 \nabla^2 \varphi' = \frac{\partial H'}{\partial t} \tag{16}$$

Since H' is purely planar by the above developments, a plane wave solution to Eq. (16) is adequate. After taking the Fourier transform of Eq. (16), the solution is

$$\varphi_\omega = \frac{i\omega}{A\bar{c}^2} \int dV(x_o) \, g_\omega(x, x_o) \int dA \, (u_1 u_1)'_\omega \tag{17}$$

where g_ω is the plane wave Green's function for the duct. It, again, may be constructed by standard means and depends upon the impedance of the duct walls and end planes. If, as in the experiment, it may be assumed that the walls are hard, the open end is like an open ended organ pipe and the nozzle end behaves like a hard wall,[6] an especially simple form for g_ω emerges. It is

$$g_\omega = \frac{\sin k(\ell - x_o - x) - \sin k(\ell - x_o + x)}{2ikA \cos k\ell} \qquad x < x_o$$

$$g_\omega = \frac{\sin k(\ell + x_o - x) + \cos k(x_o - \ell + x)}{2ikA \cos k\ell} \qquad x \geq x_o \tag{18}$$

Since all terminations and walls were assumed perfectly reflecting, Eq. (18) contains resonances of infinite magnitude. It is not hard to show, however, that Eq. (18) is valid around the troughs even when the walls are nearly perfectly reflecting. Equation (18) will be used, therefore, away from the resonance frequencies.

Finally, the linearized, low Mach number form of the equation of state, Eq. (5), using Eq. (6) becomes

$$p' = \rho_o (H' - \frac{\partial \varphi'}{\partial t})$$

$$p_\omega = \rho_o (H_\omega + i\omega\varphi_\omega)$$

Using this with Eqs. (15) and (17), the final relation for the pressure transform becomes

$$p_\omega(x) = \rho_o \frac{1}{A} \int dA\ (u_1 u_1)_\omega + \rho_o k^2 \int dx_o\ g_\omega(x,x_o) \int dA_o (u_1 u_1)_\omega$$

$$\equiv I + II \qquad (19)$$

The pressure fluctuation therefore consists of two superimposed parts. I is a local noise due to the local turbulence field. II is a propagational sound, because of the appearance of g_ω, and is the sound pumped up by the entire volume of turbulence. The frequency content of I is the frequency of the the square of the axial velocity fluctuation, and that of II is modified by g_ω.

Now consider the construction of the cross spectral density of a pressure at two different points, x_1 and x_2. Using Eq. (19),

$$S_{12} = S_{I(x_1)\ I(x_2)} + S_{I(x_1)\ II(x_2)} + S_{II(x_1)I(x_2)} + S_{II(s_1)II(x_2)}$$

Using the notation $T_\omega(x) = (u_1 u_1)'_\omega$, it is seen

$$S_{I(x_1)\ I(x_2)} = \frac{\rho_o^2}{A^2} \left(\frac{\int dA\ T^*_\omega(x_1) \int dA\ T_\omega(x_2)}{t_o} \right)$$

But if x_1 and x_2 are sufficiently separated there is expected no correlation between $T_\omega(x_1)$ and $T_\omega(x_2)$ so $S_{I(x_1)\ I(x_2)} \approx 0$. On the other hand, if $x_1 = x_2$ so that an autospectrum of the pressure is considered S_{II} is nonzero and is given by

$$S_{II} = \left(\frac{\rho_o}{A}\right)^2 \int dA(r,\theta) \int dA(\tilde{r},\tilde{\theta})\ \frac{T^*_\omega(x,r,\theta)\ T_\omega(x,\tilde{r},\tilde{\theta})}{t_o} \qquad (20)$$

Investigation of the magnitude of Eq. (20) reveals that it is expected to be of order

$$S_{II} \text{ is } \mathcal{O}\left[S_{TT}\, \rho_o^2\, A_{cor}/A\right]$$

Similar manipulations on $S_{II(x_1)II(x_2)}$ yield that even when x_1 and x_2 are separated there is correlation between the signals due to the fact that II corresponds to propagational sound. In fact

$$S_{II(x_1)\ II(x_2)} = \rho_o^2\, k^4 \int_0^{\ell} dx_o \int_0^{\ell} d\tilde{x}_o\ g_\omega^*(x_1, x_o) g_\omega(x_2, \tilde{x}_o) \times \int_A dA(r,\theta) T_\omega^*(x_o, r, \theta) \int_A dA(\tilde{r},\tilde{\theta}) T_\omega(\tilde{x}_o, \tilde{r}, \tilde{\theta}) \quad (21)$$

The point is that both x_o and $\tilde{x}_o$ run from 0 to ℓ and where $x_o \approx \tilde{x}_o$ the T values are correlated. Careful examination yields the order of magnitude result

$$S_{II(x_1)\ II(x_2)} \text{ is } \left[\rho_o^2\, k^4\, S_{TT}\, V_{cor}\, \ell\, |g_\omega|^2 A\right]$$

Consider $x_1 = x_2$ so an autospectrum is being considered, and the ratio of S_{II} to $S_{II\ II}$ is

$$\frac{S_{II}}{S_{II\ II}} \text{ is } \mathcal{O}\left[\frac{\cos k\ell\, A_{cor}}{k^2\, V_{cor}\, \ell}\right]$$

The exact nature of this ratio depends upon the behavior of the correlation area and volume with frequency, but generally it is expected that a) the propagational sound may dominate near resonance peaks ($\cos k\ell \approx 0$) and b) away from resonance S_{II} will dominate since $k\ell$ is of order unity or larger but $k\, V_{cor}/A_{cor}$ is roughly like $k\, \ell_{cor} \approx \omega a/c \approx (\omega a/\bar{u})(\bar{u}/\bar{c}) << 1$ for low Mach number flows with turbulence centered about frequencies $\omega\, a/\bar{u} \approx 1$. It may further be shown that the cross terms $S_{I\ II}$ and $S_{II\ I}$ are small compared with either $S_{I\ I}$ or $S_{II\ II}$ Consequently, the situation is as follows: a) If x_1 and x_2 are widely separated only $S_{II\ II}$ should be sensed by a cross spectrum of two pressure transducers, b) If $x_1 = x_2$ the auto spectrum of the pressure will contain mainly $S_{I\ I}$ with contamination by $S_{II\ II}$ at resonant frequencies and c) If enough information is available on the spatial correlation of T_ω the pressure should be calculable.

It is argued that the pressure computed from Eq. (18) is a lower bound to the actual pressure. This conjecture is due to the retention of only one term, the plane approximation, in H'. Actually, the Green's function of Eq. (13) contains an infinite number of terms. However, each term is somewhat uncorrelated with every other term because of different transverse function weighting in the integration operation of

Eq. (12). Consequently, the mean square pressure should consist of a sum of squared terms, the first of which is given by the solution as given here. Further work in completion of such a solution to include transverse dependence of g should be carried out.

Experimental

The tube of Fig. 1 is 20 ft long, 2 inches in diameter, and instrumented with flush mounted microphones and hot film anemometers. Because $(u_1\ u_1)'$ is desired from the hot films, the individual signals are first passed through a linearizer, then squared and then filtered to remove the d.c. part. All signals are recorded on magnetic tape for later Fourier analysis.

The nozzle for most runs has a contraction ratio to give an average Mach number of 0.1 at the entrance plane. To insure fully developed pipe flow by this station measurements were made of the mean velocity and axial turbulence intensity. These measurements are shown in Fig. 2 and are compared with Laufer's[5] pipe flow data. The axial extent of the fully developed flow was not determined.

First consider the pressure auto spectrum shown in Fig. 3. The pressure is here being measured 2 inches upstream of the nozzle. The spectrum consists of a broad band noise on which there are superimposed weak resonance peaks at the 1/4 wave resonance points (here 15, 40, 70; etc. Hz). This is the situation expected from the theory above. Figure 4 displays the cross spectral density magnitude between two microphones placed 8 inches apart. Clearly what has been done is to suppress $S_{I(x_1)\ I(x_2)}$, as expected, and to reveal only the propagational sound. These observations are in accord with the qualitative expectations from theory; the question now is the quantitative agreement.

To see if the pressure is calculable, what is needed for S_{II} is given in Eq. (20). Using the cylindrical coordinate system of Fig. 5, this becomes

$$S_{II} = \frac{\rho_o}{A^2} \int dA(r,\theta) \int_0^{2a} d\rho \int_{\varphi_1(\rho,r,\theta)}^{\varphi_2(\rho,r,\theta)} d\varphi\, \rho\ S_{T(r,\theta)}\, T(r,\theta,\rho,\varphi)$$

While axial symmetry helps somewhat, this still requires an enormous number of cross spectral densities of space separated hot films to obtain accurate numbers. Accordingly, an approximate procedure is used. A representative r, point is taken as $r = a/2\ \theta = \pi/2$ and a fixed anemometer is placed at this point. A traverse of separation distance $\rho = 0$ to $a/2$ is taken with $\varphi = \pi/2$ and then a traverse $\rho = 0$ to $3a/2$ is made with $\varphi = 3\pi/2$. S_{II} is then approximated by numerical integration of the results.

$$S_{II} \approx \frac{\rho_o}{A}\ 2\pi \left[\int_0^{a/2} S_{TT}\Big)_{\varphi=\pi/2} \rho d\rho + \int_0^{3a/2} S_{TT}\Big)_{\varphi=3\pi/2} \rho d\rho \right]$$

Shown in Fig. 6 is the behavior of S_{TT} as a function of separation distance, ρ, for various frequencies. As expected, the size scale over which neighboring anemometers are correlated decreases with an increase in frequency. S_{II} is then calculated by integration and the result is shown on Fig. 3. It is seen that a) indeed a lower bound is produced for the broadband noise, b) the frequency content is roughly correct and c) this lower bound is about 10 dB lower than the experimental curve (that is, the theory under estimates the actual linear rms pressure by about a factor of 3).

S_{III} is more difficult to come by because there is an axial integration also involved in Eq. (21). Looking at the auto spectrum, letting $x_o = x_o + \zeta$, and assuming the Green's function varies slowly over the distance scale where the axial correlation of T drops to zero, there results the approximation

$$S_{III} = \rho_o^2 k^4 \int dx_o\ g_\omega^*(x,x_o) g_\omega(x,x_o) \int_{-\infty}^{\infty} d\zeta \int dA(r,\theta) \times$$

$$\int dA(\rho,\varphi)\ S_{T(x_o,r,\theta)T(x_o+\zeta,r,\theta,\rho,\varphi)}$$

The difficulty here is that now S_{TT} has a phase, dependent on ζ, because of convection of disturbances. However S_{IIII} is real so that the integration must cancel out all phase. Consequently, only the real part of S_{TT} is used above. A typical example of $S_{T(x_o,r,\theta)T(x_o+\zeta,r,\theta)}$ is shown in Fig. 7. The above formula is estimated by

$$S_{III} = \rho_o^2 k^4 \left(\frac{S_{II} A}{\rho_o} \right) \left[\int_0^{\ell} |g_\omega|^2 dx_o \right] \ell_{cor} \qquad (22)$$

where

$$\ell_{cor} = \frac{1}{S_{TT}} \int_{-\infty}^{\infty} S_T(x_o, r, \theta) T(x_o + \zeta, r, \theta) d\zeta$$

and the integral is numerically computed from the data. This is clearly a rather coarse estimate, and, recall, the Green's function is not accurate near the resonance peaks. The calculation of Eq. (22) is shown near the troughs in g_w on Fig. 3. Again, a lower bound is evident and the troughs, as expected, are significantly down from the lower bound estimate of S_{II}.

In the experimental configuration, the S_{II} term is dominating the pressure fluctuation. Integration of the spectrum to yield the mean square pressure is made difficult because of the A_{cor} term in the order of magnitude estimate below Eq. (20). If A_{cor} were independent of frequency

$$\langle p'^2 \rangle \propto \bar{u}^4$$

would result. However, since A_{cor} may be expected to fall with frequency, a dependence on $\bar{u}$ to somewhat less than the fourth power would be expected. Checking this with nozzles of differing contraction ratio, the result is shown in Table 1.

Table 1

Scaling of Pressure Level with Flow Velocity

Mass Weighted Flow Velocity (ft/sec)	Sound Pressure Level (dB re 2×10^{-5} n/m^2)
112	108.5
162	111.8
214	115.8

The result is that $\langle p'^2 \rangle \propto \bar{u}^3$, approximately.

Concluding Remarks

What has now been gained is an understanding of the pressure fluctuation generation by turbulence in an interior flow. This understanding is semi-quantitative in the sense that a lower bound to the pressure field may be calculated from knowledge of spatial

correlations of the turbulence velocities. The next step would be to use information on rocket motor turbulence, if available, together with an accurate calculation of g as, for example, in Ref. (2), and to use these pieces of information to calculate pressure fluctuations in a rocket motor cavity. The problem is that the necessary correlations are not available. While progress is being made in calculation of the kinetic energy of turbulence[5] the spatial correlations necessary here do not appear to be forthcoming. Consequently, current work is centering on measurement of the necessary turbulence quantities in a tube as in Fig. 1 but with blowing from the side walls, to simulate a solid rocket cavity.

Acknowledgements

This work was supported by the Air Force Office of Scientific Research under Contract No. FA9620-78-C-0003. Mr. R. Christiansen gave invaluable help during the data reduction portion of the program.

References

1. Mathes, H. B., "Assessment of Chamber Pressure Oscillations in the Shuttle SRB," 16th JANNAF Combustion Meeting, Monterey, CA, September, 1979.

2. Strahle, W. C. and Handley, J. C., "Prediction of Combustion Induced Vibration in Rocket Motors," Final Report on Contract No. DASG60-77-C-0054, April, 1978.

3. Beddini, R. A. and Varma, A. K., "The Erosive Burning of Ammonium Perchlorate," 16th JANNAF Combustion Meeting, Monterey, CA, September, 1979.

4. Yates, J. E. and Sandri, G., "Bernouli Enthalpy: A Fundamental Concept in the Theory of Sound," Aeroacoustics: Jet Noise, Combustion and Core Engine Noise, (ed. I. R. Schwarz), MIT Press, 1976, p. 65.

5. Laufer, J., "The Structure of Turbulence in Fully Developed Pipe Flow," NACA Tech. Report No. 1174, 1957.

6. Crocco, L. and Sirignano, W. A., "Behavior of Supercritical Nozzles under Three Dimensional Oscillatory Conditions," AGARDograph 117, 1967.

---

* Regents' Professor of Aerospace Engineering. Associate Fellow AIAA

† Senior Research Engineer, Member AIAA.

Figure Captions

Fig. 1. Schematic drawing of the experimental configuration.

Fig. 2. Comparison of Laufer's pipe flow data with that obtained in the current experimental configuration.

Fig. 3. Measured pressure spectrum at the wall and at the nozzle entrance plane. Calculated contributions to the pressure from the velocity fluctuation data.

Fig. 4. Cross spectral density between two microphones separated by eight inches.

Fig. 5. Coordinate system for spacewise cross correlations of velocity fluctuations and actual experimental points.

Fig. 6. Cross spectral density of transversely separated hot film anemometers for various frequencies.

Fig. 7. Real part of cross spectral densities of axially separated hot film anemometers for various frequencies.

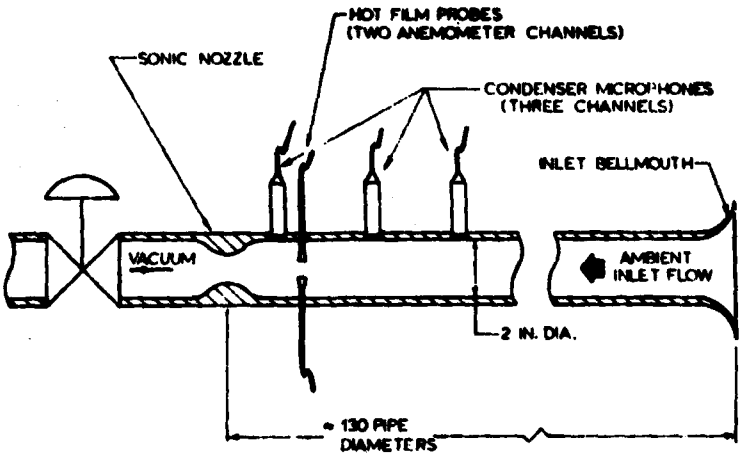

ACOUSTIC TUBE SCHEMATIC

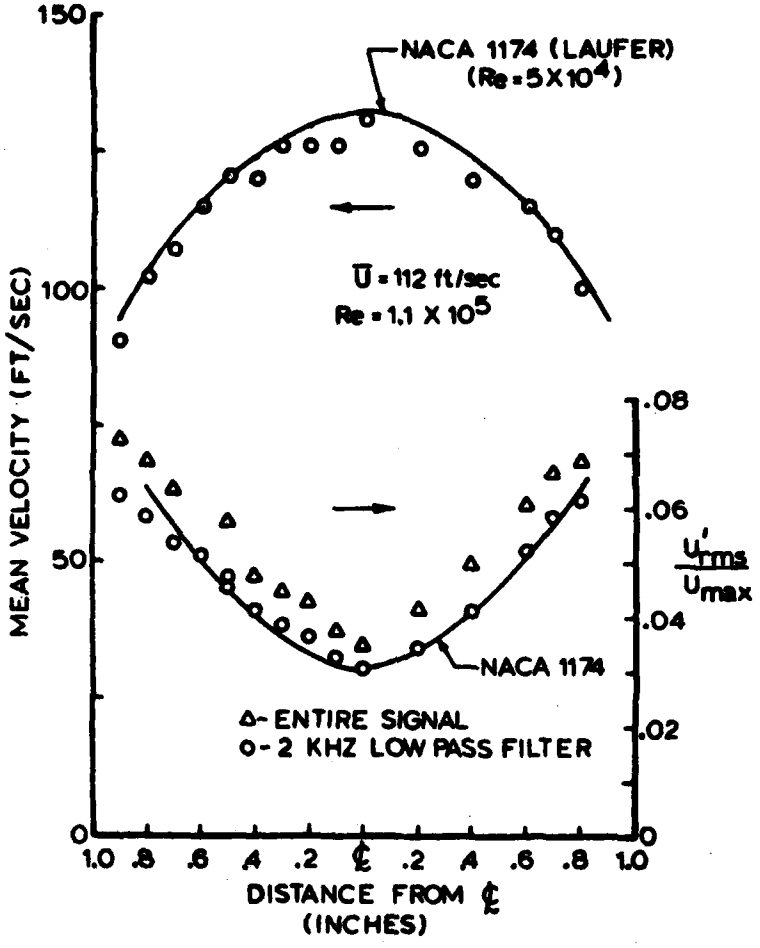

Figure 3. Mean and fluctuating axial velocity distributions across the tube

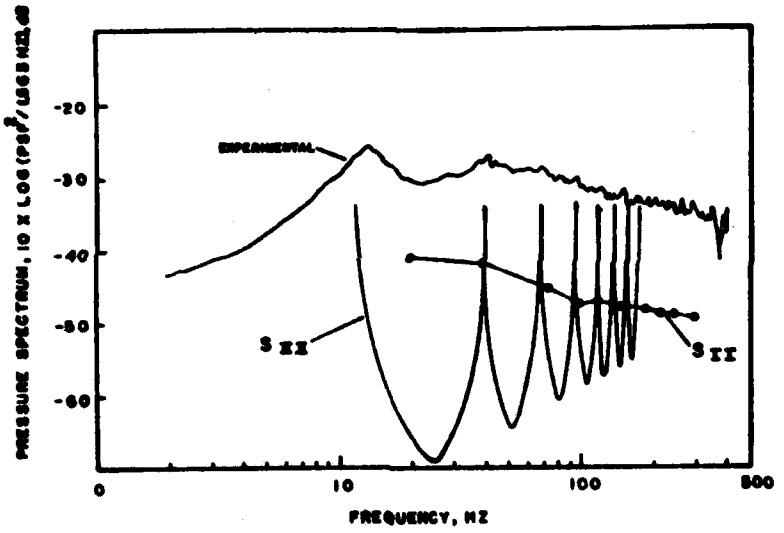
-20
-30
-40
-50
-60
0
10
100
500
FREQUENCY, HZ
S XX
S XX

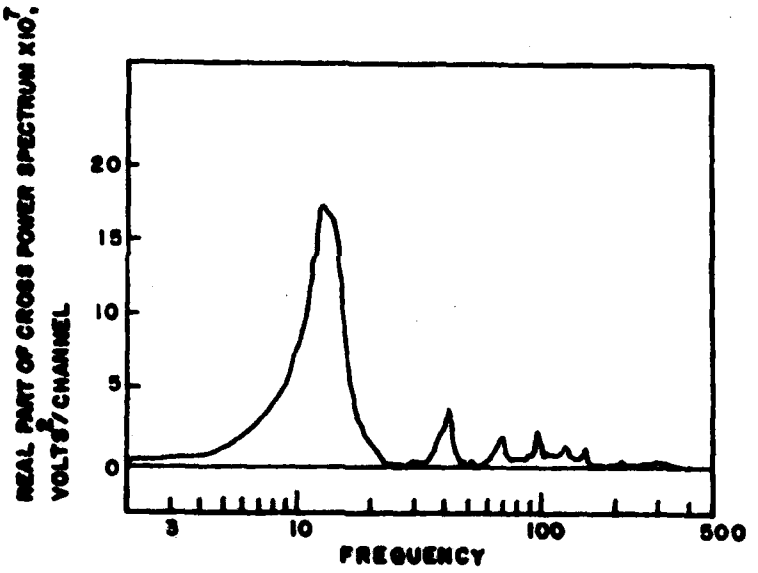
REAL PART OF CROSS POWER SPECTRUM X10^7, VOLTS^2/CHANNEL
20
15
10
5
0
3
10
100
500
FREQUENCY

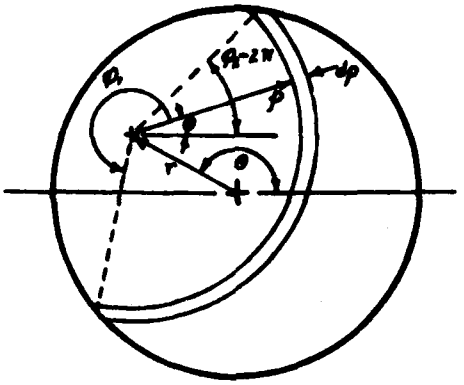

COORDINATE SYSTEM FOR CROSS CORRELATION INTEGRALS

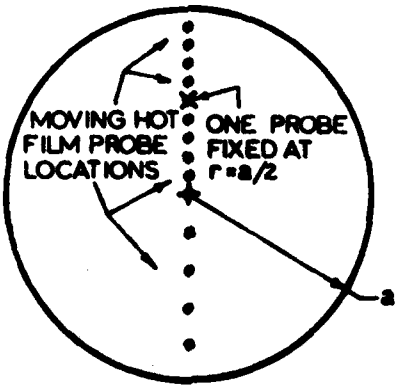

EXPERIMENTAL TRAVERSE CONDUCTED

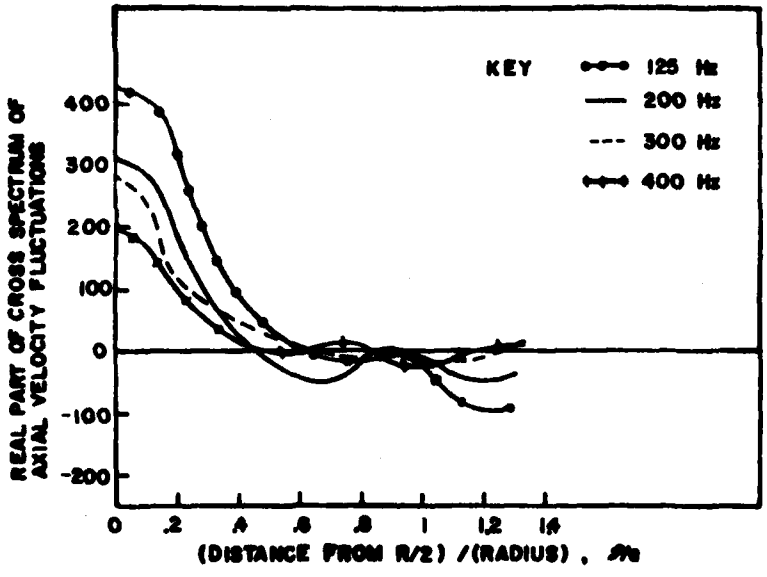
KEY
125 Hz
200 Hz
300 Hz
400 Hz
REAL PART OF CROSS SPECTRUM OF AXIAL VELOCITY FLUCTUATIONS
400
300
200
100
0
-100
-200
0
.2
.4
.6
.8
1
1.2
1.4
(DISTANCE FROM R/2) /(RADIUS)

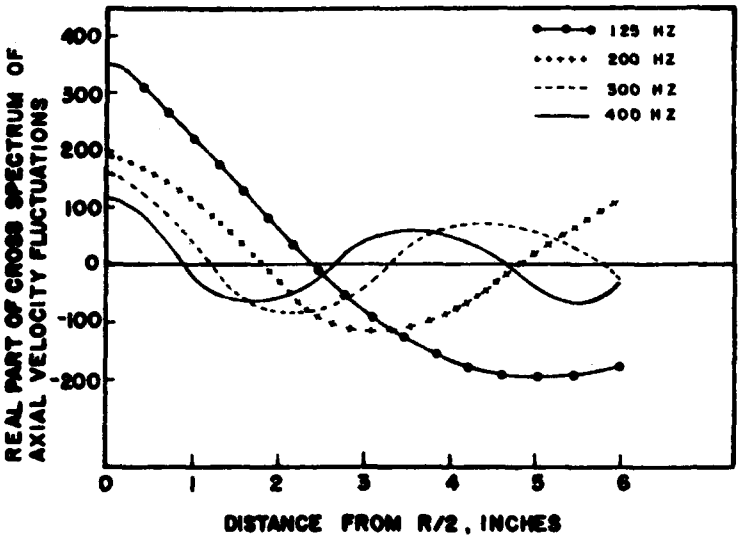
125 HZ
200 HZ
300 HZ
400 HZ
400
300
200
100
0
-100
-200
0
1
2
3
4
5
6
REAL PART OF GROSS SPECTRUM OF AXIAL VELOCITY FLUCTUATIONS
DISTANCE FROM R/2, INCHES